# IMPLICATIONS OF PLUMBING SYSTEM ON HEAVY METAL CONCENTRATIONS IN TAP WATER

BY

FAYZUL KABIR

A Thesis Presented to the
DEANSHIP OF GRADUATE STUDIES

**KING FAHD UNIVERSITY OF PETROLEUM & MINERALS**

DHAHRAN, SAUDI ARABIA

In Partial Fulfillment of the
Requirements for the Degree of

## MASTER OF SCIENCE

In

CIVIL ENGINEERING

DECEMBER 2017

KING FAHD UNIVERSITY OF PETROLEUM & MINERALS

DHAHRAN- 31261, SAUDI ARABIA

**DEANSHIP OF GRADUATE STUDIES**

This thesis, written by [FAYZUL KABIR] under the direction of his thesis advisor and approved by his thesis committee, has been presented to and accepted by the Dean of Graduate Studies, in partial fulfillment of the requirements for the degree of [**MASTER OF SCIENCE IN CIVIL ENGINEERING**].

Dr. [Md. Shakhawat Hossain Chowdhury]
(Advisor)

Dr. [Mohammad Abu Jafar Mazumder]
(Member)

Dr. [Salah U. Al-Dulaijan]
Department Chairman

Dr. [Muhammad S. Vohra]
(Member)

Dr. Salam A. Zummo
Dean of Graduate Studies

17/12/17
Date

*Dedicated to my parents Md. Osman Gani and Rowshanara Begum*

# ACKNOWLEDGMENTS

All the praise to the Almighty Allah, the most Merciful, the most Beneficent, for His guidance and protection throughout this study. Shalawat and blessings be upon the Prophet Muhammad Shallallahu ’Alaihi Wa sallam, his family, and his companions.

I am grateful to my parents, Md. Osman Gani and Rowshanara Begum for their continuous support, motivation and sacrifices throughout my study. I would also like to thank my beloved sisters, Shirin, Shaila, Jabin, Moni, and other family members for their love, prayers, and support

I sincerely thank my academic advisor, Dr. Md. Shakhawat Hossain Chowdhury for his excellent guidance, enormous support, inspiration and motivation throughout the entire journey. I would like to express appreciation for my thesis committee members Dr. Muhammad S. Vohra and Dr. Mohammad Abu Jafar Mazumder for their valuable suggestions, evaluations and admirable cooperation. I would also like to thank all of my Professors for their cordial support and cooperation.

I am deeply grateful to King Fahd University of Petroleum and Minerals (KFUPM) for their excellent research facilities and provide me the scholarship to study here. Furthermore, I am gratitude to the Bangladeshi students, teachers and staffs community of KFUPM for their continuous support and prove me a homely environment throughout my journey at KFUPM.

# TABLE OF CONTENTS

# LIST OF TABLES

# LIST OF FIGURES

# LIST OF ABBREVIATIONS

| | | |
|---|---|---|
| **ANOVA** | : | Analysis of Variance |
| **APHA** | : | American Public Health Association |
| **As** | : | Arsenic |
| **ATSDR** | : | Agency for Toxic Substances and Disease Registry |
| **AUS** | : | Australia |
| **Ba** | : | Barium |
| **BCM** | : | Billion Cubic Meter |
| **Be** | : | Beryllium |
| **BEM-4P** | : | Four Parameter Bi-exponential Model |
| **CBM** | : | Cubic model |
| **Cd** | : | Cadmium |
| **CDI** | : | Chronic Daily Intake |
| **Cr** | : | Chromium |
| **Cu** | : | Copper |
| **CV** | : | Coefficient of Variation |
| **DBP** | : | Disinfection Byproduct |

| | | |
|---|---|---|
| **DIC** | : | Dissolved Inorganic Carbon |
| **DOC** | : | Dissolved Organic Carbon |
| **EU** | : | European Union |
| **FCl** | : | Free Residual Chlorine |
| **Fe** | : | Iron |
| **GI** | : | Galvanized Iron |
| **GW** | : | Groundwater |
| **HC** | : | Health Canada |
| **Hg** | : | Mercury |
| **HWT** | : | Hot Water Tank |
| **ICP-MS** | : | Inductively Coupled Plasma-Mass Spectrometry |
| **LLM** | : | Logarithmic Model |
| **LM-3P** | : | Three Parameter Logistic Model |
| **LM-4P** | : | Four Parameter Logistic Model |
| **LMF** | : | Linear Main Factors |
| **LMFI** | : | Linear Main Factors with Interactions and Higher Orders |
| **Max** | : | Maximum |

| | | |
|---|---|---|
| **Min** | : | Minimum |
| **Mn** | : | Manganese |
| **Ni** | : | Nickel |
| **NN** | : | Neural Network |
| **NOM** | : | Natural Organic Matter |
| **NOM** | : | Natural Organic Matter |
| **NZ** | : | New Zealand |
| **Pb** | : | Lead |
| **PE** | : | Polyethylene |
| **POPR** | : | Polypropylene |
| **PP** | : | Plumbing Pipe |
| **PVC** | : | Polyvinyl Chloride |
| **QRM** | : | Quartic model |
| **QUM** | : | Quintic model |
| **Sr** | : | Strontium |
| **SW** | : | Surface Water |
| **SWCC** | : | Saline Water Conversion Corporation |

| | | |
|---|---|---|
| **T** | : | Temperature |
| **TCl** | : | Total Chlorine |
| **UK** | : | United Kingdom |
| **USEPA** | : | United States Environmental Protection Agency |
| **$UV_{254}$** | : | UV absorbance at 254 nm |
| **WDS** | : | Water Distribution System |
| **WHO** | : | World Health Organization |
| **WM-4P** | : | Four-Parameter Weibull Model |
| **Zn** | : | Zinc |

# ABSTRACT

Full Name : [FAYZUL KABIR]

Thesis Title : [Implications of Plumbing System on Heavy Metal Concentrations in Tap Water]

Major Field : [Civil and Environmental Engineering]

Date of Degree : December, 2017]

Exposure to heavy metals in tap water can have various chronic and sub-chronic effects to human health. Stagnation of water in the plumbing pipes (PP) and hot water tanks (HWT) prior to reaching the tap is likely to increase the concentrations of several heavy metals, which may exceed the regulatory guidelines. This study investigates the occurrences and variability of different heavy metals in water from water distribution systems (WDS), PP and HWT. The water samples were collected and analyzed for 7 times a day on bi-weekly basis to represent the WDS, PP and HWT. The concentrations of heavy metals in HWT were 1.2-8.1 and 1.4-6.7 times to the heavy metals in the WDS and PP respectively. The concentrations of As, Cr, Cu, Pb, Hg, Ni and Zn were in the increasing order on WDS, PP and HWT. The sampling times were not found to be sensitive, while some heavy metals were seasonally variable with higher values during the summer months. Following data analysis and identification of significant factors, three types of models (linear, non-linear and neural network) were trained for predicting the changes of heavy metals from WDS to the PP and HWT. Several models showed moderate to good predictive performances in predicting the heavy metals in PP and HWT. The findings highlight the limitations of the current sampling locations for regulatory compliance, which may need further attention to achieve better control on heavy metal concentrations at the exposure point.

# ملخص الرسالة

**الاسم الكامل:** فيض ال كبير

**عنوان الرسالة:** الآثار المترتبة على نظام السباكة على تركيزات المعادن الثقيلة في مياه الحنفية

**التخصص:** الهندسة المدنية والبيئية

**تاريخ الدرجة العلمية :** ديسمبر، 2017

وجود المعادن الثقيلة في صنابير المياه يمكن ان يتسبب بمضاعفات صحية على المدى القريب والبعيد، ركود المياه في انابيب المياه وخزانات المياه الساخنة قبل وصولها الى الصنبور يتسبب في زيادة تركيز العديد من المعادن الثقيلة والذي بدوره يؤدي الى تجاوز القيم المسموح بها في المواصفات ، تقوم هذه الدراسة باستكشاف وجود ومقدار تغير المعادن الثقيلة المختلفة في الماء المستخدم في انظمة توزيع المياه (WDS) ، انابيب المياة (PP)، وخزانات المياه الساخنة (HWT). تم تجميع عينات المياه التي تمثل (WDS,PP,HWT) وتحليلها سبع مرات يوميا وبشكل اسبوعي. تركيز المعادن الثقيلة في خزانات المياه الساخنة بلغ 1,24 – 8,1 و 1,4 – 6,65 مرات أكثرمقارنة بمقدارها في انظمة توزيع المياه و انابيب المياة على التوالي. مقدار تركيز (As, Cd, Cr, Cu, Pb, Hg, Ni, Zn) ازداد تصاعديا في انظمة توزيع المياه (WDS) ، انابيب المياة (PP)، وخزانات المياه الساخنة (HWT). توقيت تجميع العينات لم يكن ذا تاثير كبير في حين كانت بعض المعادن الثقيلة موسميا متغيرة بقيم مرتفعة خلال الصيف. بعد تحليل البيانات وتحديد العوامل المؤثرة ، ثلاثة أنواع من النماذج (خطية وغير خطية وشبكات عصبية) تم استخدامها للتنبؤ بمقدار تغير المعادن الثقيلة من انظمة توزيع المياه (WDS) الى انابيب المياة (PP) وخزانات المياه الساخنة (HWT). . النتائج سلطت الضوء على جوانب قصور مواقع أخذ العينات الحالي على التوافق المنهجي والذي يحتاج الى المزيد من الاهتمام للتحكم بشكل أفضل في مقدار تركيز المعادن الثقيلة في النقاط المكشوفة.

# CHAPTER 1

# INTRODUCTION

Heavy metals are characterized by the specific density of more than 5g/cm$^3$, which are bio-accumulative and have long half-lives [1]. The residential or occupational exposure to thirty-five metals can cause human health risk while twenty-three of these metals are known as heavy metals [2]. The heavy metals have continuous impact on the environment (e.g., water, soil) and humans, which have been a concern for the past few decades. These metals are often originated from rocks and concentrated in water, soil or in air through multiple transferring media. Drinking water is one of the potential sources for human exposure to heavy metals [3]. The atmospheric heavy metals are washed away during rainfall and ultimately reach to the potential sources of drinking water (underground water, rivers, lakes or reservoirs) [4]. The manufacturing and industrial activities (e.g., chemical industries, metal smelting and electroplating) can also serve as the anthropogenic sources for heavy metals in water [5]. For example, the Kamioka Zinc Mine of Japan was responsible for cadmium contamination in the Jinzu River, which resulted in kidney problems among the surrounding populations [6]. The agricultural, industrial and mining activities around Sonora, Mexico caused elevated levels of Cu, As, Hg, Pb and Cd in groundwater [7]. Approximately 43% of samples exceeded the action level (i.e., the concentration, above which water system must follow treatment process) for Pb (i.e., 15 µg/L) and 8.9% samples exceeded the WHO recommended value of As (i.e., 10 µg/L) [7–

9]. The industrial, mining, and agricultural activities in the surrounding areas polluted the drinking water sources [7].

Despite the efforts of removing heavy metals, several metals remain in drinking water in trace concentrations. Leaching of heavy metals from water distribution system (WDS) can further increase the concentrations of these metals [10]. The diurnal and seasonal variability in water usage, temperature fluctuations and water chemistry also have implications on the concentrations of these metals in drinking water. In 2007, concentrations of Pb were reported to be higher than 10 µg/L in approximately 25% of older houses in London, ON, Canada [11]. Tamasi and Cini (2004) reported higher levels of Fe, Cu, Zn, and Pb at the dead end of WDS than in the origin (e.g. treatment plants) in Mount Amiata and downtown Siena, indicating the leaching of metals from the water distribution pipes into water [12]. Similarly, during the transportation of water through distribution pipe, the level of Cu in treatment plant (i.e., below ICAP detection limit) increased up to 3000 µg/L at consumer tap [13]. Comparatively higher concentration of Pb (0.58±0.23 µg/L), As (0.29±016 µg/L) and Zn (5.9±2.3 µg/L) in tap water of Dakhlia, Egypt were observed than bottled water [14]. Corrosion of plumbing pipe (PP) was considered as the major source for this contamination. Stagnation of water in distribution network of Riyadh caused exceeded levels of Fe than the WHO recommended value (i.e., 300 µg/L) for 2% of the total samples [15]. The concentration of Cu increased up to 67% while conveying from the first floor (Cu= 600 µg/L) to the top floor (Cu= 1000 µg/L) of a six-story building in Dhahran, Saudi Arabia [13]. A study on 127 randomly selected HWT water sample of Dalmatian county, Croatia indicated the occurrences of Zn (mean=180 µg/L), Fe (mean=40 µg/L), Cu (mean=10 µg/L) and Mn (mean=4.96 µg/L); where the

mean water temperature was 54°C and several sampling locations exceeded the maximum contaminant levels [16].

The municipal water enters the plumbing premise of a house or building from the WDS. Based on the size of the plumbing network, water may stay in the PP and hot water tank (HWT) for significant amount of time, which can cause additional metal to release into drinking water. For instance, a study on 12,000 school and workplace tap water in USA showed exceeded concentrations of lead (i.e., 15 µg/L) for 17.2% of the samples during the first-draw, while flushing the source prior to using reduced this percentage [17]. In addition, water quality parameters in the plumbing premise, types of pipe materials and faucets can also affect the release of heavy metals into drinking water. Increased concentrations of few heavy metals were reported in the water cooler compared to WDS [18,19]. The study on 400 coolers in Riyadh area revealed the maximum concentrations of Fe (411.7 µg/L), Pb (59.82 µg/L) and Ni (228.68 µg/L) in cooler output while the feed water from WDS had negligible concentrations (i.e., Fe=20.43 µg/L, Pb=2.85 µg/L and Ni=1.72 µg/L) [20].

In context to Saudi Arabia, the desalinated water is blended with the treated groundwater, pH adjusted and chlorinated prior to supply to the communities. This relatively corrosive water typically contains trace amount of several heavy metals including Pb, Zn, Fe, Ca and Mg [13,15]. In addition, the desalinated and blended water is likely to increase the release of heavy metals from the pipe materials and pipe coatings into drinking water. Past studies reported increased levels of several heavy metals (e.g., copper, iron, zinc) from desalination plants to consumer tap where the pipe lengths showed significant effects [13]. In addition, stabilization and pH adjustment of desalinated water increased the levels of As, Cd, Hg

and Se in drinking water from few desalination plants in Saudi Arabia [21]. Further, water spends significant time in the plumbing premise prior to reaching the tap in the house/building, which can also increase the concentrations of several heavy metals.

The populations are exposed to tap water, which is likely to have higher levels of heavy metals than the WDS. Some heavy metals, including Cd, As, Pb, Cr, Hg, Ni and Cu in drinking water can pose risks to human health [8,22]. Some of these effects includes mental disorder [23], brain damage, central nervous system failure [24], damage of DNA structure [25], skin infections [26], blood composition disorder, failure of lungs, heart, liver, kidneys and other major organs [26,27]. Chronic exposure to few heavy metals can induce hypertension, ischemic heart disease and allergies [28,29]. As an example, exposure to As in water caused cancer and skin damage, while Cd was reported to be responsible for kidney damage [8]. Some other impacts, such as, liver and kidney function damage form Hg, high blood cholesterol and heart diseases from Sb and gastrointestinal disorder from Cu were also reported [8].

To minimize human health risk from heavy metals in drinking water, several regulatory agencies have endorsed the maximum allowable levels for some metals [8]. The regulatory agencies, health professionals and/or monitoring programs generally collect water samples from WDS or water treatment plants to ensure regulatory compliance and to perform exposure and risk analysis. As such, the effects of plumbing premise have not been given much attention. Although many studies have focused on heavy metal occurrences from corrosion of plumbing materials and health concerns of heavy metal contaminated drinking water, limited information is available on implications of plumbing premise on the concentrations of heavy metals in tap water or changes of heavy metal concentrations from

WDS to PP and HWT. Further, no study has been reported to date on modeling the changes of heavy metals from WDS to PP and HWT.

## 1.1 Importance of the Study

The major fraction of drinking water in the Middle Eastern countries, including Saudi Arabia, is supplied through desalinating seawater from the Arabian Gulf and the Red Sea while the seawater is polluted due to biogenic and anthropogenic activities. The blended water typically contains several heavy metals [15,20]. In addition, the relatively corrosive water is likely to increase the release of heavy metals from the pipe materials and pipe coatings into drinking water. Further, water spends significant time in the plumbing premise and HWT prior to reach the tap water in the house/building, which can increase the concentrations of several heavy metals. The regulatory agencies and/or monitoring programs generally collect water samples from the WDS or the water treatment plants to ensure regulatory compliance. The impacts of water stagnation in the plumbing system and HWT on the change of heavy metals from the WDS to the exposure point have not been given much attention. Past studies focused mainly on the heavy metals release from corrosion of plumbing materials. There are limited studies on changes of heavy metal concentrations from WDS to PP and HWT.

The populations are likely to be exposed to the tap water with elevated concentrations of heavy metals compared to WDS. In this study, the related issues were investigated, which will assist in better understanding of the changes of heavy metals concentrations from WDS to tap water. The factors affecting the changes of heavy metals concentrations between the WDS and tap water and the diurnal and seasonal variability of metal release were also

investigated. The findings may provide baseline to set policies for establishing regulatory guidelines for heavy metals in drinking water.

## 1.2 Objectives of the Study

The goal of the study is to understand the occurrences and variability of heavy metals in water distribution system (WDS), plumbing pipes (PP) and hot water tanks (HWT). The goal was achieved through fulfilling the following objectives:

i. Investigating the occurrences and variability of heavy metals in WDS, PP and HWT
ii. Investigating the correlations of heavy metal release with the water quality parameters (WQP)
iii. Developing models to predict the changes in heavy metal concentrations from WDS to PP and HWT
iv. Validating the models using an additional set of data, which were not used in developing the models

## 1.3 Organization of Thesis

This thesis work is divided into six chapters. The introduction of the thesis is presented in Chapter 1.

Chapter 2 describes the background of this thesis. It includes water supply system of Saudi Arabia, sources and occurances of heavy metals, health concerns and regulatory limits of heavy metals in drinking water. The factors affecting heavy metal release in plumbing system and chemistry of metal release are also described in Chapter 2.

In Chapter 3, methodologies of sample collection, sample analysis and data analysis are described. The approaches of modeling heavy metals in PP and HWT are also discussed in this chapter.

In Chapter 4, the experimental data are analyzed to determine the correlation, diurnal, seasonal and overall variability of heavy metals in WDS, PP and HWT. The data were also summarized

In Chapter 5, the significant factors for modeling were identified. Training of different linear, nonlinear and neural network models were performed and the models were validated using an additional set of experimental data.

Chapter 6 discussed the summary of this study.

Finally, in Chapter 7, the limitations of the study and recommendations for future study is presented.

# CHAPTER 2

# LITERATURE REVIEW

## 2.1 Water Supply System of Saudi Arabia

The Kingdom of Saudi Arabia is a semi-arid country (Lat. 16.5–32.5 N; Lon. 33.75–56.25 E), where most of the populations live in the urban areas. The major populous municipal areas are Riyadh (5.19 million), Jeddah (3.43 million), Makkah (1.53 million), Madinah (1.10 million), Dammam, Al-Khobar and Dhahran (1.24 million) [30]. The domestic water demand in 2014 was approximately 2600 million $m^3$, which has been increasing at a rate of 2.1% per year [31,32]. The major sources of water supply are the desalinated water, renewable surface and groundwater sources, non-renewable groundwater sources and treated wastewater [32]. Approximately 90% of the domestic water demand in the populous cities (e.g., Riyadh, Jeddah, Makkah, Madinah, Buraidah and Dammam) are fulfilled by desalinated water [33]. The Saline Water Conversion Corporation (SWCC) operate 28 desalination plant in the coastal zone of the Arabian Gulf and the Red Sea, which have produced 1247.9 million $m^3$ of desalinated water during the year 2015 [34]. The desalinated water is blended with the treated groundwater, pH adjusted and chlorinated prior to supplying to the WDS. The relatively corrosive desalinated and blended water are transported through a network of 21 water transmission systems and 7176 km long distribution pipelines to reach the consumers throughout the country [34]. There are 56 pumping stations in operation for propelling water into 285 reservoirs with total storage

capacity of 12.7 million $m^3$ [34]. A total of 3 mixing stations are used for blending desalinated water with the treated groundwater in the country [34].

## 2.2 Occurrences of Heavy Metals

The main sources of domestic water in Saudi Arabia are: groundwater, surface water and desalinated seawater while the desalination process is the prime source for drinking water in many arid and semi-arid countries including Saudi Arabia [35]. The treatment types, source and finished water quality, distribution network and plumbing systems (i.e., length, outline and materials) serve as the major sources for heavy metals in drinking water [3]. The source water quality is often affected by the anthropogenic and biogenic activities. The agricultural, industrial and mining activities surrounding the Sonora state of Mexico caused elevated levels of Cu, As, Hg, Pb and Cd in groundwater, which was used as drinking water [28]. The groundwater sources near the industries (e.g., steel, plastic, and battery manufacturer) also had higher levels of several heavy metals (e.g., Ni, Cd, Al and Pb) [36].

The physical and chemical water quality parameters (WQP) were found to be correlated with heavy metals in the WDS [37]. Stabilization and pH adjustment of desalinated water increased the levels of As, Cd, Hg, Pb, Cr and Se in drinking water from few desalination plants in Saudi Arabia [21]. The scale formation in the WDS is due mainly to upstream or *in-situ* corrosion and post-treatment deposits. The characteristics and composition of corrosion scale varied with WQP and pipe materials. Deposition of several heavy metals including, Al, As and Ra were reported in the corrosion scale [38]. In the tap water from Dakhlia governorate in Egypt, elevated levels of Cd, Pb, As, Se and Zn were reported [14].

The dead end of WDS showed elevated levels of Cu, Fe, Pb and Zn in drinking water, indicating the potential leaching of metals from WDS [12].

## 2.3 Factors Affecting Heavy Metal Release

### 2.3.1 Effects of Pipe Materials

The pipe materials and coatings can have effects on the leaching of heavy metals into drinking water. In the past, lead pipes were commonly used for water distribution and plumbing premise. In the recent years, different polymeric pipes (e.g., polypropylene [POPR], polyvinyl chloride [PVC] and polyethylene [PE]) are used. Several stabilizers, composed of metallic salt (i.e., Ca-Zn, Ba-Zn), are often used as additive of PVC polymer, which may serve as the potential sources of metal contamination [39]. It is to be noted that the polypropylene and polyethylene pipes do not require these stabilizers. The galvanized iron (GI) pipe generally consists of zinc coating, which can be a potential source of zinc and lead release in stagnant water [40]. Lasheen et al., [37] demonstrated the variability of lead and iron release depending on pipe materials following a 72 h water stagnation experiment. The iron release was similar in POPR (0.067 mg/L) and PVC pipe (0.068 mg/L) network while around 20 times higher values were observed for GI pipe (1.379 mg/L). The release of lead from POPR pipes (0.04 mg/L) was lowest while it was highest in the PVC pipe (0.113 mg/L).

### 2.3.2 Effect of Stagnation Period and Pipe Age

Stagnation period can have significant effects on metal release from pipe network. Past study demonstrated exponential increase in metal release during 20-24 h of stagnation period [41]. Heavy metal release was also reported to increase with the increase of pipe

age [37]. The overnight stagnation of water in cooler was reported to increase Cr, Al, Cu, Fe, Zn, Ni, Mn, and Pb in tap water [20]. Al-Malack [42] showed the increase of lead release from 0.43 to 0.78 mg/L between 10 to 72 hrs of stagnation in PVC pipe. Approximately 26% increase in lead release was reported for an increase in stagnation from 2 to 20 weeks while approximately 100% increase in iron release was observed during this period [37].

### 2.3.3 Effect of pH

Decrease of pH from neutral to acidic can increase the metal release from plumbing materials. At lower pH, dissolution rate of lead increases with increase of dissolved inorganic carbon (DIC) in water [43]. Kim et al. [11] reported approximately 50% reduction of lead concentration in drinking water when pH was increased from 7.1 to 7.7 in several houses in ON, Canada. The results were consistent to the batch and pipe loop experiments [11]. Release of iron and copper was reported to increase with lowering pH to acidic range [44] while decrease in iron release was observed when the pH was increased from 7.5 to 9.5 [45]. The rate of ferric hydroxide formation increased with increasing of pH above the neutral range, where ferric hydroxides are less likely to dissolve than ferrous solid and the scales formed are less porous [46].

### 2.3.4 Effect of Alkalinity

Increase of alkalinity in water reduces the release of few metals (e.g., iron, copper and lead) from pipe materials [45]. At equilibrium of lead carbonate, higher alkalinity decreases solubility of lead and reduces lead concentrations in water [47]. The increase of alkalinity at anoxic conditions reduces the solubility of ferrous carbonate phase and thus decrease

iron release. On the contrary, dissolution of carbonate-containing iron (i.e., $FeCO_3$) increases iron concentration in water at lower alkalinity [45]. The higher alkalinity offers higher buffer capacity and the denser scale structure can decrease iron release [46].

### 2.3.5 Impact of Chlorine Disinfectant

In the lead pipe, elevated lead concentrations in WDS may be due to the deposition of corrosion products (i.e., lead (II) carbonates and Oxides, lead(IV) oxides ($PbO_2$)) [48,49]. Among the different types of lead products, $PbO_2$ is rare and it can be formed in the pipe network due to the presence of free chlorine (i.e., HOCl and OCl-), which is often used as the residual disinfectant to protect water quality in the WDS [50]. Generally, $PbO_2$ is less soluble and its stability is changed with the presence of residual disinfectant (e.g., free chlorine or chloramines). To reduce the formation of disinfectant byproducts, the Washington DC tap water system substituted the free residual chlorine by chloramines, which resulted in higher lead concentrations in water [51]. An intermediate species, formed during the mono-chloramine deterioration process, was considered to be responsible for lead release from $PbO_2$ [52]. A study on $PbO_2$ dissolution rate in presence of disinfectant (e.g., monochloramine and free chlorine) using a completely mixed continuous-flow reactor reported free chlorine as the most active inhibitor for $PbO_2$ dissolution [53]. However, the WDS with the free chlorine and monochloramine reported lower levels of lead than the WDS without disinfectant. At acidic pH, $PbO_2$ dissolution rate was faster in presence of monochloramine, which could be lowered using the free chlorine as residual disinfectant [53].

### 2.3.6 Effects of Temperature and Seasonal Variability

Change of temperature and seasonal variability can play an important role on the release of heavy metals from WDS. Water temperature has impacts on the physical properties of water, corrosion scale, chemical reaction rates and thermodynamic properties (i.e., activity coefficients, solubility, and enthalpy of reaction) of corrosion scale. The cyclic variation of temperature over a short period (i.e, diurnal variation) might affect the rates of iron corrosion [46]. The change in water temperature may lead to formation of heterogeneous scale of multiple compounds on an iron surface. Volk et al. [54] reported lower iron concentrations and corrosion rates in WDS during the winter months while more red water incidents (i.e., higher iron release) was reported during the warmer summer months [46]. Temperature variability in different seasons caused variable levels of lead in drinking water from several houses in ON (Canada) at constant pH [11,55]. Temperature dependent variation was also observed in corrosion of copper [55] and lead [56] in WDS.

### 2.3.7 Sequence of Pipe and Flow Rate

The distribution network is consists of different metal piping system. Partial replacement of lead (Pb) pipe with copper (Cu) pipe reduced lead exposure at consumer level [57]. During continuous flow of water through Pb-Cu combined network, galvanic corrosion was reported to be negligible [58]. However, due to 48-72 h stagnation of water, galvanic corrosion was much higher and caused long-term effects [59]. Through changing flow acceleration, on/off flow regimes and/or varying water demand at different time of the day, corrosion could be controlled [60]. The medium flow (≅ 8 L/min) and high flow (≅ 32 L/min) conditions generated turbulent flow regimes in WDS leading to increased lead release in comparison to low flow (≅ 1.3 L/min) condition [61]. A pilot study on replacing

50% of lead pipes by copper pipes at upstream and downstream showed slightly lower lead release comparted to 100% lead pipe system during the low flow condition [61]. During medium and high flow conditions, lead release in the combined pipe system (Pb - Cu) were significantly higher. The same study showed that installation of a copper pipe at upstream of a lead pipe increased lead release to 1.6 folds compared to copper pipe at downstream of lead pipe. Presence of two electrochemically dissimilar metal (Pb - Cu) could induce galvanic corrosion, resulting in more lead particulates in water even in presence of zinc orthophosphate corrosion inhibitor.

### 2.3.8 Plumbing Fixtures

Although there are regulatory standards on faucet materials to ensure health safety, the aptitude of licensed elements to meet the standards is yet to be fulfilled [62]. Use of brass faucets in plumbing system can be a potential source of metal release [63,64]. The brass faucets consist of Zn and Cu, which can be corroded continuously. Corrosion of zinc coating (dezincification) may serve as a major booster for lead release at the end of service line [65,66]. Higher chloride in distribution network (> 200 mg/L), lower alkalinity, pH of approximately 8, higher ammonia (> 15 mg/L) and higher level of natural organic matter (NOM) (> 1 mg/L) are the main factors for dezincification [67,68]. Leaching of nickel from nickel/chromium-plated taps and corrosion of stainless steel pipes and fittings may also induce metal releases into tap water. An increase in pH to optimal level may provide a partial solution to Cu and Ni corrosion [69].

### 2.3.9 Presence of Other Metals

Presence of iron oxide particles in distribution network enhances particulate lead release in water. Iron oxide/hydroxide has high affinity to lead [70,71]. Kim et al., [11] reported higher level of particulate lead in presence of high concentrations of iron in WDS, indicating possible correlations between particulate lead release and iron concentration. Further, mechanical disturbance may also increase the release of several metals (e.g., Pb, Fe and Al) [72].

## 2.4 Chemistry of Metals in Drinking Water

The metals with relatively high densities, atomic weights, or atomic numbers are defined as heavy metals. Several low-molecular-weight cations that do not have the physical properties of metals (i.e, magnesium, calcium, sodium) are also considered with significance, due mainly to their role in mammalian metabolism [73]. The following sections discusses the chemistry of some metals in drinking water.

### 2.4.1 Magnesium

Magnesium (Mg) has the atomic weight and density of 24.312 g/mole and 1740 kg/m$^3$ respectively. The Mg containing main minerals are dolomite ($CaMg(CO_3)_2$) and magnesite ($MgCO_3$). It is one of the commonly occurring metals in seawater with average concentrations of approximately 1300 mg/L. The presence of Mg with other alkali caused the hardness of water. Water at room temperature has no considerable effect on Mg due to its slow-reaction nature while the presence of oxygen changes its reactivity. The reaction of Mg with water vapor forms magnesium hydroxide and hydrogen gas as follows:

$$Mg\ (s) + 2H_2O\ (g) \longrightarrow Mg(OH)_2\ (aq) + H_2\ (g) \quad (2.1)$$

The $Mg^{2+}$ ion is commonly occurring form of Mg in water, while $MgOH^+$ and $Mg(OH)_2$ may also present. The solubility of $Mg(OH)_2, MgCO_3$ in water are 12 mg/L and 600 mg/L respectively.

### 2.4.2 Chromium

Chromium (Cr) has atomic weight of 51.996 g/mole and density of 7.19 g/cm$^3$. The main chromium mineral is chromite and it does not occur freely in nature. The concentration of Cr in seawater varies between 0.2 and 0.6 µg/L, while in river, its around 1 µg/L. In water, Cr may be present in trivalent $Cr(OH)_3$ or hexavalent $CrO_4^{2-}$ form. However, the later one is abundant in natural water. Water at room temperature have no considerable reaction with Cr. The trivalent Cr(III) are generally insoluble in water while the hexavalent Cr (VI) are water soluble. The Cr(VI) compounds are stable in aerobic condition, but reduces to trivalent form under anaerobic condition.

### 2.4.3 Iron

Iron (Fe) has the atomic weight of 55.85 g/mole and density of 7.8 g/cm$^3$. The concentration of Fe in seawater, rivers and groundwater are in the ranges of 1-3 µg/L, 0.5-1 mg/L and 100 - 125 mg/L respectively. The common form of Fe in water is $Fe(OH)_2$ in the acidic or neutral condition. The solubility of iron carbonate, iron sulfide and iron vitriol in water are 60 mg/L, 6 mg/L and 295 g/L respectively. The water solubility of some iron compounds increases at lower pH. The reaction of Fe under aerobic condition can be presented as:

$$4Fe + 3O_2 + 6H_2O \longrightarrow 4Fe^{3+} + 12OH^- \longrightarrow 4Fe(OH)_3\ or\ 4FeO(OH) + 4H_2O \quad (2.2)$$

### 2.4.4 Lead

Lead (Pb) is a soft and highly malleable metal with atomic weight of 207.2 g/mole and density of 11.34 g/cm$^3$. The concentration of Pb in seawater and rivers are 2-30 g/L and 3-30 µg/L respectively. Lead is not soluble in water in normal condition while its reactivity increases in contact with moist air. A thin layer of lead oxide (PbO) is formed on the metal surface under oxidized condition. In presence of oxygen and water, the following reaction is occurred.

$$2Pb\ (s) + O_2\ (g) + 2H_2O \longrightarrow Pb(OH)_2\ (s) \tag{2.3}$$

Lead may bond to carbonate and form $\boldsymbol{PbCO_3\ or\ Pb(CO_3)_2^{2-}}$. Lead compounds are generally soluble in soft, slightly acidic water. Inside the pipes, a layer of hardly soluble alkaline lead carbonate is formed. This layer functions as a protective coating for the underlying lead of pipes.

### 2.4.5 Zinc

Zinc (Zn) is a lustrous bluish-white metal with atomic weight of 65.37 g/mole and density of 7.11 g/cm$^3$. The most significant zinc ores include sphalerite (ZnS) and smithsonite ($ZnCO_3$). It is a reactive metal and it combines with oxygen and other non-metals. Zn is naturally present in water. The concentration of Zn in seawater and rivers are in the ranges of 0.6-5 µg/L and 5-10 µg/L respectively. Elementary zinc does not react with water while the ion forms a protective layer as follows:

$$Zn^{2+} + 2OH^- \longrightarrow Zn(OH)_2\ (s) \tag{2.4}$$

The higher concentrations of Zn salts cause milky turbidity in water and imparts an unwanted taste to water. The solubility of Zn in water varies with temperature and pH. The solubility increases with increasing acidity and remains insoluble under neutral pH. The solubility of $ZnCO_3$ and $ZnSO_4.7H_2O$ in water are 0.21 g/L and 580 g/L respectively.

### 2.4.6 Strontium

Strontium (Sr) is a soft metal with atomic weight of 87.62 g/mole and density of 2.6 g/cm$^3$. The most significant strontium mineral is celestite ($SrSO_4$) and strontianite ($SrCO3$). It has high reactivity with water and present in $Sr^{2+}$ or $SrOH^+$ form. The concentration of Sr in seawater and rivers are approximately 8 mg/L and 50 µg/L respectively. The Sr is dissolved in water as follows:

$$Sr\ (s) + 2H_2O \longrightarrow Sr(OH)_2(aq) + H_2\ (g) \qquad (2.5)$$

### 2.4.7 Arsenic

Arsenic (As) has atomic weight of 74.9216 g/mole and density of 5.7 g/cm$^3$. Arsenic in water mainly present as: $HAsO_4^{2-}$, $H_2AsO_4^-$, $H_3AsO_4$, $AsO_4^{3-}$ or $H_2AsO_3^-$ forms. The major species of arsenic in natural waters are As(III) and As(V). The concentration of As in seawater and rivers are in the ranges of 2-4 µg/L and 0.5-2 µg/L respectively. In water, arsenic exists in the forms of particulate (>0.45 µm), colloidal (3000 Da - 0.45 µm) and dissolved states (<3000 Da). With the increase of dissolved organic matter in groundwater, As in dissolved and colloidal states increase significantly. The molecular distributions of humic acid and Fe to Carbon (C) ratios influence the colloidal fraction of As. The particulate form of As varies with pH and the maximum particulate fraction was reported at pH of 4 [74]. The following reactions are common for arsenic in natural water:

$$H_3AsO_4 + 2H^+ + 2e^- \leftrightarrow H_3AsO_3 + H_2O \quad (2.6)$$

### 2.4.8 Nickel

Nickel (Ni) has the atomic weight of 58.71 g/mole and density of 8.9 g/cm$^3$. The concentration of Ni in seawater and rivers are in the ranges of 0.5-2 µg/L and 0.3 µg/L respectively. The common form of Ni in water are $Ni^{2+}$ or $NiCO_3$, and may be either dissolved, or complexed with inorganic ligands. It may also be bound to particles. Ni is not reactive to water under normal conditions, but its compounds may be water-soluble.

### 2.4.9 Mercury

Mercury (Hg) is a silvery-white liquid metal with atomic weight of 200.59 g/mole and density of 13.6 g/cm$^{3.}$ It remains liquid at ordinary temperatures. The commonly occurring Hg salts are $HgCl_2, Hg_2Cl_2$ or $HgS$.

### 2.4.10 Copper

Copper (Cu) is a reddish metal with atomic weight of 63.546 g/mole and density of 8.9 g/cm$^3$. Cu is stable in its metallic state and forms monovalent (cuprous) and divalent (cupric) cations. Dissolved Cu may cause unpleasant metallic, bitter taste to drinking water. The dissolved Cu in tap water can form the blue to green staining on porcelain sinks and plumbing fixtures.

The reactivity of Cu with water is complex and influenced by pH, dissolved oxygen and the presence of oxidizing agents and chelating compounds or ions [75]. Surface oxidation of copper produces copper (I) oxide or hydroxide. The common copper compounds include: Copper(II) acetate monohydrate [$Cu(C_2H_3O_2)_2 \cdot H_2O$], Copper(II) chloride

[$CuCl_2$], Copper(II) nitrate trihydrate [$Cu(NO_3)_2 \cdot 3H_2O$], Copper(II) oxide [$CuO$] and Copper(II) sulfate pentahydrate [$CuSO_4 \cdot 5H_2O$]. In most instances, copper (I) ion is oxidized to copper (II) ion. Copper (II) ion is the major species in water for pH up to 6. At pH of 6 – 9.3, aqueous $CuCO_3$ is prevalent while at pH of 9.3–10.7, the aqueous $[Cu(CO_3)_2]^{2-}$ ion predominates.

### 2.4.11 Manganese

Manganese is a chemically active metal with atomic weight of 54.9380 g/mole and density of 7.43 g/cm$^3$. It is one of the most abundant metals in Earth's crust, usually occurring with Fe. It has high reactivity with water and dissolves in dilute acids. It may cause staining of plumbing fixtures, clothing, or has an off-taste or odor.

## 2.5 Health Effects of Heavy Metals and Regulatory Limits

The populations are likely to be exposed to higher concentrations of heavy metals from tap water. Some heavy metals, including Cd, As, Pb, Cr, Hg, Ni and Cu in drinking water can pose risks to human health [76,77]. Table 2.1 summarizes the effects of some of this heave metals in drinking water.

Some of these effects were mental disorder [78], brain damage, central nervous system failure , damage of DNA structure [79], skin infections [80], blood composition disorder, failure of lungs, heart, liver, kidneys and other major organs [80,81]. Chronic exposure to few heavy metals can induce cancer, hypertension, ischemic heart disease and allergies [82,83].

Table 2.1: Possible human health effects from priority metals in drinking water [84]

| Metal Type | Possible human health effects |
|---|---|
| Arsenic | Problems with circulatory systems, vascular and neurological effects, skin damage, heart disease, embryotoxicity, developmental disabilities, hyperpigmentation, cancer of lung, bladder, liver and skin. |
| Mercury | Kidney and liver damage, Irreversible neurological symptoms, developmental disabilities, minamata disease |
| Lead | Neurobehavioural effects of children, slight deficits in attention span and learning abilities for children, high blood pressure, kidney problems, anaemia, probably carcinogenic to humans, embryotoxicity, neoplasia, bone marrow suppression, seizures etc. |
| Copper | Liver or kidney damage, gastrointestinal distress |
| Chromium | Irritation of the skin, allergic dermatitis, asthma, cholestasis of liver, neoplasia, respiratory and gastrointestinal tracts problem by Cr (VI) |
| Cadmium | Damage of kidney, neonatal death, pulmonary edema, developmental disabilities, neoplasia, and softening of bone |
| Beryllium | Intestinal lesions, granuloma in lungs and respiratory tracts |
| Barium | Blood pressure increase, cardiovascular disease |
| Nickel | Nausea, vomiting, diarrhea, giddiness, lassitude, headache, shortness of breath, gastrointestinal effects, allergic contact dermatitis, asthma, neoplasia, kidney problem |
| Manganese | Pneumonia, neurotoxicity, bronchitis, cirrhosis of liver, influenza, schizophrenia, dullness, weak muscles, headaches and insomnia. |
| Zinc | Pulmonary edema, corneal ulceration, esophagus damage, nausea, vomiting, dizziness, colics, fevers and diarrhea |
| Iron | Excessive dosage my cause damage of pancreas, liver, spleen and heart of haemochromatose patients |
| Strontium | Accumulates in hypophysis and ovaries, disrupts infant hormonal development and infant growth. increase infant mortality, Problems in cell division |

The possible health concerns of these heavy metals have forced many organizations to establish guidelines and/or limitations on metals concentrations in drinking water (e.g. maximum contaminant levels). Few organizations, including the European Union (EU), Health Canada (HC), World Health Organization (WHO) and the United States Environmental Protection Agency (USEPA) have established the regulatory limits on heavy metal concentrations in drinking water. Table 2.2 summarizes the guideline values of different metals that are currently endorsed by different organizations.

Table 2.2: Regulatory limits on metals in drinking water (µg/L)

| Metal Type | USEPA 2017 [85] | HC 2017 [86] | WHO 2011 [87] | NZ 2005 [88] | AUS 2011 [89] | UK 2015 [90] |
|---|---|---|---|---|---|---|
| As | 10 | 10 | 10 | 10 | 10 | 10 |
| Hg | 2 | 1 | 6 (Inorganic) | 7 (Inorganic) | 1 | 1 |
| Pb | 15 | 10 | 10 | 10 | 10 | 10 |
| Cu | 1300 | ≤ 1000 | 2000 | 2000 | 2000 | 2000 |
| Cr | 100 | 50 | 50 | 50 | 50 | 50 |
| Cd | 5 | 5 | 3 | 4 | 2 | 5 |
| Be | 4 | - | - | | 60 | - |
| Ba | 2000 | 1000 | 1300 | 700 | 700 | - |
| Fe | 300 | ≤ 300 | 100 | 200 | 300 | 200 |
| Mn | 50 | ≤ 50 | 0 | 40 | 500 | 50000 |
| Zn | 5000 | ≤ 5000 | 5000 | 1500 | 3000 | - |
| Na | - | ≤ 200000 | 50000 | 200000 | 180000 | 20000 |
| Ni | - | - | 70 | 80 | 20 | 20 |
| Mo | - | - | - | 70 | 50 | - |

USEPA: United States Environmental Protection Agency; UK: United Kingdom; AUS: Australia; NZ: New Zealand; HC: Health Canada; WHO: World Health Organization

# CHAPTER 3

# METHODOLOGY

## 3.1 Sample Collection

Water leaves the WDS to flow through plumbing pipe (PP) and hot water tank (HWT) prior to reaching the consumer tap. In this study, water samples were collected from WDS, PP and HWT at different times of the day. A typical water supply system is illustrated in Figure 3.1, where the water passes the WDS and subsequently flows through PP and HWT to reach consumer tap. The water samples were collected in duplicates from a housing complex in King Fahd University of Petroleum and Minerals (KFUPM), Dhahran, Saudi Arabia.

The samples were collected on bi-weekly basis during November 2015 to June 2016. A total of seven samples were collected in each sampling cycle (Figure 3.2). The seven samples in a day represented the diurnal variability of heavy metals in WDS, PP and HWT. The first sample (S1) was collected at the late evening after 10 minutes of free flush in tap water to represent the WDS. The second sample (S2) was the first flush of water collected in the early morning of the next day from the same tap. The second sample represented the effects of overnight (e.g., 8 - 12 hours) stagnation of water in PP. During this period, there was no use of water from the tap. The third sample (S3) was collected in the morning from hot water tap to represent the HWT samples. The fourth sample (S4) was collected after 10 minutes of free flow of cold water through the tap, which represented the water from WDS.

The fifth and sixth samples (S5 and S6) were collected from the taps of cold and hot water respectively, in the afternoon following normal usages during the day. These samples represented the PP and HWT respectively. The seventh sample (S7) was collected at afternoon after 10 minutes of free flow through the tap to represent the sample from WDS. Each sample was collected in 100 mL glass bottle for metal analysis and and the samples for other parameters (e.g., pH, temperature, $UV_{254}$, DOC etc.) were collected in 125 mL plastic bottles. The samples were transported to the laboratory in a cooler (< 4 ºC). Figure 3.2 summarizes the overall sampling and analysis programs.

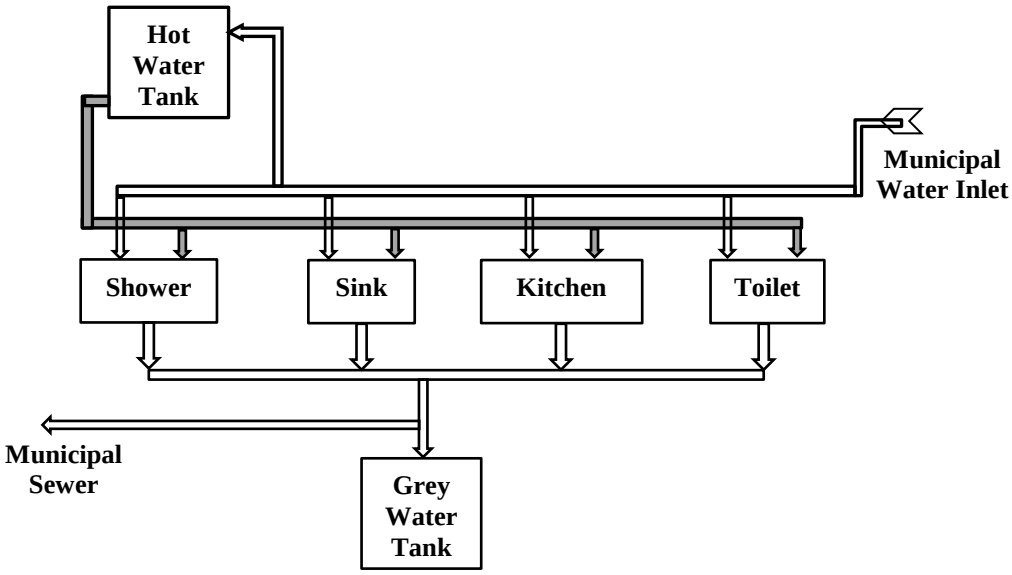


Figure 3.1: Typical plumbing system of a house with water intake points

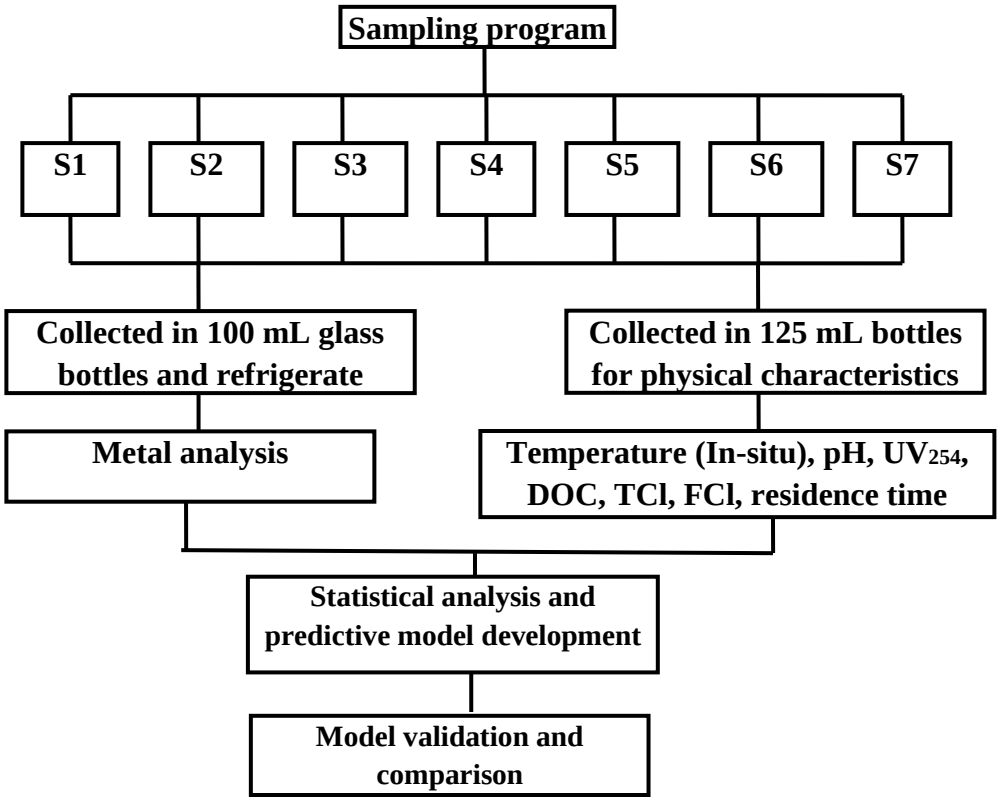


Figure 3.2: Sampling program for data collection and methodology

## 3.2 Laboratory Analysis

Concentrations of heavy metals and relevant water quality parameters for each sample were analyzed in the laboratory. The water samples were collected and analyzed following standard methods [91]. The total chlorine (TCl), free residual chlorine (FCl), UV absorbance at 254 nm ($UV_{254}$), dissolved organic carbon (DOC), temperature, pH, turbidity and residence time were measured for each sample. Temperature and pH were measured *in-situ*. The total chlorine (TCl) and free residual chlorine (FCl) were measured by HACH spectrophotometer (HACH DR 3900 model) following HACH methods 8021 and 8167

respectively. DOC was measured using a Shimadzu TOC analyzer (Model: TOC-L-CSN) according to standard method 5310B developed by American Public Health Association [92]. The $UV_{254}$ was measured using a spectrophotometer (Genesys 10 UV VIS model) at 254 nm wavelength with a 10-mm optical path quartz cell. Before measuring DOC and $UV_{254}$, samples were filtered through 0.45 µm membrane filters. The heavy metals were measured with Inductively Coupled Plasma - Mass Spectrometry (ICP-MS) (Thermo electron corporations, Model: ICP-MS XSERIES-II) followed by USEPA method-200.8 and the data were processed by PlasmaLab windows platform software [93].

## 3.3 Statistical Analysis

The experimental data for the WDS, PP and HWT were analyzed using the JMP™ and Minitab™ statistical software [94,95]. The data summary were generated. These data were analyzed for trends, diurnal and seasonal variability, outliers and correlation structure. The data varaibility and statistical distributions were investigated. The coefficient of variation (CV) was calculated to determine the dispersion of data as:

$$CV = \frac{Standard\ Deviation}{Mean} \tag{3.1}$$

Box plots were generated to identify the outliers of dataset. The bottom and top of the boxes represent the first quartile (Q1) and the third quartile (Q3) respectively. The lower whisker extends up to [Q1 – 1.5*(Q3–Q1)] and upper whisker extends up to [Q3+1.5*(Q3–Q1)]. The horizontal lines within the box represent the medians of the data. The value

larger than Q3 or smaller than Q1 by at least 1.5 times the interquartile range (IQR) are considered as the outliers. All the data were compared for the WDS, PP and HWT.

## 3.4 Model Development

The predictions of heavy metals in the PP and HWT were performed through training the linear, nonlinear and neural network models. The models were validated using an additional set of experimental data, which were not used in model development. The statistical packages: JMP™ and Minitab™ were used to perform the data analysis and model development works.

### 3.4.1 Linear Models

Among different linear models, the linear main factors (LMF), linear main factors with interactions and higher orders (LMFI), and linear logarithmic (LL) models were investigated. The simplest form of multiple linear models are the LMF models, where the predictor variables and model coefficients are linear. The significant main factors are only considered in this model [96]. The matrix plot of the dataset and the Pearson correlation ($r$) of WQP and metal concentrations were used as basis for initial selection of significant factors. The final section of signification factors was performed through effect analysis using the JMP™ statistical package.

The generic form of linear models with main factors is shown in Equation 3.2. In the LMFI models, the significant main factors, interactions of two factors and higher order relationships (e.g., cubic, quadratic and) are incorporated. Equation 3.3 represents the generic form of LMFI models. In case of LL models, the dataset obtained for different

factors are converted into logarithmic form and the linear regression is performed for transformed data. The logarithmic from of factors and parameters are linear. The generic form of LL models is presented by Equation 3.4.

$$y = \beta_0 + \sum_{i=1}^{n} \beta_i x_i + ..... + \varepsilon \tag{3.2}$$

$$y = \beta_0 + \sum_{i=1}^{n} \beta_i x_i + \sum_{i,j=1}^{n} \beta_{i,i+j} x_i x_{i+j} + \sum_{i=1}^{n} \beta_{ii} x_i^2 + ..... + \varepsilon \tag{3.3}$$

$$\ln(y) = \beta_0 + \sum_{i=1}^{n} \beta_i [\ln(x_i)] + ..... + \varepsilon \tag{3.4}$$

Where,

y = model output; $\beta_0$ = model intercept; β = model parameters; ε = residuals and *x* = predictor variables; i, j = 1, 2, 3……n.

### 3.4.2 Nonlinear Models

The nonlinear models (NL) are complex than the linear models. In these models, the parameters are nonlinear. Two parameters and one predictor variable generate the simplest form of nonlinear model. The construction of nonlinear models follows the procedure of defining the preliminary model based on the correlation structure in the matrix plot and the Pearson correlation (*r*) of WQP and metal concentrations. By using the JMP™ "Nonlinear models" library, the initial models were tested with the data [94]. The parameters for nonlinear models were defined by attaining convergence using the Analytic Gauss Newton method [94]. Upon the convergence, the corresponding RMSE were observed. The plot of predicted versus experimental data and their corresponding $R^2$ values were used to confirm

the model adequacy. Seven types of nonlinear models were tested in this study. The forms of different non-linear models are shown in Equations 3.5-3.11.

Logistic model (3 parameters):

$$y = \frac{\theta_1}{(1 + \theta_2 Exp(\theta_3 x))} \tag{3.5}$$

Logistic model (4 parameters):

$$y = \theta_1 + \frac{(\theta_2 - \theta_1)}{(1 + Exp\{\theta_3[x - \theta_4]\})} \tag{3.6}$$

Weibull model (4 parameters):

$$y = \theta_1 - \theta_2 Exp(-Exp[\theta_3 + \theta_4 Ln\{Zn - WDS\}]) \tag{3.7}$$

Biexponential model (4 parameters):

$$y = \theta_1 Exp(-\theta_2 x) + \theta_3 Exp(-\theta_4 x) \tag{3.8}$$

Quartic model:

$$y = \theta_1 + \theta_2 x + \theta_3 (x)^2 + \theta_4 (x)^3 + \theta_5 (x)^4 \tag{3.9}$$

Quintic model:

$$y = \theta_1 + \theta_2 x + \theta_3 (x)^2 + \theta_4 (x)^3 + \theta_5 (x)^4 + \theta_6 (x)^5 \tag{3.10}$$

Cubic model:

$$y = \theta_1 + \theta_2 x + \theta_3 (x)^2 + \theta_4 (x)^3 \tag{3.11}$$

Where,

y = model output

x = predictor variables and

$\theta_1$ to $\theta_6$ = model parameters

### 3.4.3 Neural Network Models

A neural network (NN) is a series of algorithms that attempts to identify the underlying relationships in a set of data by using a process analogous to the vast network of neurons in a brain. The NN structure consists of an input layer, an output layer and one/several hidden layers (Figure 3.3). The neuron or nodes are the basic elements of the layers. The hidden nodes explain the hyperbolic tangent function of input variables (i.e., WQP and metal concentrations). Each node in a layer is connected to the node of next layer, but not within the same layer [97]. The dataset for WQP defines the number of nodes in each layer. Equations 3.12 and 3.13 represent the generic forms of a three-hidden-node NN model.

$$y = \lambda_0 + \sum_{\gamma=1}^{3} \lambda_\gamma H_\gamma \tag{3.12}$$

$$H_y = \tan H\left[0.5*(\alpha_0 + \alpha_1 x_i\right] \tag{3.13}$$

Where,

$H_\gamma = \gamma^{th}$ hidden node

$\lambda$ = coefficients for the NN model.

$\alpha_0$ = intercept of predictor variables

$\alpha_i$ = coefficients of predictor variables associated with each hidden node.

The hidden node ($H_\gamma$) is a hyperbolic tangent function, which is a sigmoid function. The output ranges from -1 to 1 and is the centered and scaled version of logistic function. For each node of this model, the hidden node ($H_\gamma$) is estimated as the hyperbolic tangent function of linear combinations of the predictor variables.

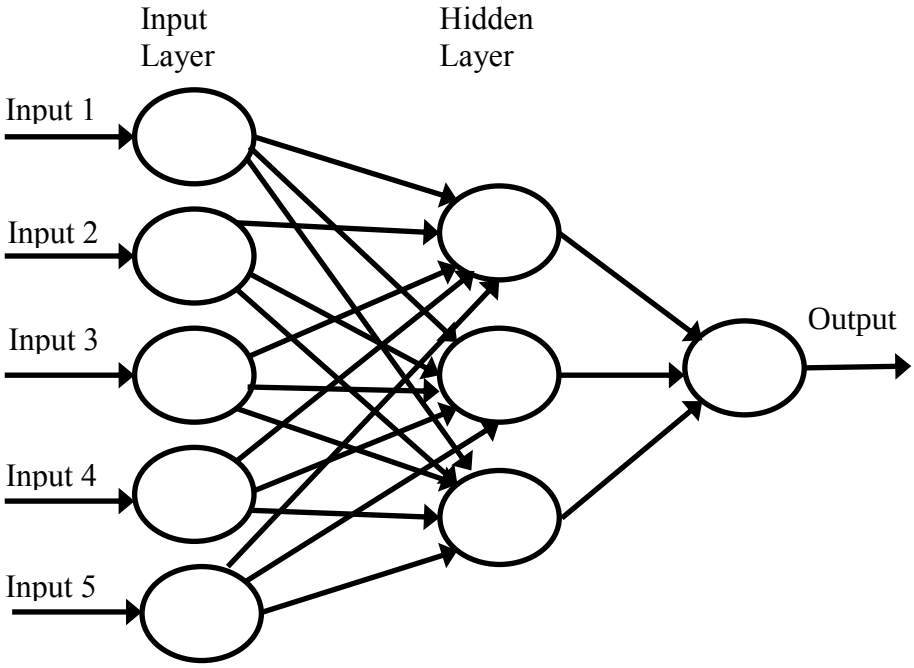


Figure 3.3: Structure of a typical neural network diagram

# CHAPTER 4

# OCCURANCES AND VARIABILITY OF METAL

## 4.1 Data

The water quality parameters in WDS, PP and HWT for seven sampling scenarios are summarized in Table 4.1. The average temperature in WDS, PP and HWT were 27.2 °C, 26.7 °C and 60.4 °C respectively and the corresponding ranges were 23-33 °C, 22.5-32 °C and 58-62 °C respectively. The averages of FCl in WDS, PP and HWT were 0.04, 0.055 and 0.045 mg/L respectively and the ranges were 0.01-0.21, 0.02-0.33 and 0.01-0.17 mg/L respectively. The averages of pH in WDS, PP and HWT were 6.93, 6.83 and 6.77 respectively with the ranges of 6.37-8.2, 6.17-7.4 and 6.26-8.04 respectively. The average of pH were below the neutral value, indicating possible corrosive nature of water. The $UV_{254}$ in WDS, PP and HWT were in the ranges of 0-0.005 $cm^{-1}$, 0-0.009 $cm^{-1}$ and 0-0.009 $cm^{-1}$ respectively with the averages of 0.001 $cm^{-1}$, 0.0025 $cm^{-1}$ and 0.002 $cm^{-1}$ respectively. The averages of DOC in WDS, PP and HWT were 0.65 mg/L, 0.73 mg/L and 0.84 mg/L respectively with the wide ranges of 0.11-10.24 mg/L, 0.24-3.98 mg/L and 0.30-4.48 mg/L respectively. Further details will be explored in the following sections.

Table 4.1: Water quality parameters at different sampling points

| Samples | | Temp (°C) | FCl (mg/L) | TCl (mg/L) | pH | $UV_{254}$ (/cm) | DOC (mg/L) |
|---|---|---|---|---|---|---|---|
| | Mean | 27.04 | 0.04 | 0.03 | 7.06 | 0.002 | 1.13 |
| | Std. Dev | 3.04 | 0.04 | 0.03 | 0.44 | 0.002 | 2.75 |
| S1 | Min | 24.00 | 0.02 | 0.02 | 6.60 | 0.000 | 0.11 |
| | Max | 33.00 | 0.12 | 0.11 | 8.20 | 0.007 | 10.24 |
| | CV | 0.11 | 0.91 | 0.83 | 0.06 | 0.964 | 2.43 |
| | Mean | 25.91 | 0.06 | 0.05 | 6.81 | 0.003 | 0.81 |
| | Std. Dev | 1.81 | 0.09 | 0.08 | 0.38 | 0.002 | 1.00 |
| S2 | Min | 23.00 | 0.02 | 0.02 | 6.17 | 0.000 | 0.24 |
| | Max | 29.00 | 0.33 | 0.29 | 7.40 | 0.009 | 3.98 |
| | CV | 0.07 | 1.52 | 1.50 | 0.06 | 0.847 | 1.25 |
| | Mean | 60.77 | 0.04 | 0.05 | 6.75 | 0.002 | 0.99 |
| | Std. Dev | 1.11 | 0.04 | 0.07 | 0.47 | 0.001 | 1.29 |
| S3 | Min | 58.00 | 0.01 | 0.02 | 6.26 | 0.000 | 0.32 |
| | Max | 62.00 | 0.17 | 0.26 | 8.04 | 0.005 | 4.48 |
| | CV | 0.02 | 1.16 | 1.37 | 0.07 | 0.652 | 1.30 |
| | Mean | 27.23 | 0.04 | 0.05 | 6.93 | 0.001 | 0.40 |
| | Std. Dev | 2.82 | 0.04 | 0.10 | 0.29 | 0.002 | 0.21 |
| S4 | Min | 24.00 | 0.01 | 0.01 | 6.53 | 0.000 | 0.16 |
| | Max | 32.00 | 0.15 | 0.37 | 7.67 | 0.005 | 0.83 |
| | CV | 0.10 | 1.06 | 1.85 | 0.04 | 1.303 | 0.53 |
| | Mean | 27.50 | 0.05 | 0.03 | 6.84 | 0.002 | 0.64 |
| | Std. Dev | 2.92 | 0.07 | 0.02 | 0.43 | 0.002 | 0.33 |
| S5 | Min | 22.50 | 0.02 | 0.02 | 6.33 | 0.000 | 0.31 |
| | Max | 32.00 | 0.22 | 0.10 | 7.87 | 0.005 | 1.27 |
| | CV | 0.11 | 1.26 | 0.77 | 0.06 | 0.983 | 0.51 |
| | Mean | 60.05 | 0.05 | 0.07 | 6.79 | 0.002 | 0.69 |
| | Std. Dev | 1.09 | 0.03 | 0.07 | 0.47 | 0.003 | 0.43 |
| S6 | Min | 58.00 | 0.01 | 0.01 | 6.31 | 0.000 | 0.30 |
| | Max | 61.00 | 0.09 | 0.25 | 8.02 | 0.009 | 1.90 |
| | CV | 0.02 | 0.58 | 0.96 | 0.07 | 1.188 | 0.62 |
| | Mean | 27.41 | 0.04 | 0.04 | 6.79 | 0.001 | 0.41 |
| | Std. Dev | 3.33 | 0.05 | 0.06 | 0.29 | 0.001 | 0.18 |
| S7 | Min | 23.00 | 0.02 | 0.02 | 6.37 | 0.000 | 0.24 |
| | Max | 33.00 | 0.21 | 0.24 | 7.19 | 0.004 | 0.87 |
| | CV | 0.12 | 1.45 | 1.65 | 0.04 | 0.957 | 0.45 |

Std. Dev: Standard deviation; Min: Minimum; Max: Maximum; CV: Coefficient of variation; TCl: Total chlorine; FCl: Free residual chlorine; $UV_{254}$: UV absorbance at 254 nm; DOC: Dissolved organic carbon

The concentrations of metal at different sampling points are summarized in Table 4.2. There was significant variability in metal concentrations at different scenarios and several metals showed wide ranges (e.g., high coefficient of variation [CV]). Few metals had higher concentrations and higher variability in HWT than the WDS and PP. Concentrations of Ca and Mg in HWT were higher and showed higher variability (e.g., higher CV) in

comparison to the samples from the WDS and PP. The average concentrations of Cr in S6 and S1 were 0.79 and 0.60 µg/L with the ranges of 0.19-1.34 and 0.23-0.98 µg/L respectively. Concentrations of Fe, Zn, Br, Sr, Ba and Co were also higher in HWT than WDS. Concentrations of Cu, As, Hg and Ni were higher in PP (S2 and S5) than the WDS (S1, S4 and S7), due possibly to overnight stagnation of water in plumbing premise. In the PP, average concentrations of Cu, Hg and Ni were 4.3, 2.6 and 28.9 µg/L respectively while in the WDS, the averages were 0.4, 0.8 and 1.6 µg/L respectively. In PP, the ranges of Cu, Hg and Ni were 0.02-38.28, 0.08-25.40 and 0.12-113.7 µg/L respectively while in WDS, the ranges were 0.04-4.76, 0.05-14.87 and 0.15-59.22 µg/L respectively.

Table 4.2: Metal concentrations at different sampling points (in µg/L)

| Samples | | Na | Mg | Ca | V | Cr | Mn | Fe | Cu | Zn | As | Sr | Mo | Ba | Hg | Pb | Ni | Co |
|---|---|---|---|---|---|---|---|---|---|---|---|---|---|---|---|---|---|---|
| | Mean | 186229 | 5487 | 9570 | 4.58 | 0.60 | 1.04 | 60.89 | 0.43 | 6.72 | 1.09 | 324.9 | 2.36 | 74 | 2.00 | 3.95 | 1.79 | 0.19 |
| | Std. Dev | 291009 | 10464 | 17290 | 7.38 | 0.22 | 1.22 | 28.83 | 0.69 | 12.22 | 1.48 | 623.3 | 3.94 | 987 | 4.03 | 3.23 | 2.05 | 0.07 |
| S1 | Min | 248 | 21.51 | 38.65 | 0.03 | 0.23 | 0.02 | 8.01 | 0.04 | 0.07 | 0.09 | 1.7 | 0.01 | 1.52 | 0.09 | 0.29 | 0.18 | 0.04 |
| | Max | 788040 | 27219 | 45100 | 21.05 | 0.98 | 3.45 | 99.70 | 2.67 | 45.32 | 4.16 | 1649 | 13.16 | 3394 | 14.87 | 8.90 | 5.40 | 0.27 |
| | CV | 1.56 | 1.91 | 1.81 | 1.61 | 0.36 | 1.17 | 0.47 | 1.62 | 1.82 | 1.35 | 1.9 | 1.67 | 1.33 | 2.01 | 0.82 | 1.15 | 0.39 |
| | Mean | 109405 | 2764 | 5886 | 5.05 | 0.57 | 2.70 | 51.23 | 4.30 | 398 | 0.88 | 170.9 | 34.94 | 1241 | 2.64 | 4.08 | 28.89 | 1.09 |
| | Std. Dev | 202231 | 7029 | 11823 | 7.90 | 0.23 | 5.06 | 29.40 | 10.9 | 931 | 1.14 | 432.2 | 72.14 | 2200 | 6.89 | 3.34 | 46.74 | 1.38 |
| S2 | Min | 266 | 31.68 | 60.11 | 0.03 | 0.18 | 0.03 | 3.83 | 0.04 | 0.72 | 0.06 | 2.5 | 0.01 | 1.17 | 0.08 | 0.13 | 0.12 | 0.06 |
| | Max | 747648 | 24921 | 40506 | 21.64 | 0.92 | 18.6 | 93.14 | 38.3 | 3032 | 3.88 | 1564 | 209.8 | 7525 | 25.40 | 10.57 | 113.7 | 3.89 |
| | CV | 1.85 | 2.54 | 2.01 | 1.56 | 0.40 | 1.87 | 0.57 | 2.53 | 2.34 | 1.29 | 2.5 | 2.06 | 1.77 | 2.61 | 0.82 | 1.62 | 1.26 |
| | Mean | 257644 | 13910 | 32144 | 5.62 | 0.68 | 1.06 | 68.51 | 0.79 | 201 | 1.69 | 723.4 | 1.78 | 2772 | 1.70 | 3.67 | 14.23 | 0.31 |
| | Std. Dev | 331341 | 19473 | 57468 | 7.56 | 0.33 | 1.37 | 23.86 | 1.14 | 642 | 1.62 | 949.9 | 2.38 | 4379 | 2.31 | 3.61 | 29.73 | 0.35 |
| S3 | Min | 4000 | 143 | 493 | 0.04 | 0.12 | 0.03 | 36.24 | 0.01 | 0.22 | 0.22 | 8.2 | 0.01 | 1.42 | 0.12 | 0.16 | 0.12 | 0.01 |
| | Max | 994600 | 67050 | 213600 | 23.98 | 1.29 | 4.23 | 114.1 | 3.73 | 2334 | 4.91 | 3023 | 8.97 | 15010 | 7.48 | 9.21 | 87.55 | 0.85 |
| | CV | 1.29 | 1.40 | 1.79 | 1.35 | 0.48 | 1.29 | 0.35 | 1.44 | 3.19 | 0.96 | 1.3 | 1.34 | 1.58 | 1.36 | 0.98 | 2.09 | 1.12 |
| | Mean | 126848 | 3403 | 6982 | 5.20 | 0.63 | 0.69 | 54.45 | 0.92 | 9.47 | 0.86 | 193 | 35.90 | 1248 | 0.81 | 3.60 | 1.58 | 0.45 |
| | Std. Dev | 174413 | 6217 | 11957 | 7.21 | 0.23 | 0.88 | 22.19 | 1.31 | 15.87 | 0.96 | 351.6 | 83.60 | 2369 | 0.92 | 3.15 | 1.81 | 0.66 |
| S4 | Min | 2863 | 41 | 120.2 | 0.04 | 0.33 | 0.02 | 14.81 | 0.05 | 0.57 | 0.08 | 3.7 | 0.02 | 0.76 | 0.05 | 0.18 | 0.16 | 0.01 |
| | Max | 521444 | 16824 | 30545 | 19.61 | 1.03 | 2.78 | 93.57 | 4.76 | 55.99 | 3.09 | 991.8 | 239.8 | 7960 | 3.10 | 9.02 | 4.51 | 1.99 |
| | CV | 1.37 | 1.83 | 1.71 | 1.39 | 0.36 | 1.28 | 0.41 | 1.42 | 1.68 | 1.11 | 1.8 | 2.33 | 1.90 | 1.14 | 0.87 | 1.15 | 1.45 |
| | Mean | 90651 | 1964 | 4258 | 3.61 | 0.57 | 1.12 | 54.57 | 2.00 | 10.42 | 1.05 | 103.5 | 26.04 | 1931 | 1.50 | 4.25 | 11.11 | 0.42 |
| | Std. Dev | 126509 | 4644 | 8248 | 4.31 | 0.24 | 1.01 | 20.26 | 5.05 | 12.49 | 1.61 | 222.8 | 47.39 | 3500 | 1.77 | 3.29 | 28.93 | 0.40 |
| S5 | Min | 2479 | 44.22 | 119.6 | 0.03 | 0.22 | 0.01 | 28.22 | 0.02 | 0.48 | 0.07 | 3.5 | 0.05 | 2.96 | 0.18 | 0.17 | 0.27 | 0.02 |
| | Max | 471086 | 15915 | 26934 | 10.57 | 0.99 | 2.48 | 91.11 | 18.7 | 47.6 | 5.78 | 770.8 | 122.8 | 11160 | 4.51 | 10.90 | 82.66 | 1.00 |
| | CV | 1.40 | 2.36 | 1.94 | 1.19 | 0.42 | 0.90 | 0.37 | 2.52 | 1.20 | 1.53 | 2.2 | 1.82 | 1.81 | 1.18 | 0.78 | 2.60 | 0.97 |
| | Mean | 352681 | 18042 | 39152 | 9.97 | 0.79 | 0.85 | 75.40 | 1.16 | 3.62 | 2.39 | 969.7 | 19.12 | 3998 | 1.74 | 3.74 | 4.62 | 0.30 |
| | Std. Dev | 366156 | 17405 | 49941 | 9.63 | 0.36 | 1.16 | 25.25 | 1.28 | 4.02 | 1.84 | 842.9 | 44.58 | 6897 | 2.93 | 3.81 | 2.13 | 0.16 |
| S6 | Min | 5482 | 148.61 | 199.9 | 0.15 | 0.19 | 0.01 | 11.40 | 0.06 | 0.10 | 0.16 | 9.2 | 0.02 | 0.59 | 0.03 | 0.14 | 0.12 | 0.05 |
| | Max | 895500 | 64280 | 195300 | 24.59 | 1.34 | 3.92 | 113.3 | 3.47 | 15.14 | 4.73 | 2726 | 159.6 | 24180 | 10.62 | 10.58 | 6.60 | 0.59 |
| | CV | 1.04 | 0.96 | 1.28 | 0.97 | 0.46 | 1.37 | 0.33 | 1.10 | 1.11 | 0.77 | 0.9 | 2.33 | 1.72 | 1.68 | 1.02 | 0.46 | 0.55 |
| | Mean | 145387 | 3287 | 6195 | 5.64 | 0.63 | 1.45 | 61.63 | 1.12 | 114.2 | 0.96 | 190.8 | 33.21 | 1365 | 1.79 | 3.56 | 8.79 | 0.76 |
| | Std. Dev | 207850 | 7503 | 12326 | 7.78 | 0.22 | 1.39 | 21.38 | 1.25 | 383.7 | 1.11 | 429.5 | 81.38 | 2486 | 2.33 | 3.24 | 20.45 | 1.17 |
| S7 | Min | 3155 | 44 | 165.2 | 0.02 | 0.27 | 0.11 | 17.84 | 0.05 | 0.29 | 0.08 | 3.5 | 0.01 | 2.22 | 0.10 | 0.18 | 0.15 | 0.01 |
| | Max | 689535 | 23692 | 39462 | 22.28 | 0.99 | 3.22 | 94.19 | 4.04 | 1390 | 3.64 | 1443 | 272.5 | 8877 | 6.68 | 8.90 | 59.22 | 3.00 |
| | CV | 1.43 | 2.28 | 1.99 | 1.38 | 0.35 | 0.96 | 0.35 | 1.12 | 3.36 | 1.16 | 2.3 | 2.45 | 1.82 | 1.30 | 0.91 | 2.33 | 1.54 |

Std Dev: Standard deviation; Min: Minimum; Max: Maximum; CV: Coefficient of variation

## 4.2 Correlation and Variability of Metals

The Pearson correlation coefficients (*r*) for the metals and WQP are presented in Table 4.3. To show the patterns and linear correlations (*r*) among the factors, a matrix plot of the dataset is shown in Figure 4.1. The initial selection of important variables for model development is performed based on the matrix plot. Temperature showed positive correlations with several metals (e.g., Zn, Cu, Mo, V), indicating possible implications due to temperature variation. The $UV_{254}$ was positively correlated with Cu, Zn, As and V with *r* of 0.48, 0.41, 0.24 and 0.23 respectively while Pb and Fe were negatively correlated with $UV_{254}$ with r of -0.32 and -0.21 respectively. The FCl were positively correlated with Hg, Mn, Ba and Pb with *r* of 0.6, 0.37, 0.35 and 0.22 respectively. The TCl were positively correlated with Hg, Ba, Ca, Mn and Mg with r of 0.56, 0.42, 0.35, 0.25 and 0.22 respectively. In addition to the WQP, few metals showed moderate to strong correlations among themselves. Concentrations of Sr showed moderate to strong correlations with Na, Mg, Ca, V, Fe and As with *r* of 0.75, 0.98, 0.89, 0.56, 0.48 and 0.79 respectively. Concentrations of Pb were negatively correlated with Na, V and As with r of -0.63, -0.65 and -0.48 respectively. Further details can be found in Table 4.3.


Figure 4.1: Matrix plot of the dataset

Table 4.3: Pearson correlation (*r*) between water quality parameters

| | Temp. | FCl | TCl | pH | $UV_{254}$ | DOC | Na | Mg | Ca | V | Cr | Mn | Fe | Cu | Zn | As | Sr | Mo | Ba | Hg | Pb |
|---|---|---|---|---|---|---|---|---|---|---|---|---|---|---|---|---|---|---|---|---|---|
| Temp. | 1.00 | -0.08 | 0.03 | -0.03 | 0.18 | 0.03 | 0.11 | 0.18 | 0.18 | 0.22 | -0.06 | 0.09 | -0.04 | 0.23 | 0.37 | 0.12 | 0.18 | 0.22 | 0.10 | -0.01 | -0.10 |
| FCl | -0.08 | 1.00 | 0.70 | 0.19 | 0.03 | -0.06 | -0.17 | 0.07 | 0.16 | -0.23 | -0.21 | 0.37 | -0.15 | 0.06 | -0.05 | 0.08 | 0.04 | -0.16 | 0.35 | 0.60 | 0.22 |
| TCl | 0.03 | 0.70 | 1.00 | 0.33 | 0.03 | -0.04 | -0.13 | 0.23 | 0.35 | -0.19 | -0.23 | 0.25 | -0.13 | 0.05 | -0.05 | 0.07 | 0.18 | -0.14 | 0.42 | 0.56 | 0.17 |
| pH | -0.03 | 0.19 | 0.33 | 1.00 | -0.08 | -0.01 | 0.07 | 0.10 | 0.10 | 0.02 | -0.10 | -0.03 | -0.14 | -0.09 | -0.12 | 0.07 | 0.10 | -0.05 | -0.04 | 0.14 | -0.15 |
| $UV_{254}$ | 0.18 | 0.03 | 0.03 | -0.08 | 1.00 | 0.25 | 0.18 | 0.03 | 0.01 | 0.23 | 0.14 | 0.22 | -0.21 | 0.48 | 0.41 | 0.24 | 0.03 | 0.19 | -0.16 | 0.19 | -0.32 |
| DOC | 0.03 | -0.06 | -0.04 | -0.01 | 0.25 | 1.00 | 0.06 | -0.01 | -0.01 | 0.02 | -0.08 | 0.06 | -0.17 | -0.04 | 0.11 | 0.03 | 0.00 | -0.03 | -0.09 | -0.03 | -0.22 |
| Na | 0.11 | -0.17 | -0.13 | 0.07 | 0.18 | 0.06 | 1.00 | 0.64 | 0.39 | 0.82 | 0.41 | 0.16 | 0.39 | 0.08 | -0.03 | 0.87 | 0.75 | -0.04 | -0.29 | 0.03 | -0.63 |
| Mg | 0.18 | 0.07 | 0.23 | 0.10 | 0.03 | -0.01 | 0.64 | 1.00 | 0.95 | 0.46 | 0.16 | 0.04 | 0.44 | -0.02 | -0.11 | 0.72 | 0.98 | -0.15 | 0.44 | 0.24 | -0.22 |
| Ca | 0.18 | 0.16 | 0.35 | 0.10 | 0.01 | -0.01 | 0.39 | 0.95 | 1.00 | 0.26 | 0.00 | 0.04 | 0.32 | -0.03 | -0.08 | 0.54 | 0.89 | -0.13 | 0.61 | 0.31 | -0.09 |
| V | 0.22 | -0.23 | -0.19 | 0.02 | 0.23 | 0.02 | 0.82 | 0.46 | 0.26 | 1.00 | 0.22 | 0.23 | 0.12 | 0.11 | 0.05 | 0.66 | 0.56 | 0.53 | -0.34 | -0.06 | -0.65 |
| Cr | -0.06 | -0.21 | -0.23 | -0.10 | 0.14 | -0.08 | 0.41 | 0.16 | 0.00 | 0.22 | 1.00 | -0.29 | 0.73 | -0.07 | -0.15 | 0.32 | 0.22 | -0.20 | -0.17 | -0.21 | 0.15 |
| Mn | 0.09 | 0.37 | 0.25 | -0.03 | 0.22 | 0.06 | 0.16 | 0.04 | 0.04 | 0.23 | -0.29 | 1.00 | -0.31 | 0.23 | 0.32 | 0.24 | 0.07 | 0.18 | -0.10 | 0.62 | -0.29 |
| Fe | -0.04 | -0.15 | -0.13 | -0.14 | -0.21 | -0.17 | 0.39 | 0.44 | 0.32 | 0.12 | 0.73 | -0.31 | 1.00 | -0.11 | -0.21 | 0.35 | 0.48 | -0.42 | 0.18 | -0.26 | 0.34 |
| Cu | 0.23 | 0.06 | 0.05 | -0.09 | 0.48 | -0.04 | 0.08 | -0.02 | -0.03 | 0.11 | -0.07 | 0.23 | -0.11 | 1.00 | 0.70 | 0.22 | -0.01 | 0.09 | 0.01 | 0.02 | -0.17 |
| Zn | 0.37 | -0.05 | -0.05 | -0.12 | 0.41 | 0.11 | -0.03 | -0.11 | -0.08 | 0.05 | -0.15 | 0.32 | -0.21 | 0.70 | 1.00 | -0.04 | -0.11 | 0.16 | -0.09 | -0.03 | -0.18 |
| As | 0.12 | 0.08 | 0.07 | 0.07 | 0.24 | 0.03 | 0.87 | 0.72 | 0.54 | 0.66 | 0.32 | 0.24 | 0.35 | 0.22 | -0.04 | 1.00 | 0.79 | -0.13 | 0.06 | 0.26 | -0.48 |
| Sr | 0.18 | 0.04 | 0.18 | 0.10 | 0.03 | 0.00 | 0.75 | 0.98 | 0.89 | 0.56 | 0.22 | 0.07 | 0.48 | -0.01 | -0.11 | 0.79 | 1.00 | -0.14 | 0.32 | 0.20 | -0.29 |
| Mo | 0.22 | -0.16 | -0.14 | -0.05 | 0.19 | -0.03 | -0.04 | -0.15 | -0.13 | 0.53 | -0.20 | 0.18 | -0.42 | 0.09 | 0.16 | -0.13 | -0.14 | 1.00 | -0.19 | -0.12 | -0.27 |
| Ba | 0.10 | 0.35 | 0.42 | -0.04 | -0.16 | -0.09 | -0.29 | 0.44 | 0.61 | -0.34 | -0.17 | -0.10 | 0.18 | 0.01 | -0.09 | 0.06 | 0.32 | -0.19 | 1.00 | 0.26 | 0.52 |
| Hg | -0.01 | 0.60 | 0.56 | 0.14 | 0.19 | -0.03 | 0.03 | 0.24 | 0.31 | -0.06 | -0.21 | 0.62 | -0.26 | 0.02 | -0.03 | 0.26 | 0.20 | -0.12 | 0.26 | 1.00 | -0.08 |
| Pb | -0.10 | 0.22 | 0.17 | -0.15 | -0.32 | -0.22 | -0.63 | -0.22 | -0.09 | -0.65 | 0.15 | -0.29 | 0.34 | -0.17 | -0.18 | -0.48 | -0.29 | -0.27 | 0.52 | -0.08 | 1.00 |

TCl: Total chlorine; FCl: Free residual chlorine $UV_{254}$: UV absorbance at 254 nm; DOC: Dissolved organic carbon

## 4.3 Variability in WDS, PP and HWT

Among the metals (Table 4.2), As, Pb, Cr, Hg, Ni and Cu can pose risks to humans [77,84]. For example, inorganic arsenic (As) is a known human carcinogen while Pb can complicate the neural development among the children [98]. Cu can have gastro-intestinal effects while Hg has been reported to have risk to kidney [77]. Further details on the effects of metals in drinking water can be found in literature [99,100]. The concentration profile of Cr, Mn, Fe, Cu, Zn, As, Hg, Pb, Mg and Ni at different sampling scenarios are shown by the box plot in Figure 4.2. The data for Pb and Cr showed no outlier while the other metals had several outliers (Figure 4.2). The box plots for Fe, Ni and Zn showed 1, 3 and 4 data points, respectively, as outliers while Mg, Hg, As and Cu had higher number of outliers indicating higher levels of data variability. For an example, average concentrations of Cu in S1 - S7 were less than 2 µg/L while the maximum was 38 µg/L. The average concentration of As in S5 was less than 0.5 µg/L with the maximum of 5.8 µg/L. The wide interquartile ranges of Pb, Fe and Cr in S1-S7 indicated higher variability of data (Figure 4.2).

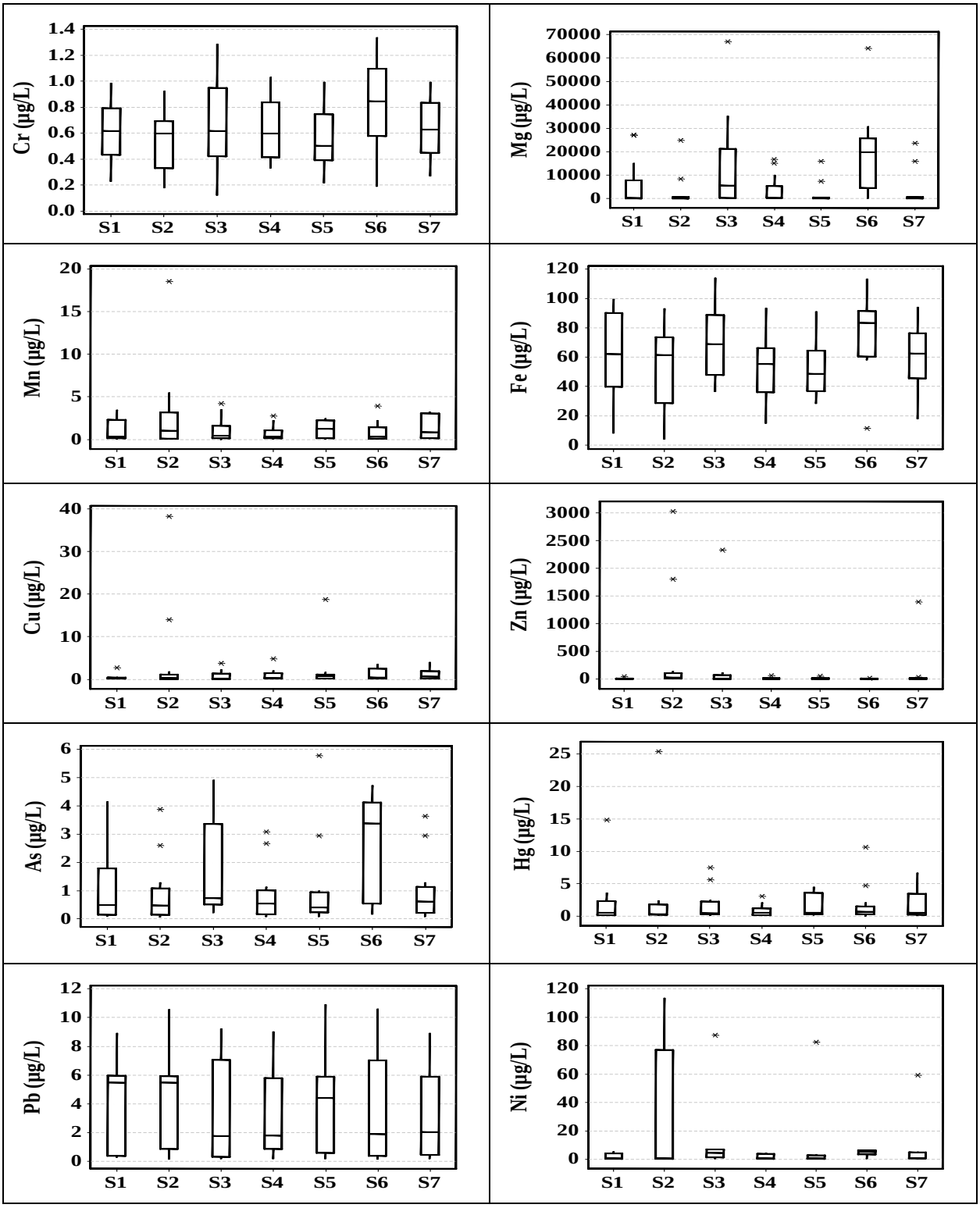


Figure 4.2: Box plot of metal variability in different sampling scenarios

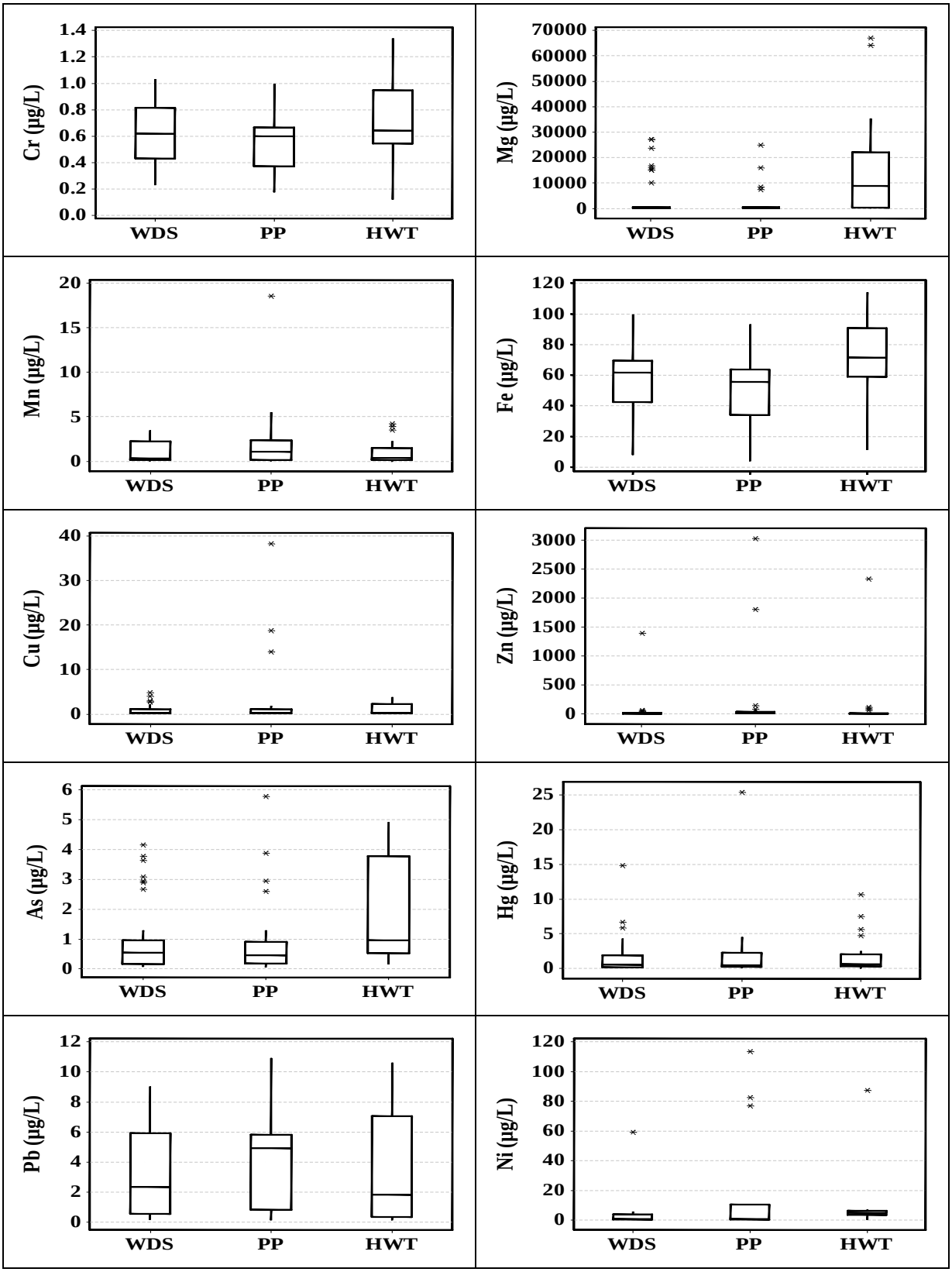


Figure 4.3: Box plot of metal variability in WDS, PP and HWT
(WDS: water distribution system; PP: plumbing pipes; HWT: hot water tanks)

In hot water tank samples (S3), the interquartile ranges of Pb and Cr were 0.2-7.0 µg/L and 0.4-0.95 µg/L respectively (Figure 4.2). Similar findings were noted for Mg and As in S3 and S6 (Figure 4.2). In contrast, the smaller interquartile ranges of Cu, Zn and Ni indicated the closeness of the data to the averages (Figure 4.2). It is to be noted that the outliers are often discarded to achieve statistical consistency and modeling works. However, the outliers are likely to be important for human exposure and risk analysis due to their extremities and possible health concerns [76].

Figure 4.3 shows the variability of metal concentrations in WDS, PP and HWT. The average concentration in WDS was calculated by taking the mean value from S1, S4 and S7. The mean of S3 and S6 represented HWT concentration while the average of PP was calculated by taking the mean of S2 and S5. Concentrations of most of the metals were higher in HWT than those in the WDS and PP. Concentrations of Fe and As in WDS were 60 and 0.5 µg/L respectively, which were increased to 72 and 1.0 µg/L, respectively, in HWT. The average concentrations and interquartile ranges of Cr, Mg, Cu, Hg and Ni were higher in HWT than those in the WDS. The sediments and precipitates along with the corroded metal were likely to be accumulated in HWT from its time of installation, which might be partially responsible for higher concentration in HWT sample [101]. In addition, the higher temperature might have accelerated the release of these metals during stagnation in HWT. The average concentrations Mn, Pb, Cu and Hg were higher in PP than those in the WDS. Average concentration of Mn in PP (1.91 µg/L) was almost two times the average concentration in WDS (1.05 µg/L). Average concentrations of Pb and Hg in WDS were 3.7 and 0.9 µg/L respectively, which were increased to 4.2 and 1.1 µg/L in PP respectively (Figure 4.3).

## 4.4 Diurnal Variability

The diurnal variability of metal concentrations for the S1-S7 sampling scenarios are presented in Figure 4.4. The S1, S4 and S7 represented the WDS samples in the evening, early morning and afternoon. The S2 and S5 represented the PP samples in early morning and afternoon respectively while S3 and S6 represented the HWT samples in early morning and afternoon respectively. The time of sampling showed variable effects on the concentrations of metals (Figure 4.4). The diurnal variability for WDS, PP and HWT samples were also tested for the equality of medians through the non-parametric tests (Kruskal-Wallis and Mann–Whitney tests) due to the non-Gaussian distributions of the data. The $\alpha$ - value was considered to be 0.05, meaning the similarity of the medians when $p > 0.05$. For $p \leq 0.05$, the medians were statistically different.

Average concentrations of Cr in the WDS samples (S1, S4 and S7) were similar (median: 0.6-0.63 µg/L; p = 0.9) indicating insignificant effects of sampling time. In the PP samples, averages of Cr were similar for S2 and S5 (median: 0.5-0.6 µg/L; p = 0.92). Averages of Cr in HWT (S3 and S6) were statistically different (median: S3 = 0.62 µg/L; S6 = 0.85 µg/L), indicating the impacts of sampling period. Average concentrations of As in S1, S4 and S7 were similar (median: 0.86-1.09 µg/L; p = 0.88). Averages of As in all PP samples (S2 and S5) were also similar (median: 0.88-1.05 µg/L; p = 0.8) while As in HWT samples S3 and S6 (median: S3 = 1.69 µg/L; S6 = 2.39 µg/L) were different, which have also indicated significant effects of sampling time on the concentrations of As. The exact mechanisms of the release of Cr and As in HWT are yet to be established.

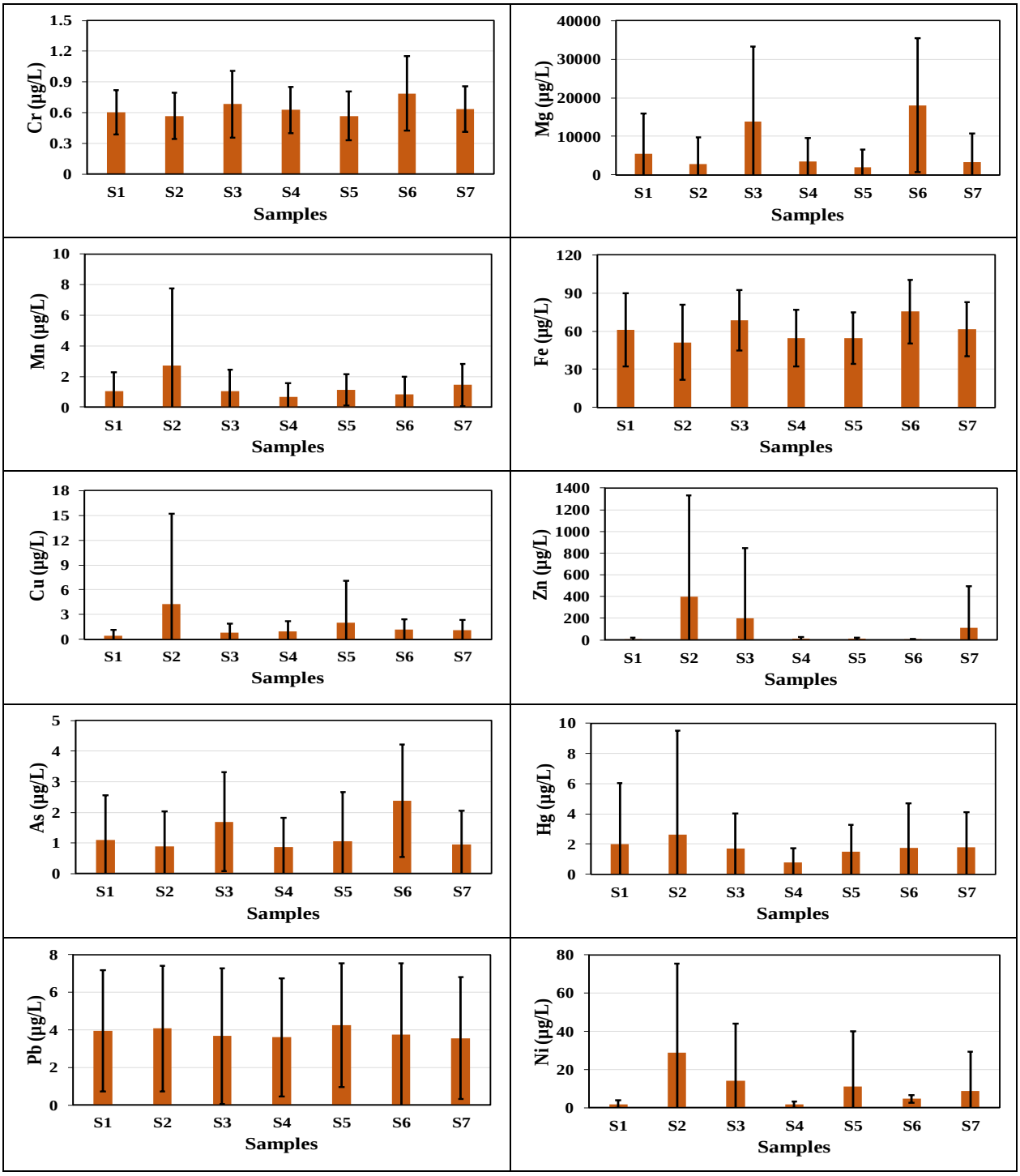


Figure 4.4: Diurnal variability of some significant metals

(S1: WDS samples after last use of water in the late evening; S2: cold water samples in the early morning prior to the first water use; S3: hot water samples in the morning; S4: WDS samples in the morning; S5: samples collected from the cold water tap in the afternoon following normal uses; S6: hot water samples in the afternoon; S7: WDS samples in the afternoon)

The Cr might have released from the Ni-Cr heater alloys and stainless steel while As could have entered from the wall of HWT due to scale formation [102]. Following the usage of hot water, the scales are being sloughed off and released into hot water [103].

Average concentrations of Pb in all WDS samples (S1, S4 and S7) were similar (median: 3.56-3.95 µg/L; p = 0.92). In the PP samples (S2 and S5), these were also similar (median: 4.08-4.25 µg/L; p = 0.96). The HWT samples (S3 and S6) also had similar concentrations (median: 3.67 - 3.74 µg/L; p = 0.92). The concentrations of Hg in S1, S4 and S7 samples showed significant variability in the average values (median: 0.81-2 µg/L) (Figure 4.4). The diurnal variation was observed for the average concentrations of Hg in all PP samples (median: S2 = 2.64 µg/L; S5 = 1.50 µg/L) while HWT samples (median: S3 = 1.7 µg/L; S6 = 1.74 µg/L; p = 0.88) showed insignificant variability.

## 4.5 Seasonal Variability

Figure 4.5 shows the seasonal variability of Cr, Mg, Mn, Cu, Fe, As, Zn, Hg and Pb in the WDS, PP and HWT samples. The concentration in WDS was calculated by taking the mean values of metals in S1, S4 and S7. The means of S3 and S6 represented the HWT concentrations while the concentration in PP was calculated by taking the averages of S2 and S5. The sampling duration (Nov 01, 2015 – May 29, 2016) was divided into three periods: P1, P2 and P3 representing Nov 01 – Dec 31, Jan 01 – Mar 31 and Apr 01 – May 31 respectively. The average temperatures of water in the WDS during P1, P2 and P3 were 26.31°C, 25.38°C and 30.67°C respectively.

In WDS, average concentrations of Pb, Fe, Mn and Cr in P3 were 4.78, 72.01, 1.29 and 0.71 µg/L respectively. In P2, these values were reduced to 2.6, 54.18, 1.16 and 0.61 µg/L respectively. The higher concentrations of Pb, Fe, Mn and Cr in P3 might be partially attributed to higher temperature and increased water demand during P3, which could have increased the metal release from the WDS and/or plumbing system [101,104].

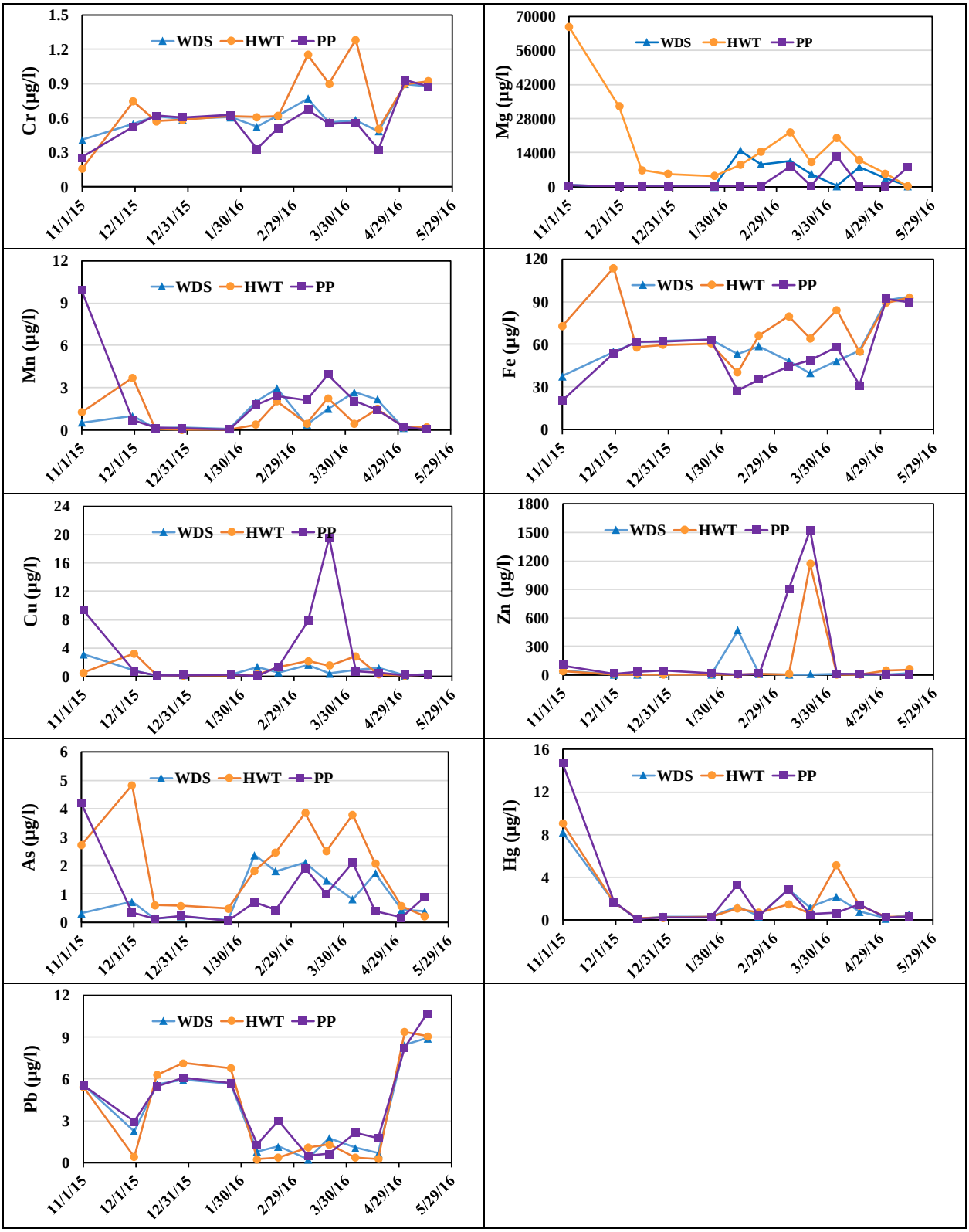


Figure 4.5: Seasonal variability of some significant metal

(WDS: water distribution system; PP: plumbing pipes; HWT: hot water tanks)

In WDS, averages of Pb, Hg and Cu during P1 were 4.49, 3.34 and 1.31 µg/L respectively, which were 2.6, 1.05 and 0.71 µg/L, respectively, during P2. The lower values of these metals in P2 might be attributed to lower water temperature.

However, averages of Mg, Cu, Zn, As and Hg were higher in P2 than in P3. The average concentrations of Mg, Cu, Zn, As and Hg were 6658.1, 0.71, 80.7, 1.34 and 1.05 µg/L respectively, in P2. In P3, these values were 2992.9, 0.63, 8.4, 0.84, 0.91 µg/L respectively. In P1, the average concentrations of Cr, Mn, Fe, Zn and As were 0.52, 0.53, 51.25, 15.76 and 0.39 µg/L respectively, which were 0.61, 1.16, 54.18, 80.68 and 1.34 µg/L, respectively in P2. In PP, average concentrations of Mg, Cr, Fe, As and Pb were higher during P3 than those in P2. Average concentrations of Mg, Cr, Fe, As and Pb in P2 were 1542, 0.55, 46.88, 0.72 and 2.87 µg/L respectively while in P3, these values were 5176, 0.67, 67.67, 0.89 and 5.72 µg/L respectively. The higher concentrations of Mg and As in P3 might be partially due to accumulation of Mg and As in the PP [103]. The higher consumption rate and water temperature during P3 might have increased the dissolution of Mg, As and Fe in the stagnant water (e.g., PP). However, average concentrations of Mn, Cu, Zn and Hg were higher in P2 and those in P3. The average concentrations of Mn, Cu, Zn and Hg in P2 were 1.73, 4.87, 417.36 and 1.27 µg/L respectively while in P3, these were 0.95, 0.39, 4.37 and 0.67 µg/L respectively. The average concentrations of Cr, Fe and Cu during P1 and P2 have not shown significant variation. The averages of Mn, As, Hg and Pb were higher during P1 than in P2 while the averages of Mg and Zn were lower during P1 than in P2.

In HWT, average concentrations of Mg, Mn, Cu, Zn and As were much higher during P2 than in P3. The average concentrations of Mg, Mn, Cu, Zn and As in P2 were 10889, 0.85, 0.91, 197.25 and 1.94 µg/L respectively. In P3, these were 9191, 0.57, 0.84, 25.79 and 1.66 µg/L respectively. The average concentrations Cr, Fe, Hg and Pb were lower in P2 than in P3. The averages of Cr, Fe, Hg and Pb in P2 were 0.75, 61.71, 0.73 and 2.82 µg/L respectively. In P3, these were 0.90, 80.23, 1.78 and 4.78 µg/L respectively. In HWT, several metals (e.g., Mg, Mn, Fe, Cu, Zn, As, Hg and Pb) showed insignificant decrease from P1 to P2. However, averages of Cr and Zn were increased from P1 to P2.

Overall, the average concentrations of Pb in WDS, PP and HWT were highest during P3 followed by P1 and P2. In case of Zn, the average concentration in WDS and PP were highest during P2 followed by P1 and P3. The average concentrations of Cu in PP were highest during P2 followed by P1 and P3. Both Zn and Cu showed decreasing trends with the increase in temperature. The average concentrations of Cr in WDS, PP and HWT were highest during P3 followed by P2 and P1. The average concentrations of Fe in WDS and PP were highest in P3 followed by P2 and P1. Concentrations of Mn in WDS were highest in P3 and lowest in P1.

## 4.6 Summary on Variability of Heavy Metals

Among the heavy metals, the average concentrations of Pb, Ni, Co, Hg, Cu, Mn and Zn were highest in the water samples from the PP (Table 4.2). The average concentrations of Na, Mg, Ca, V, Cr, Fe, Sr, Ba and As were highest in the HWT samples (Table 4.2). The samples from the WDS had the lowest averages in most cases (except Mo). Overall, concentrations of heavy metals in HWT were 1.24-8.1 and 1.4-6.65 times to the concentrations in the WDS and PP respectively.

In most scenarios, the average concentrations of As, Cr, Cu, Pb, Hg, Ni and Zn were in the increasing order for WDS, PP and HWT. Among these metals, release of Pb into drinking water has drawn significant attention due to its wide spread occurrences in drinking water and possible health effects, particularly to the children [77,84].

Several physical and chemical parameters of water (e.g., temperature, pH, chlorine), and plumbing properties and configuration (e.g., pipe materials, plumbing arrangement) were reported to affect the release of heavy metals from PP. The water was the mixture of desalinated and blended water, in which pH was adjusted prior to supplying through the WDS. The averages of pH were lower than the neutral value in most cases (Table 1) resulting in the relatively corrosive water, which might have increased the release of heavy metals from PP. The extended reaction period due to stagnation of water in PP might have increased the rate of release of Pb from PP. Kim et al., [11] reported approximately 50% reduction of Pb concentration in drinking water when pH was increased from 7.1 to 7.7 in several houses in ON, Canada. The Pb dissolution rate was found to increase with the increase of dissolved inorganic carbon (DIC) in water [105]. Further, FCl was found to maintain the constant rate of Pb dissolution into drinking water [105,106]. However, alteration of FCl by mono-chloramine was reported to increase the concentration of Pb in drinking water significantly [107,108]. The Pb concentrations were observed to increase to 31-113 µg/L from 15 µg/L (90th percentile). An intermediate species, formed during mono-chloramine decay process, was responsible for Pb release from $PbO_2$ [108].

In addition, the presence of iron oxide particles might have led the particulate Pb to release into water. The iron oxide/hydroxide has relatively high affinity to Pb [109,110]. Kim et al., [11]

reported higher levels of particulate Pb in water in presence of higher concentration of iron. The positive value of correlation coefficient between Pb and Fe (r = 0.34) also support this explanation to some extent. In addition, mechanical disturbances (e.g., repeated activation of the faucet, water hammer) could have increased the release of Pb and Fe [72]. The pipe materials and coatings could have affected the leaching of heavy metals into drinking water during stagnation in the PP. The galvanized iron (GI) pipes with zinc coating were the main components in the PP, which could have increased the concentration of Pb in the stagnant water [40]. Lasheen et al., [111] demonstrated the release of Pb and Fe into stagnant water using different pipe materials. Past study also demonstrated exponential increase in metal concentration (e.g., Pb and Cu) during 20-24 h of stagnation period [41]. Concentration of Pb and Fe were increased by 26% and 100% respectively, when the stagnation period was increased from 2 to 20 weeks [111]. The overnight stagnation of water in cooler was reported to increase Cr, Cu, Fe, Zn, Ni, Mn, and Pb in tap water [20], which were consistent to the findings in this study. The concentration of Cu was significantly higher in the PP than the WDS, due possibly to extended reaction during the overnight stagnation in PP [112]. The higher concentrations of Zn, Fe, Cu and Mn in HWT might be due to temperature driven extended reaction in the HWT [16].

The higher concentrations of heavy metals in the PP and HWT might be a concern from monitoring, regulatory, human exposure and risk perspectives [9,97,112,113]. The regulatory agencies typically monitor the water quality in the treatment plant or in few locations of the WDS prior to entering the buildings. However, the plumbing premise can alter the concentrations of several heavy metals in the tap water significantly. The regulatory agencies may further look into

the strategy of water quality monitoring and regulatory compliance for the best protection of human health.

Most of the metals in WDS, PP and HWT did not show noticeable diurnal variability. The sampling time had minimal effects on the concentrations of many metals. However, considerable variations were observed in the concentrations of As and Cr in HWT for the early morning and afternoon samples. The exact mechanisms for this variability are yet to be established. The corrosion in stainless steel wall of HWT and Ni-Cr heater alloys might have released Cr while As could have entered from the wall of HWT due to scale formation [102]. Following the whole day usage of hot water, the scales were sloughed off and increased the levels of As and Cr in afternoon samples [103].

Many of the metals in WDS, PP and HWT showed seasonal variability. The average concentrations of Pb in WDS, PP and HWT were highest during summer followed by pre-winter and winter seasons, due possibly to the highest temperature and water demands in summer followed by pre-winter and winter. Similar increasing trends were observed for Cr in WDS, PP and HWT, Fe in WDS and PP and Mn in WDS. The average concentrations of Zn and Cu in WDS, PP and HWT showed decreasing trends with the increase in temperature (e.g., from winter to summer). The variability of these metals (e.g., Zn, Cu, Cr, Fe, Mn) in different periods needs further analysis through the cause and effect studies. The trends of metal release with seasons are different for different metals, and this phenomenon may pose enhanced risk to the consumers. Installation of a household filter to facilitate the treatment prior to consumption may be a potential option.

# CHAPTER 5

# MODELING OF HEAVY METAL

## 5.1 Model Development

The models for predicting heavy metals in PP and HWT were developed through training of several linear, nonlinear and neural network models. The first step for model development was to identify the statistically significant factors through numerical and graphical analysis. The matrix plot (Fig. 4.1) and the Pearson correlation (*r*) of WQP and metal concentrations (Table 4.3) were used as basis for initial selection of significant factors. The final selection of signification factors was performed through effect analysis using statistical packages JMP$^{TM}$.

Among different linear models, linear main factors (LMF), main factors with interactions and higher orders (LMFI), and logarithmic models (LL) were investigated for predicting heavy metals in PP and HWT. The effect analysis was performed using the Analysis of Variance (ANOVA) to select the significant factors. The effects of significant factors were also tested using graphical techniques (i.e., half-normal plot, prediction profiler). The plot of residuals versus predicted, residuals versus row number and predicted versus experimental data were used to confirm the model adequacy.

By using JMP$^{TM}$ 'nonlinear models' library, three parameter Logistic model (LM-3P), four parameter Logistic model (LM-4P), four-parameter Weibull model (WM-4P), four parameter

Biexponential model (BEM-4P), Quartic model (QRM), Quintic model (QUM) and Cubic model (CBM) were trained with the measured data [94]. Different nonlinear models were trained for modeling the concentrations of several significant metals (i.e., Mg, As, Cr, Pb, Hg, Cu, Mn, Zn, Fe) in PP an HWT. The NL models were tested for significant WQP and other metals in PP and WDS separately. The parameters for nonlinear models were selected by attaining convergence using the Analytic Gauss Newton method [94]. Upon fitting the best convergence, the corresponding RMSE were observed. The plot of predicted versus experimental data and their respective $R^2$ were used to explain the model adequacy.

The neural network (NN) model is a series of algorithms that attempt to identify the underlying relationships in a set of data using a process analogous to the network of neurons in a brain. The neural network structure for modeling heavy metals in PP and HWT consist of an input layer, one hidden layer with three nodes and the output layer. The input layer contains the WQP and metal concentrations in WDS, PP and HWT while the output layer denotes the concentrations of the metals in PP or HWT. The three hidden nodes explain the hyperbolic tangent function of input variables. Training of each NN model was accomplished by two thirds of the data from the dataset. The models were validated by "Excluded Rows" method, where one third of the data were used. The NN model was tested for modeling several significant metals (i.e., Mg, As, Cr, Pb, Hg, Cu, Mn, Zn, Fe) in PP and HWT samples. The plot of predicted versus experimental data for training and validation were used to assess the model adequacy. Finally, the models were validated using an additional set of experimental data, which were not used in model development. The statistical packages JMP™, and Minitab™ were used to perform the model development works.

## 5.2 Models for Predicting Lead (Pb)

### 5.2.1 Modeling Pb in PP

**Linear Model:**

Figure 5.1 summarizes the procedure of selecting factors and adequacy check for modeling of Pb in PP. Table 5.1 summarizes the ANOVA with significant factors (p-value < 0.01). Among the different linear models, the LMF model was found to be the best and was selected (Equation 5.1). The model had the $R^2$ value of 0.96. The experimental data and predicted values were found to be consistent (Fig. 5.1d).

Table 5.1: Screening effects of the factors for modeling Pb-PP

| Term | Estimate | Std Error | *t* Ratio | Prob>\|*t*\| |
|---|---|---|---|---|
| Intercept | -0.894658 | 0.383462 | -2.33 | 0.0302 |
| Pb-WDS | 1.12266 | 0.056813 | 19.76 | <0.0001 |
| Mo-PP | 0.0201685 | 0.003139 | 6.43 | <0.0001 |
| Zn-PP | -0.000645 | 0.000217 | -2.97 | 0.0075 |
| DOC-PP | 0.9390127 | 0.236508 | 3.97 | 0.0008 |
| Ca-WDS | -0.000042 | 1.253e-5 | -3.35 | 0.0032 |

$$Pb-PP = \beta_0 + \beta_1 Pb-WDS + \beta_2 Mo-PP + \beta_3 Zn-PP + \beta_4 DOC-PP + \beta_5 Ca-WDS \qquad (5.1)$$

Where: $\beta_0 = -0.89;\ \beta_1 = 1.12;\ \beta_2 = 0.02;\ \beta_3 = -0.0006;\ \beta_4 = 0.94;\ \beta_5 = -0.000042$

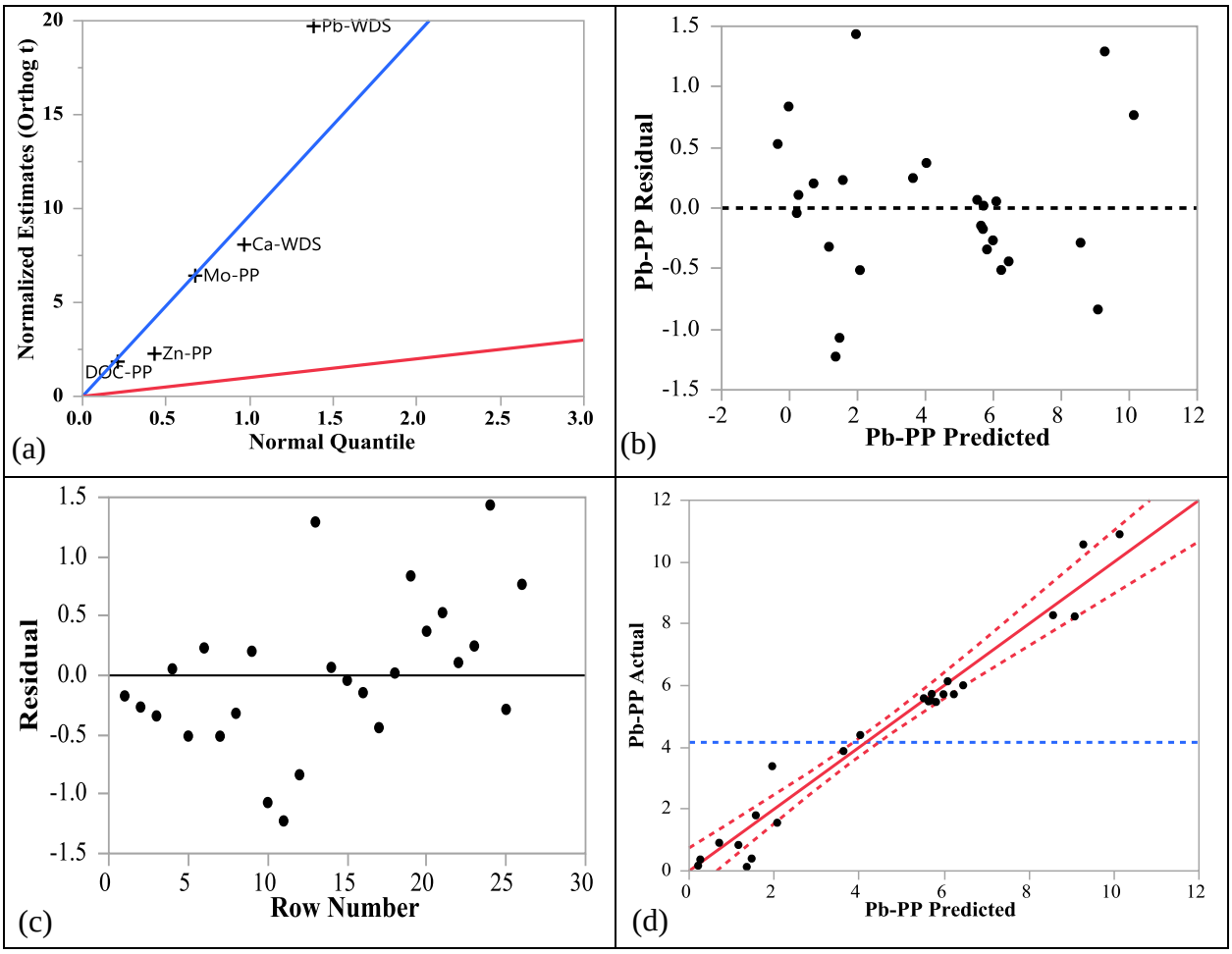


Figure 5.1: For Pb-PP model: (a) half-normal plot (b) residual vs predicted (c) residual vs row number and (d) actual vs predicted data

The plot of residuals versus predicted values (Fig. 5.1b) showed the data randomness. The plot of residuals versus row number (Fig. 5.1c) indicated that the residuals were uncorrelated. No evidence of lack of fit (P >= 0.1) was also observed. The screening effects of the main factors (Table 5.1) and the half-normal plot (Fig. 5.1a) show that Pb-WDS, Mo-PP, DOC-PP had positive effects on the occurrence of Pb in PP, while Zn-PP and Ca-WDS had negative effects.

**Nonlinear Model:**

The nonlinear model selection for Pb in PP is explained in Fig. 5.2. The Pb in WDS showed the best performance for Pb-PP with the three parameter Logistic model (Fig. 5.2a). The other factors and models did not show similar performance. The three parameter Logistic model was developed for predicting Pb-PP (Equation 5.2), and the model had the RMSE of 1.15. The experimental data and predicted values ($R^2$=0.88) were found to be consistent (Fig. 5.2b).

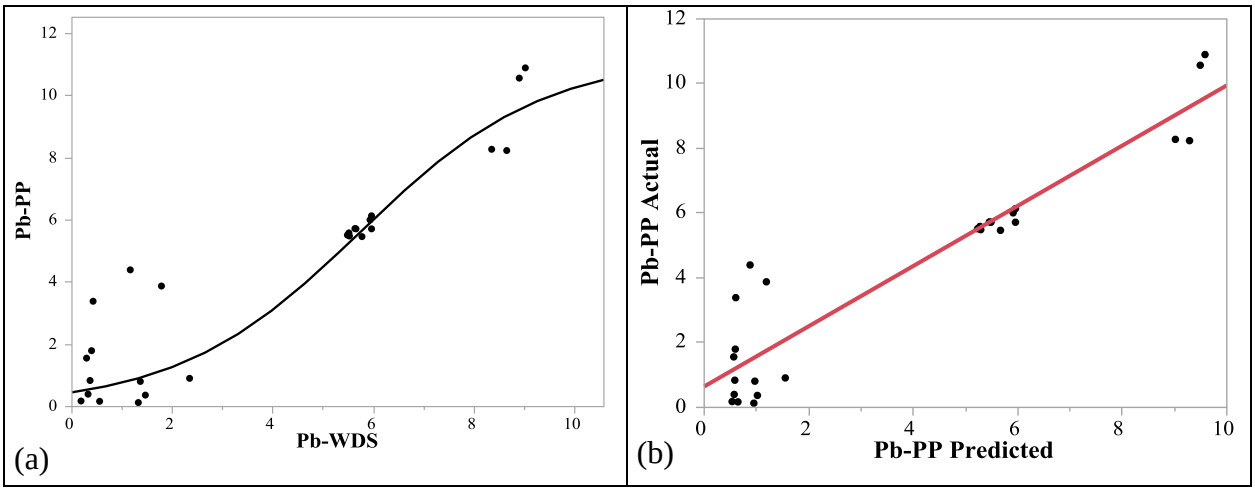


Figure 5.2: For Logistic model (3 P) of Pb-PP (a) model fitting (b) actual vs predicted plot

$$Pb-PP=\frac{\theta_1}{(1+\theta_2 Exp(\theta_3 Pb-WDS))} \quad (5.2)$$

Where: $\theta_1=11.25; \theta_2=23.5; \theta_3=-0.55$

**Neural Network Model:**

The NN model for predicting the concentrations of Pb-PP is shown in Equation 5.3. The model had the $R^2$ and RMSE values of 0.91 and 0.95 respectively. The experimental data and predicted

values were consistent (Fig. 5.3). The Equations 5.4-5.6 showed that Ca-WDS, Pb-WDS and DOC-PP had influence on the concentrations of Pb in PP.

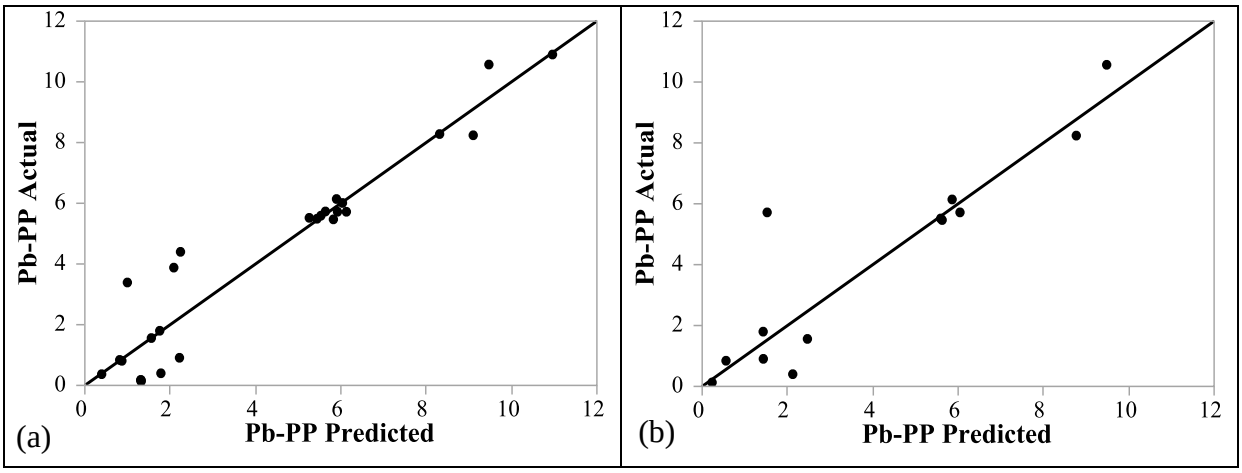


Figure 5.3: Actual vs predicted plot of Pb-PP for (a)data training (b) validation of NN model

$$Pb-PP = 7.49 + (-6.996 \times \mathrm{H1}) + (-5.287 \times \mathrm{H2}) + (-6.063 \times \mathrm{H3}) \quad (5.3)$$

$$\mathrm{H1} = \tanh[0.5 \times \{-1.347 + (0.828\,\mathrm{DOC\text{-}PP}) + (0.00007\,\mathrm{C}a\text{-}\mathrm{WDS}) + (-0.053\,\mathrm{P}b\text{-}\mathrm{WDS})\}] \quad (5.4)$$

$$\mathrm{H2} = \tanh[0.5 \times \{4.39 + (-2.97\,\mathrm{DOC\text{-}PP}) + (0.00004\,\mathrm{C}a\text{-}\mathrm{WDS}) + (-0.23\,\mathrm{P}b\text{-}\mathrm{WDS})\}] \quad (5.5)$$

$$\mathrm{H3} = \tanh[0.5 \times \{1.73 + (0.99\,\mathrm{DOC\text{-}PP}) + (-0.00009\,\mathrm{C}a\text{-}\mathrm{WDS}) + (-0.25\,\mathrm{P}b\text{-}\mathrm{WDS})\}] \quad (5.6)$$

### 5.2.1.1 Model Comparison for Pb in PP

The comparison of the models for predicting Pb in PP are shown in Figure 5.4. The LMF, NL (LM-3P) and NN models had the $R^2$ values of 0.96, 0.88 and 0.95 respectively (Table 5.2). The lower RMSE of LMF model (RMSE=0.71) than the NN model (RMSE=0.95) and NL (LM-3P) model indicates better performance of LMF model than the other models. The LMF model used

two additional factors (e.g., Mo-PP, Zn-PP) than the NN model, which might have improved its performance (Table 5.2). The relatively lower performance of the NL (LM-3P) model might be attributed to the inclusion of a single factor for modeling (i.e., Pb-WDS). All models had better fits with measured data for low to medium concentrations of Pb (0-7.0 µg/L) while the LMF model predictions were closer to the line of equal concentration (LOEC) than the other models. Depending on the data availability, all models can be applied for predicting Pb in PP.

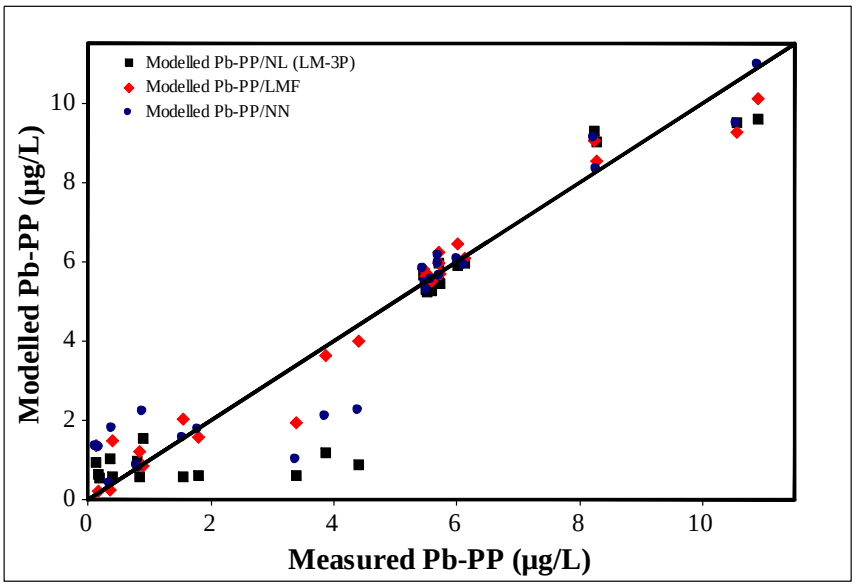


Figure 5.4: Measured and modeled concentration of Pb in PP

(LM-3P: 3 P Logistic model; LMF: Main factors linear model; NN: Neural network model)

Table 5.2: Comparison of different models for Pb in PP

| Output | Model Type | Parameters | $R^2$ | RMSE |
|---|---|---|---|---|
| Pb-PP | LMF | DOC-PP, Ca-WDS, Pb-WDS, Mo-PP, Zn-PP | 0.96 | 0.71 |
| | NL (LM-3P) | Pb-WDS | 0.88 | 1.15 |
| | NN | DOC-PP, Ca-WDS, Pb-WDS | 0.95 | 0.95 |

### 5.2.1.2 Model Validation for Pb in PP

The predictive models for Pb in PP were validated using an additional set of data, which were not used in model development. The average concentrations of Pb-PP, obtained from validation study of LMF, NL (LM-3P) and NN models, were 4.05, 3.59 and 3.94 µg/L respectively and the ranges were 1.09-9.25, 0.51-9.57 and 0.23-9.49 µg/L respectively. The average concentrations the measured data was 4.08 µg/L with the range of 0.13-10.57 µg/L. From the plot of predicted vs. measured data, the values of correlation coefficients (*r*) were determined and shown in Table 5.3. The values of *r* for LMF, NL (LM-3P) and NN models were 0.76, 0.90 and 0.91 respectively. The comparison of different models for validation study are shown in Figure 5.5. The NN and NL (LM-3P) models were much closer to LOEC and showed better fit with measured data than LMF model.

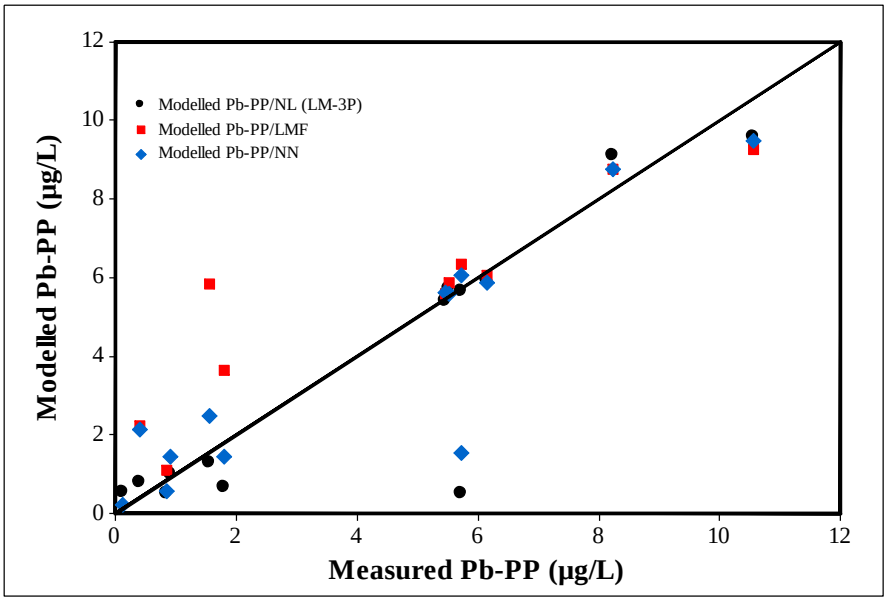


Figure 5.5: Measured and modelled concentration of Pb-PP in validation

Table 5.3: Correlation coefficients for model validation of Pb in PP

| Output | Model Type | *r* (Corr. Coef.) |
|---|---|---|
| Pb-PP | LMF | 0.76 |
| | NL (LM-3P) | 0.90 |
| | NN | 0.91 |

### 5.2.2 Modeling Pb in HWT

**Linear Model:**

Figure 5.6 summarizes the procedure of selecting parameters and adequacy check for modeling of Pb concentrations in HWT samples. Table 5.4 summarizes the ANOVA with significant factors (p value < 0.01). Among the different linear models, the LMF model was found to be the best and

was selected (Equation 5.7). The model had the $R^2$ value of 0.85. The experimental data and predicted values were found to be consistent (Fig. 5.6d). The plot of residuals versus predicted values (Fig. 5.6b) showed data randomness. No evidence of lack of fit (P >= 0.1) was also observed. The screening effects of the main factors (Table 5.4) and half-normal plot (Fig. 5.6a) showed that Pb-WDS, Cr-HWT and Ba-HWT positively influenced the occurrence of Pb in HWT samples while Na-HWT showed negative effect.

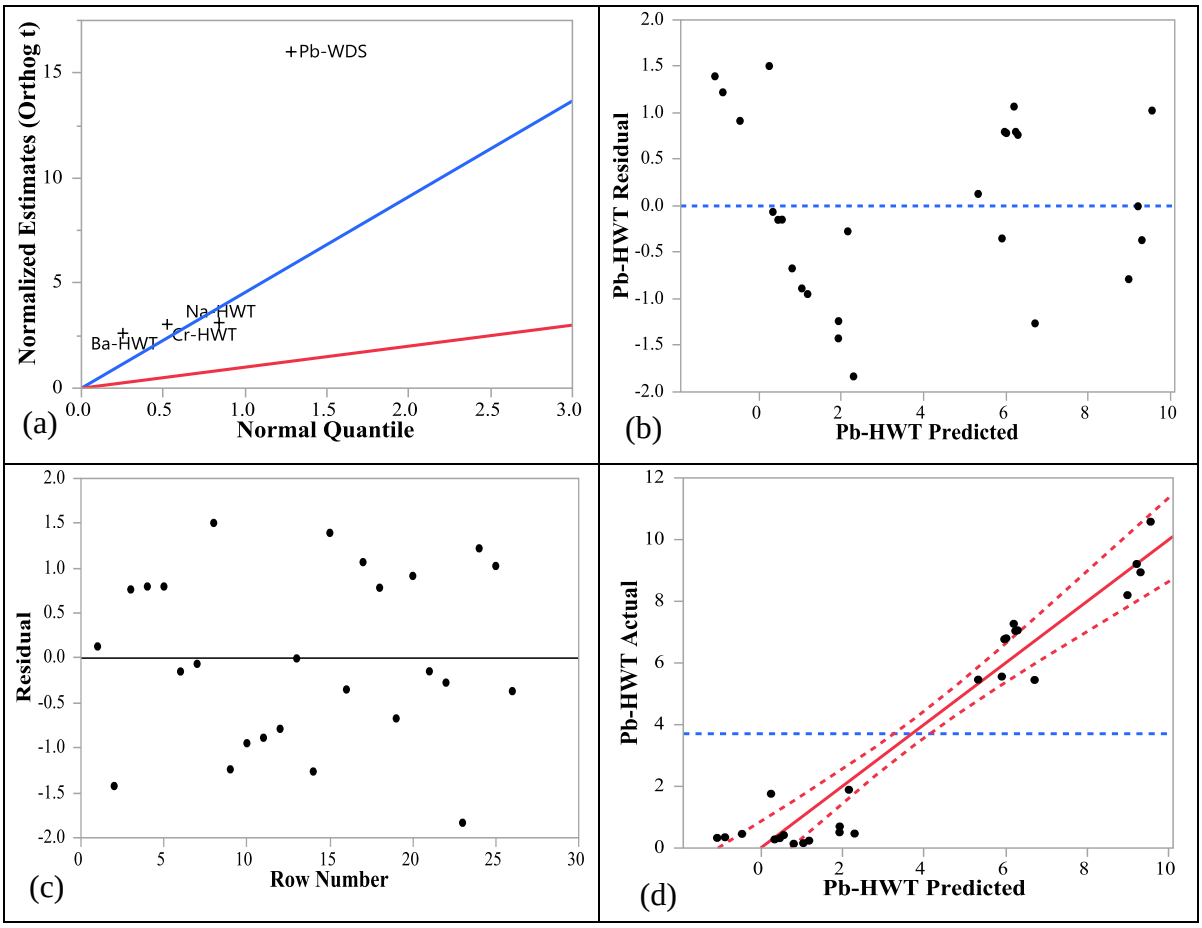


Figure 5.6: For Pb-HWT model (a) half normal plot (b) residual vs predicted (c) residual vs row number and (d) actual vs predicted data

Table 5.4: Screening effects of the factors for modeling Pb-HWT

| Term | Estimate | Std Error | t Ratio | Prob>\|t\| |
|---|---|---|---|---|
| Intercept | -0.65179 | 0.694267 | -0.94 | 0.3585 |
| Pb-WDS | 0.7563172 | 0.094491 | 8.00 | <.0001 |
| Na-HWT | $-3.887\times10^{-6}$ | $9.05\times10^{-7}$ | -4.30 | 0.0003 |
| Cr-HWT | 3.0806746 | 0.797723 | 3.86 | 0.0009 |
| Ba-HWT | 0.0001236 | $4.726\times10^{-5}$ | 2.61 | 0.0162 |

$$Pb-HWT=\beta_0+\beta_1 Pb-WDS+\beta_2 Na-HWT+\beta_3 Cr-HWT+\beta_4 Ba-HWT \qquad (5.7)$$

Where: $\beta_0=-0.65;\ \beta_1=0.756;\ \beta_2=-3.89\times10^{-6};\ \beta_3=3.08;\ \beta_3=0.00012$

**Nonlinear Model:**

The nonlinear model selection for Pb in HWT samples is explained in Figure 5.7. Among the different factors, Pb in the Pb-WDS showed the best performance with the three parameter Logistic model (Fig. 5.7a). The model for predicting Pb-HWT is shown in Equation 5.8 and the model had the RMSE of 1.39. The experimental data and predicted values ($R^2$=0.86) were found to be consistent (Fig. 5.7b).

$$Pb-HWT=\frac{\theta_1}{(1+\theta_2 Exp(\theta_3 Pb-WDS))} \qquad (5.8)$$

Where: $\theta_1=9.78;\ \theta_2=48.53;\ \theta_3=-0.77$

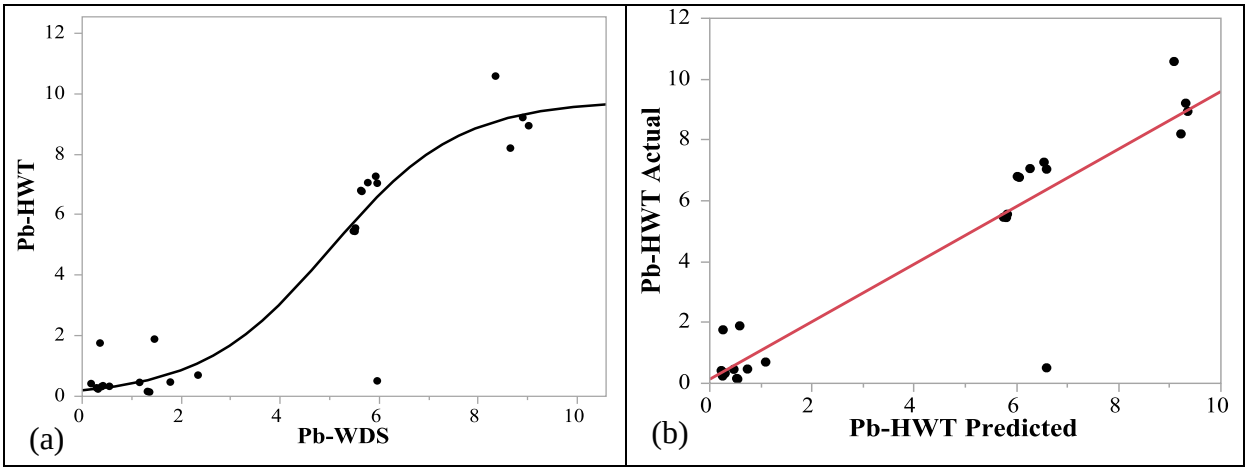


Figure 5.7: For three parameter Logistic model of Pb-HWT (a) model fitting (b) actual vs predicted plot

**Neural Network Model:**

Equation 5.9 shows the NN model for predicting Pb-HWT. The model had the $R^2$ value of 0.99 and RMSE of 0.34. The experimental data and predicted values were found to be consistent (Fig. 5.8). The Equations of hidden nodes (Equation 5.10-5.12) showed that Pb-WDS, Na-HWT, Cr-HWT and Ba-HWT had influence on the occurrence of Pb in HWT.

$$Pb-HWT = 4.638 + (-2.717 \times H1) + (-2.467 \times H2) + (4.337 \times H3) \quad (5.9)$$

$$H1 = \tanh[0.5 \times \{2.9 + (0.21\,Pb\text{-}WDS) + (-0.61\,Cr\text{-}HWT) + (-0.003\,Ba\text{-}HWT)\}] \quad (5.10)$$

$$H2 = \tanh[0.5 \times \{-15.23 + (3.09\,Pb\text{-}WDS) + (-7.31\,Cr\text{-}HWT) + (-0.0003\,Ba\text{-}HWT)\}] \quad (5.11)$$

$$H3 = \tanh[0.5 \times \{-37.90 + (3.68\,Pb\text{-}WDS) + (22.59\,Cr\text{-}HWT) + (0.0003\,Ba\text{-}HWT)\}] \quad (5.12)$$

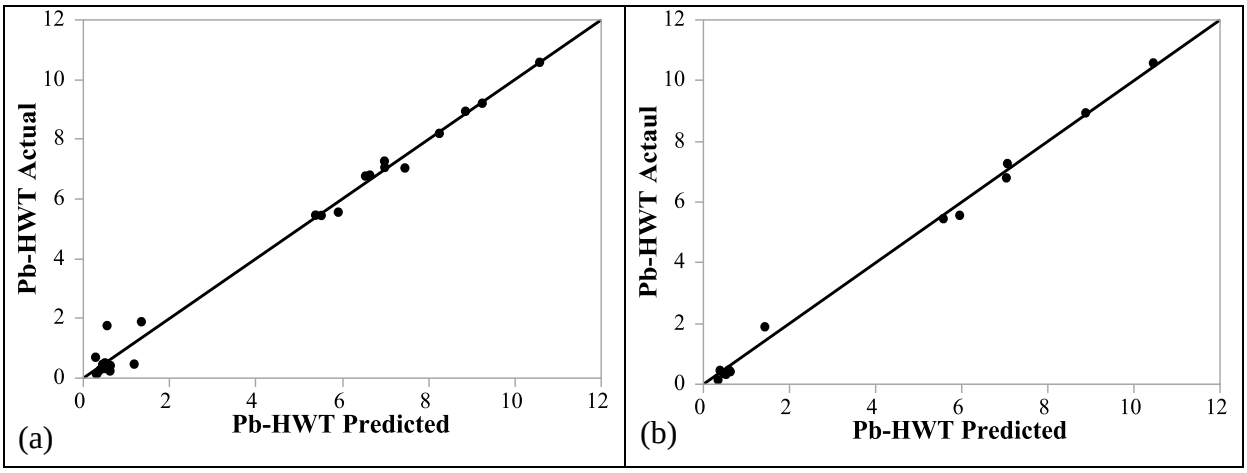


Figure 5.8: Actual vs predicted plot of Pb-HWT for (a) data training (b) validation of NN model

### 5.2.2.1Model Comparison for Pb in HWT

The comparison of the models for predicting Pb in HWT are shown in Figure 5.9. The NN model showed better performance ($R^2$ = 0.99; RMSE = 0.34) than LMF ($R^2$ = 0.93; RMSE = 1.04). However, these two models had the same input factors (Table 5.5). The NL model (LM-3P) showed poor performance than the NN and LMF models, due possibly to the single input factor (e.g., Pb-WDS) while Pb in HWT could be affected by several other factors. All models showed better fit for low and mid-level concentrations of Pb (0-8.0 µg/L) (Figure 5.9), while for NN model, the measured data were much closer to the LOEC. The NN model is the model of choice for predicting Pb in HWT.

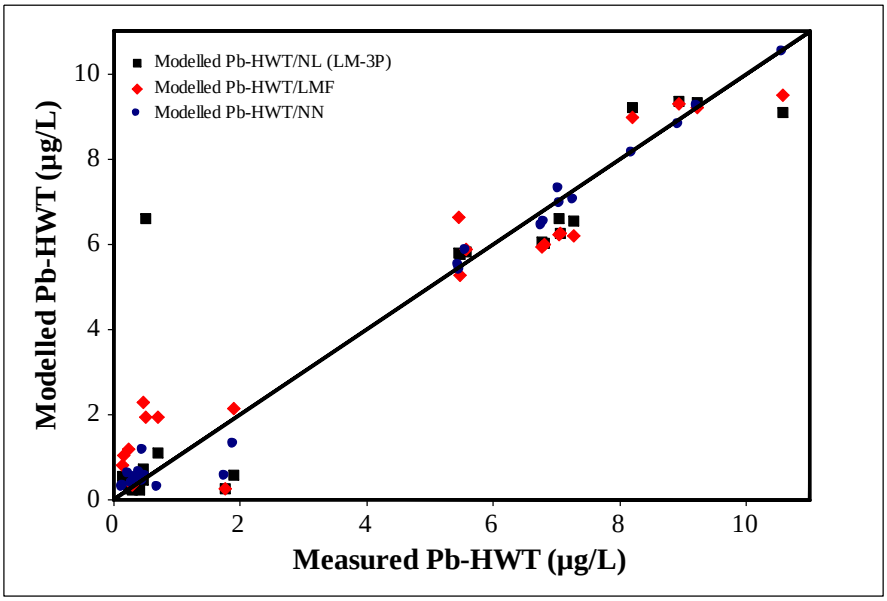


Figure 5.9: Measured and modeled concentration of Pb in HWT

(LM-3P: 3 parameters Logistic model; LMF: Main factors linear model; NN: Neural network model)

Table 5.5: Comparison of different models for Pb in HWT

| Output | Model Type | Parameters | $R^2$ | RMSE |
|---|---|---|---|---|
| Pb-HWT | LMF | Pb-WDS, Na-HWT, Ba-HWT, Cr-HWT | 0.93 | 1.04 |
| | NL (LM-3P) | Pb-WDS | 0.86 | 1.39 |
| | NN | Pb-WDS, Na-HWT, Ba-HWT, Cr-HWT | 0.99 | 0.34 |

### 5.2.2.2 Model Validation for Pb in HWT

The predictive models for Pb in HWT were validated using an additional set of data, which were not used in model development. The average concentrations of Pb-HWT, obtained from the LMF, NL (LM-3P) and NN models were 3.57, 3.55 and 3.78 µg/L respectively, and the ranges were 0.18-9.52, 0.23-9.30 and 0.34-10.41 µg/L respectively. The average concentration of measured

Pb-HWT was 3.74 µg/L with the range of 0.14-10.58 µg/L. From the plot of predicted vs. measured data, the values of correlation coefficients (*r*) were determined and shown in Table 5.6. The values of *r* for LMF, NL (LM-3P) and NN models were 0.97, 0.98 and 0.99 respectively. The comparison of different models for validation study are shown in Figure 5.10. All the models were closer to LOEC and showed almost perfect fits with measured data.

Table 5.6: Correlation coefficients for model validation of Pb in HWT

| Output | Model Type | *r* (Corr. Coef.) |
|---|---|---|
| Pb-HWT | LMF | 0.97 |
| | NL (LM-3P) | 0.98 |
| | NN | 0.99 |

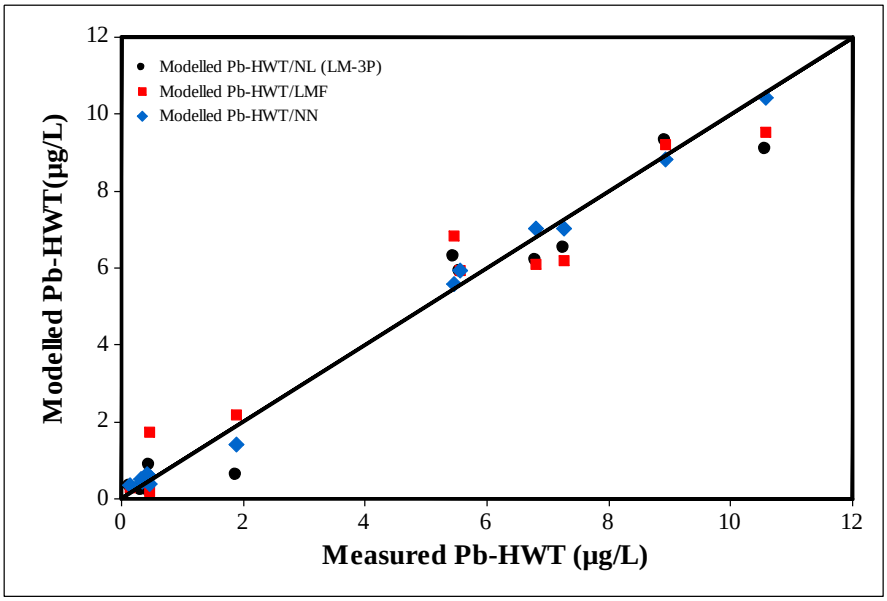


Figure 5.10: Measured and modelled concentration of Pb-HWT in validation

For the Pb-PP and Pb-HWT models, the NN models were found to be the best while the NL models were showing poor performance. The nonlinear models were developed using the most important single factors, which might have ignored the effects of one or more less important main factors and the interaction effects, resulting in relatively rating the additional factors and their interaction effects. Most of the models for Pb in PP and HWT showed moderate to excellent predictive capacities.

The factors of the models for predicting Pb-PP indicated that Pb in tap water (e.g., PP) was affected by the Pb in WDS (Pb-WDS). The relatively acidic water was likely to increase the release of metals due to increased reaction period with the pipe coatings and plumbing materials. The stagnation period also affected the corrosion of lead service line and caused the leaching effects in pipe network. In addition, mechanical disturbances (e.g., repeated activation of the faucet, water

hammer) could also release Pb along with Fe and Al [72]. The GI pipes contained the zinc coating, which could also be a source of Pb release in stagnant water [40]. The iron pipe corrosion by-products contained several metals including Pb (i.e., Cu, V, Mn, Pb, Cr), which could have released Pb into PP due to changes of WQP (i.e., changing temperature, TCl) [115]. The models indicated that the Pb in HWT was affected by the Pb in WDS. In addition, scale deposits on the heater wall along with other corroded metals from the plumbing fixtures or service line might have served as the potential sources of Pb in HWT. Following the usage of hot water, the scales were sloughed off and released into hot water [103].

## 5.3 Models for Predicting Chromium (Cr)

### 5.3.1 Modeling Cr in PP

**Linear Model:**

The ANOVA (Table 5.7) summarizes the significant factors (p value < 0.01) for modeling Cr in PP samples. Among the different linear models, the LMF model was found to be the best and was selected (Equation 5.13). The model had the $R^2$ value of 0.91. The experimental data and predicted values were found to be consistent (Fig. 5.11d). The plot of residuals versus predicted values (Fig. 5.11b) showed the randomness. The plot of residuals versus row number (Fig. 5.11c) confirmed that the residuals were uncorrelated. No evidence of lack of fit (P >= 0.1) was also observed. The screening effects of the main factors (Table 5.7) and the half-normal plot (Fig. 5.11a) showed that V-WDS, Fe-PP and Mn-PP had positive impact on the concentrations of Cr in PP.

Table 5.7: Screening effects of the factors for modeling Cr-PP

| Term | Estimate | Std Error | t Ratio | Prob>\|t\| |
|---|---|---|---|---|
| Intercept | -0.095117 | 0.057181 | -1.66 | 0.1104 |
| V-WDS | 0.01034 | 0.002329 | 4.44 | 0.0002 |
| Fe-PP | 0.0109549 | 0.000805 | 13.61 | <0.0001 |
| Mn-PP | 0.0173407 | 0.004906 | 3.53 | 0.0019 |

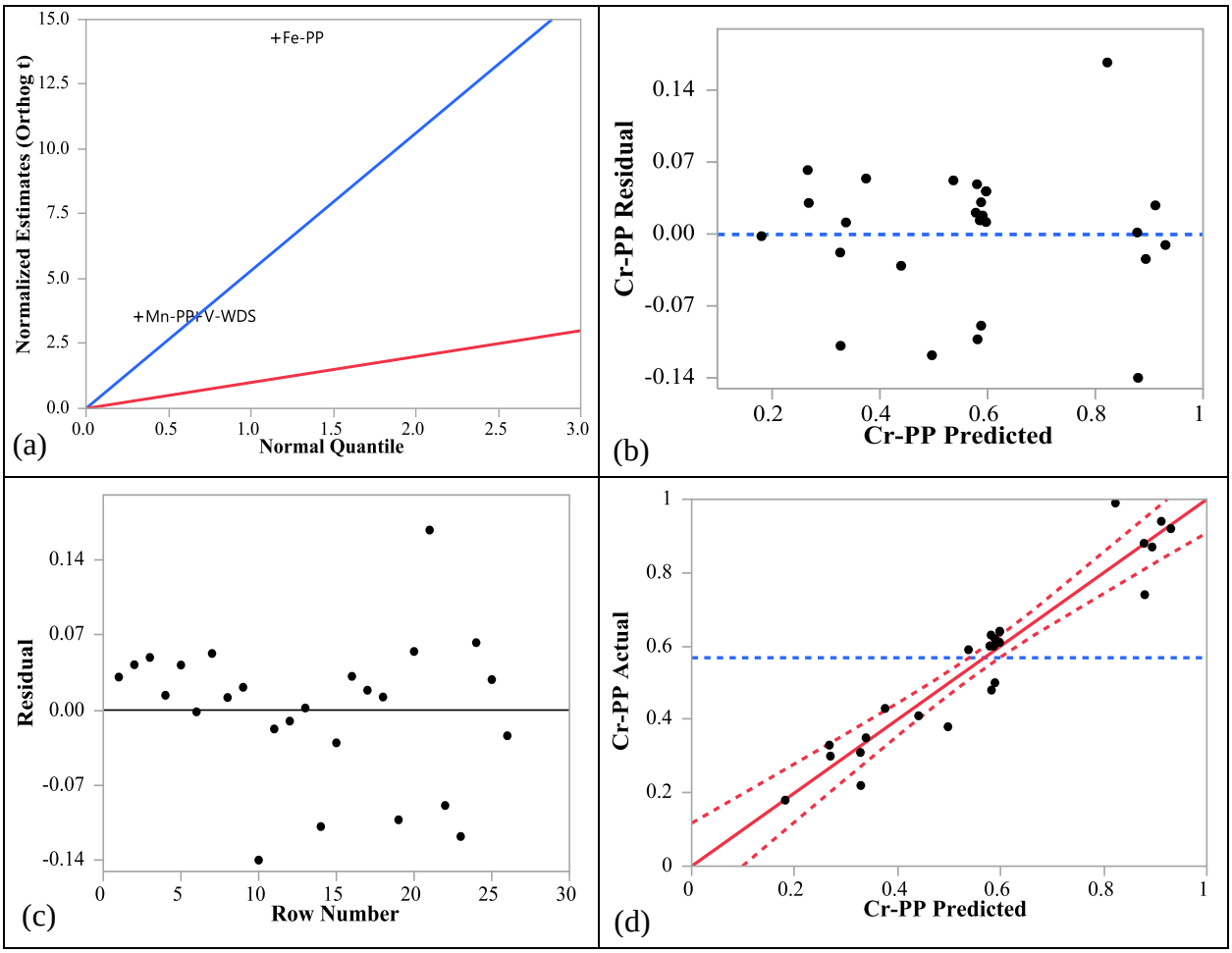


Figure 5.11: For Cr-PP model (a) half normal plot (b) residual vs predicted (c) residual vs row number and (d) actual vs predicted data

$$Cr-PP = \beta_0 + \beta_1 V - WDS + \beta_2 Fe - PP + \beta_3 Mn - PP \quad (5.13)$$

Where: $\beta_0 = -0.095; \beta_1 = 0.01; \beta_2 = 0.01; \beta_3 = -0.017$

**Nonlinear Model:**

Figure 5.12 explains the nonlinear model selection process for Cr in PP samples (Cr-PP). Among the different parameters, Fe in PP samples showed best performance with the three parameter Logistic model (Fig. 5.12a) for predicting Cr-PP. The model was developed (Equation 5.14) and it had the RMSE of 0.098. The experimental data and predicted values ($R^2$=0.82) were found to be consistent (Fig. 5.12b).

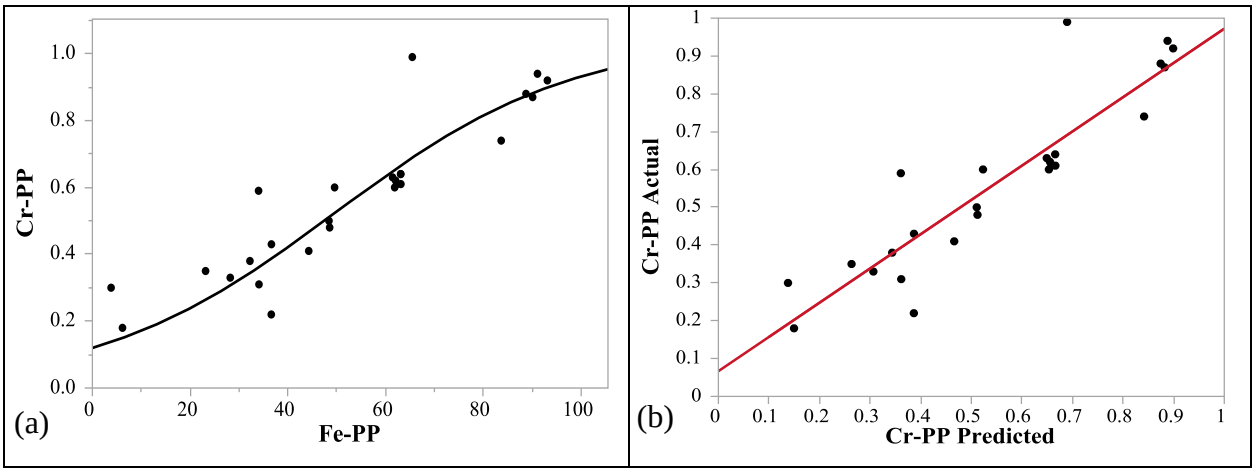


Figure 5.12: For three parameters Logistic model of Cr-PP (a) model fitting (b) actual vs predicted plot

**Neural Network Model:**

The NN model for predicting Cr-PP was found to be the best (Equation 5.15). The model had the $R^2$ value of 0.98 and RMSE of 0.027. The experimental data and predicted values were found to

be consistent (Fig. 5.13). The Equation of hidden nodes (Equation 5.16-5.18) showed that V-WDS, Fe-PP and Mn-PP have influenced the concentrations of Cr in PP.

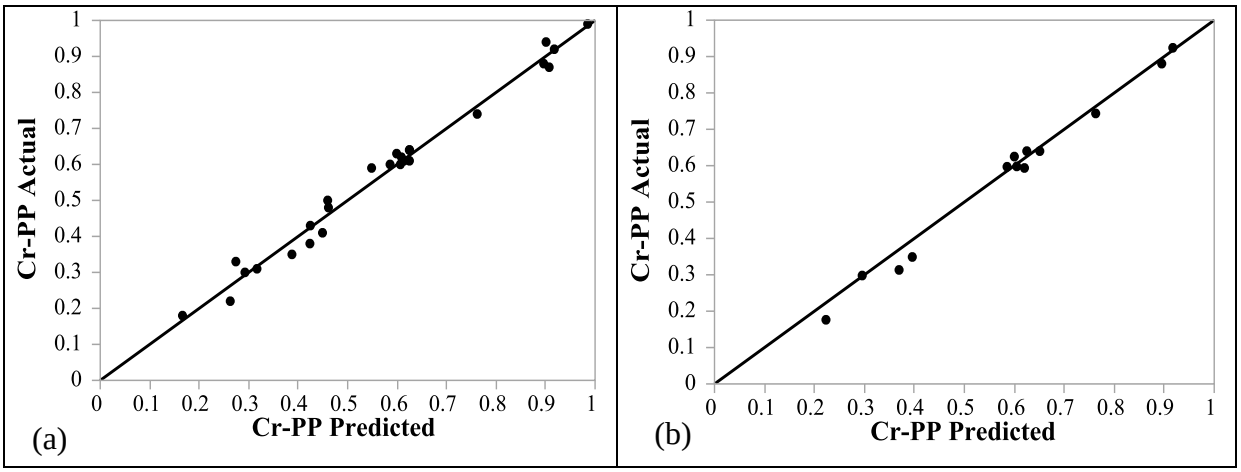


Figure 5.13: Actual vs predicted plot of Cr-PP for (a) data training (b) validation of NN model

$$Cr-PP = 1.58 + (-1.757 \times \mathrm{H1}) + (-3.732 \times \mathrm{H2}) + (1.11 \times \mathrm{H3}) \quad (5.15)$$

$$\mathrm{H1} = \tanh[0.5 \times \{0.557 + (0.0065\,\mathrm{V\text{-}WDS}) + (0.012\ Fe-PP + (-0.215\,Mn-PP)\}] \quad (5.16)$$

$$\mathrm{H2} = \tanh[0.5 \times \{1.716 + (-0.056\,\mathrm{V\text{-}WDS}) + (-0.022\ Fe-PP + (0.024\,Mn-PP)\}] \quad (5.17)$$

$$\mathrm{H3} = \tanh[0.5 \times \{4.29 + (-0.197\,\mathrm{V\text{-}WDS}) + (-0.049\,Fe-PP + (-0.223\,Mn-PP)\}] \quad (5.18)$$

### 5.3.1.1 Model Comparison for Cr in PP

The comparison of the models for predicting Cr in PP are shown in Figure 5.14. The NN model showed better performance ($R^2$=0.98; RMSE=0.027) than the LMF model ($R^2$=0.91; RMSE=0.072). However, these two models had the same input factors (Table 5.8). The NL model (LM-3P) showed poor performance than the NN and LMF models, due to the single input factor (e.g., Fe-PP) while Cr in PP could be affected by several factors. All models had better fits with

measured data for concentrations of Cr, while for NN model, the measured data were much closer to the LOEC. The NN model is the model of choice for predicting Cr in PP.

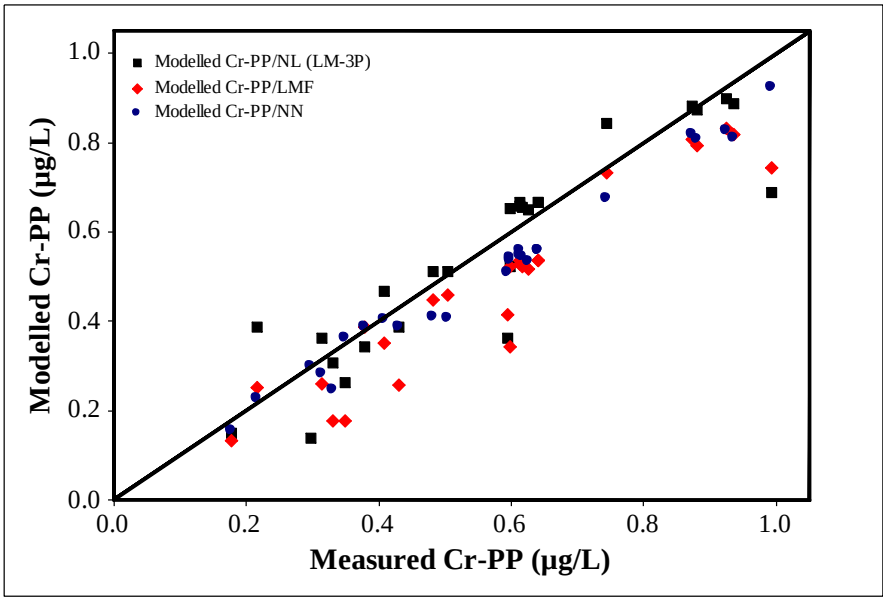


Figure 5.14: Measured and modeled concentration of Cr in PP

(LM-3P: 3 parameters Logistic model; LMF: Main factors linear model; NN: Neural network model)

Table 5.8: Comparison of different models for Cr in PP

| Output | Model Type | Parameters | $R^2$ | RMSE |
|---|---|---|---|---|
| Cr-PP | LMF | V-WDS, Mn-PP, Fe-PP | 0.91 | 0.072 |
| | NL (LM-3P) | Fe-PP | 0.82 | 0.098 |
| | NN | V-WDS, Mn-PP, Fe-PP | 0.98 | 0.027 |

### 5.3.1.2Model Validation for Cr in PP

The predictive models for Cr in PP were validated using an additional set of data, which were not used in model development. The average concentrations of Cr-PP, obtained from the LMF, NL (LM-3P) and NN models were 0.43, 0.54 and 0.53 µg/L respectively, and the ranges were 0.17-0.83, 0.14-0.90 and 0.21-0.83 µg/L respectively. The average actual concentration of Cr-PP was 0.57 µg/L with the range of 0.18-0.92 µg/L. From the plot of predicted vs. measured data, the values of correlation coefficients (*r*) were determined and shown in Table 5.9. The values of *r* for LMF, NL (LM-3P) and NN models were 0.85, 0.94 and 0.99 respectively. The comparison of different models for validation study are shown in Figure 5.15. The NN and NL (LM-3P) models were much closer to LOEC and showed better fit with measured data than LMF model.

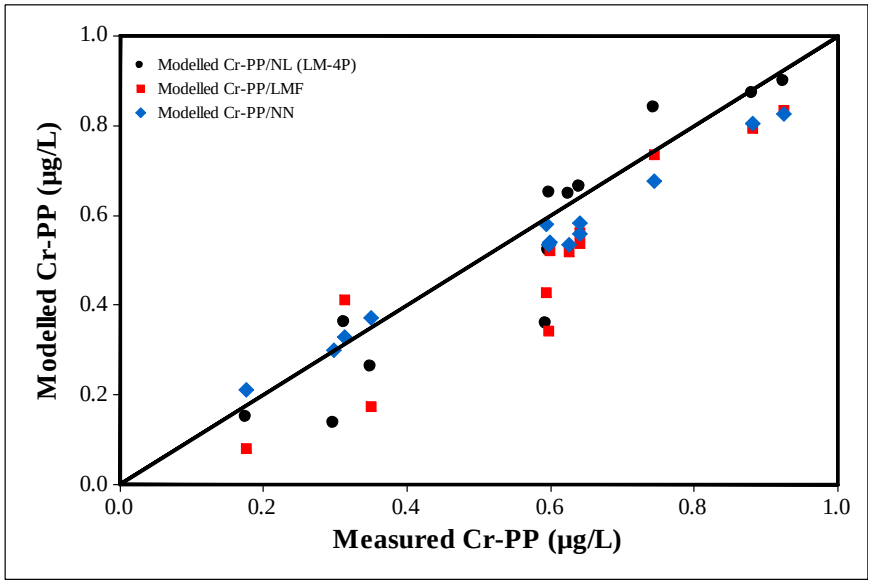


Figure 5.15: Measured and modelled concentration of Cr-PP in validation

Table 5.9: Correlation coefficients for model validation of Cr in PP

| Output | Model Type | *r* (Corr. Coef.) |
|---|---|---|
| Cr-PP | LMF | 0.85 |
| | NL (LM-4P) | 0.94 |
| | NN | 0.99 |

### 5.3.2 Modeling Cr in HWT

**Linear Model:**

Among the different linear models, the LMFI model was found to be the best and was selected (Equation 5.19). The model had the $R^2$ value of 0.92. The experimental data and predicted values were found to be consistent (Fig. 5.16d). The plot of residuals versus predicted (Fig. 5.16b) showed data randomness. No evidence of lack of fit (P >= 0.1) was also observed.

Table 5.10: Screening effects of the factors for modeling Cr-HWT

| Term | Estimate | Std Error | t Ratio | Prob>\|t\| |
|---|---|---|---|---|
| Intercept | 0.1501846 | 0.073441 | 2.04 | 0.0542 |
| Fe-HWT | 0.0160629 | 0.001125 | 14.28 | <.0001 |
| Sr-HWT | -0.000196 | 3.138e-5 | -6.25 | <.0001 |
| Pb-WDS | -0.075447 | 0.00788 | -9.57 | <.0001 |
| Mn-HWT | -0.114127 | 0.019211 | -5.94 | <.0001 |
| (Fe-HWT-71.95)*(Mn-HWT-0.96) | -0.001867 | 0.000584 | -3.20 | 0.0045 |

$$Cr-HWT=\beta_0+\beta_1 Fe-HWT+\beta_2 Sr-HWT+\beta_3 Pb-WDS+\beta_4 Mn-HWT+\beta_5(Fe-HWT-71.95)(Mn-HWT-0.96) \quad (5.19)$$

Where: $\beta_0=0.15;\ \beta_1=0.016;\ \beta_2=-0.0002;\ \beta_3=-0.075;\ \beta_4=-0.11;\ \beta_5=-0.0019$

The screening effects of the main factors (Table 5.10) and half-normal plot (Fig. 5.16a) show that Fe-HWT positively influenced the concentrations of Cr in HWT samples. The Sr-HWT, Pb-WDS, Mn-HWT and interactions of Fe and Mn in HWT had negative effects.

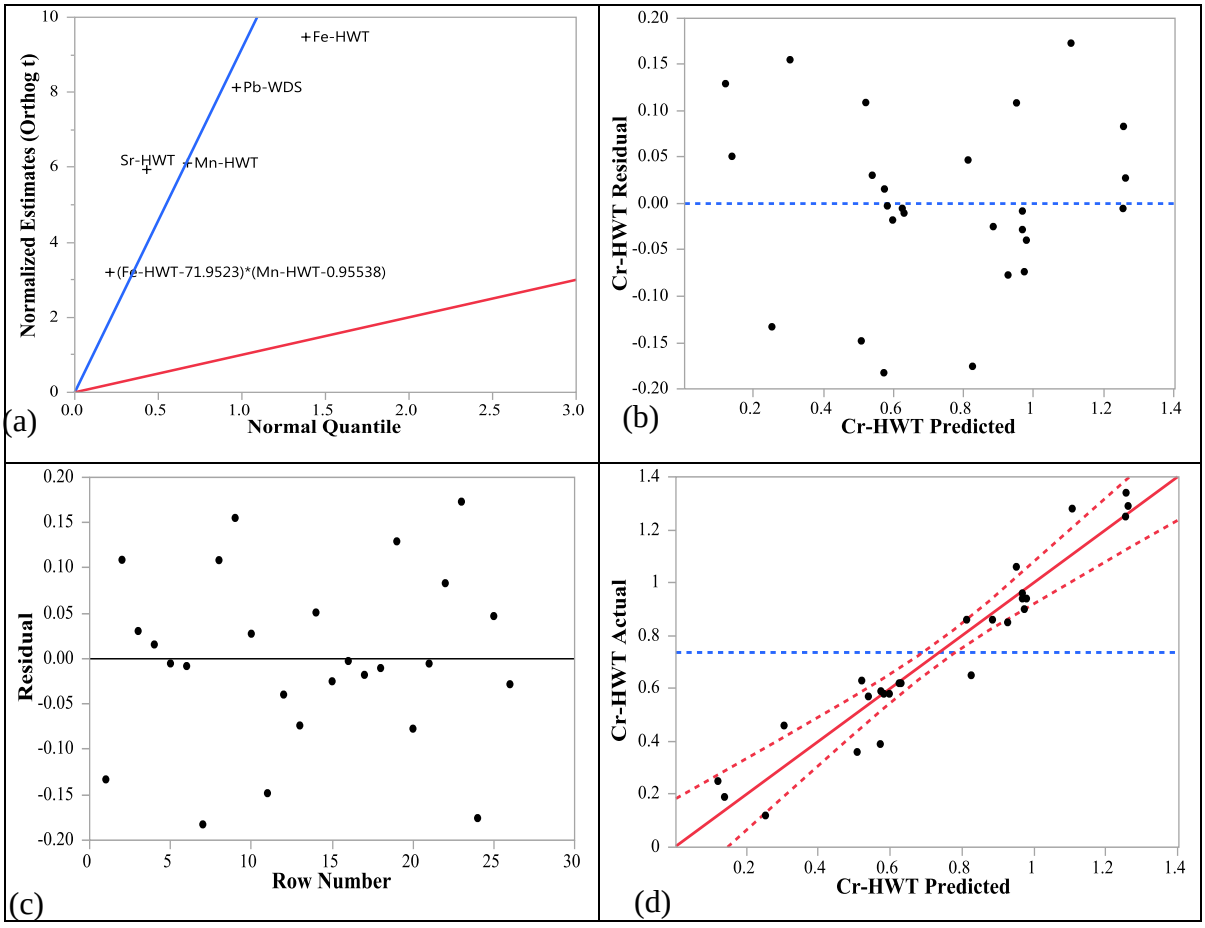


Figure 5.16: For Cr-HWT model (a) half normal plot (b) residual vs predicted (c) residual vs row number and (d) actual vs predicted data

**Nonlinear Model:**

The nonlinear model selection for Cr in HWT samples is explained in Fig. 5.17. Among the different factor, Sr in HWT showed the best performance with the Cubic model (Fig. 5.17a). The model for predicting Cr-HWT is shown in Equation 5.20 and the model had the RMSE of 0.22. The experimental data and predicted values were found to be moderately consistent (Fig. 5.17b) with $R^2$ of 0.59.

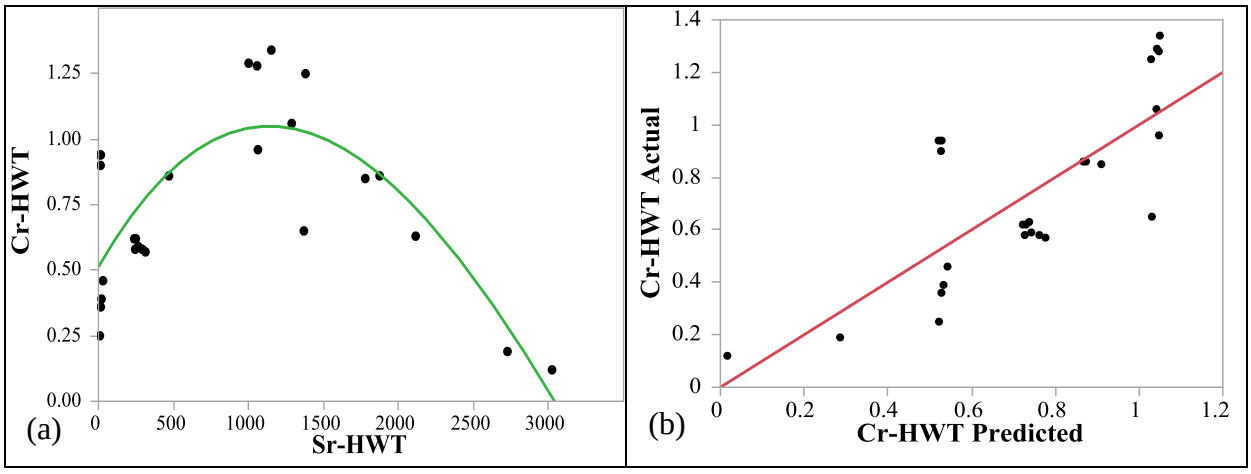


Figure 5.17: For Cubic model of Cr-HWT (a) model fitting (b) actual vs predicted plot

$$Cr-HWT = \theta_1 + \theta_2 Sr-HWT + \theta_3 (Sr-HWT)^2 + \theta_4 (Sr-HWT)^3 \qquad (5.20)$$

Where: $\theta_1 = 0.513; \theta_2 = 0.001; \theta_3 = -5.07\times10^{-7}; \theta_4 = 4.08\times10^{-11}$

**Neural Network Model:**

The NN model for predicting Cr-HWT is shown in Equation 5.21. The model had the $R^2$ value of 0.98 and RMSE of 0.05. The experimental data and predicted values were found to be consistent (Fig. 5.18). The Equations 5.22-5.24 showed that Pb-WDS, Cr-WDS, Fe-HWT and Mn-HWT had influence on the occurrence of Cr in HWT.

$$Cr-HWT = 1.02 + (-0.17 \times H1) + (-0.46 \times H2) + (-0.46 \times H3) \quad (5.21)$$

$$H1 = \tanh[0.5 \times \{-3.47 + (0.07\ Fe\text{-}HWT) + (-0.71\ Mn\text{-}HWT) + (-0.15\ Pb\text{-}WDS) + (0.97\ Cr\text{-}WDS)\}] \quad (5.22)$$

$$H2 = \tanh[0.5 \times \{8.19 + (-0.09\ Fe\text{-}HWT) + (2.88\ Mn\text{-}HWT) + (0.17\ Pb\text{-}WDS) + (-7.09\ Cr\text{-}WDS)\}] \quad (5.23)$$

$$H3 = \tanh[0.5 \times \{3.81 + (-0.07\ Fe\text{-}HWT) + (-0.38\ Mn\text{-}HWT) + (0.55\ Pb\text{-}WDS) + (1.55\ Cr\text{-}WDS)\}] \quad (5.24)$$

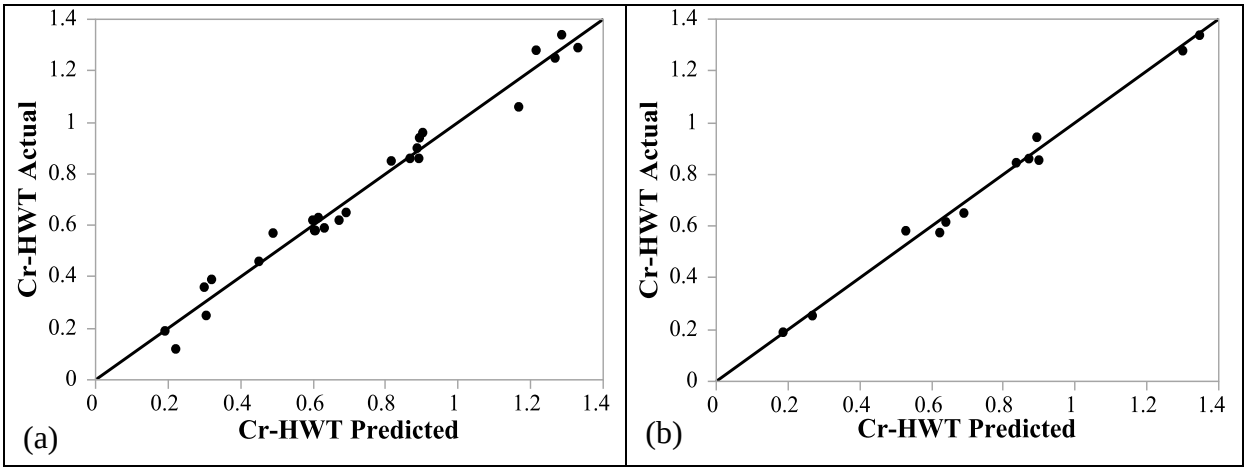


Figure 5.18: Actual vs predicted plot of Cr-HWT for (a) data training (b) validation of NN model

### 5.3.2.1 Model Comparison for Cr in HWT

The comparison of the models for predicting Cr in HWT are shown in Figure 5.19. The NN model showed better performance ($R^2$ = 0.98; RMSE = 0.05) than the LMFI model ($R^2$ = 0.92; RMSE = 0.107). The NN model used the background metal (i.e., Cr in WDS) in addition to other factors of the LMFI model, which might have improved its performance (Table 5.11). The NL model (CBM) showed poor performance than the NN and LMF models, due to the single input factor (e.g., Sr-HWT), while Cr in HWT could be affected by several factors. All the models had better fits with

measured data for the whole range of concentrations of Cr, while for NN model, the measured data were much closer to the LOEC. The NN model is the model of choice for predicting Cr in HWT.

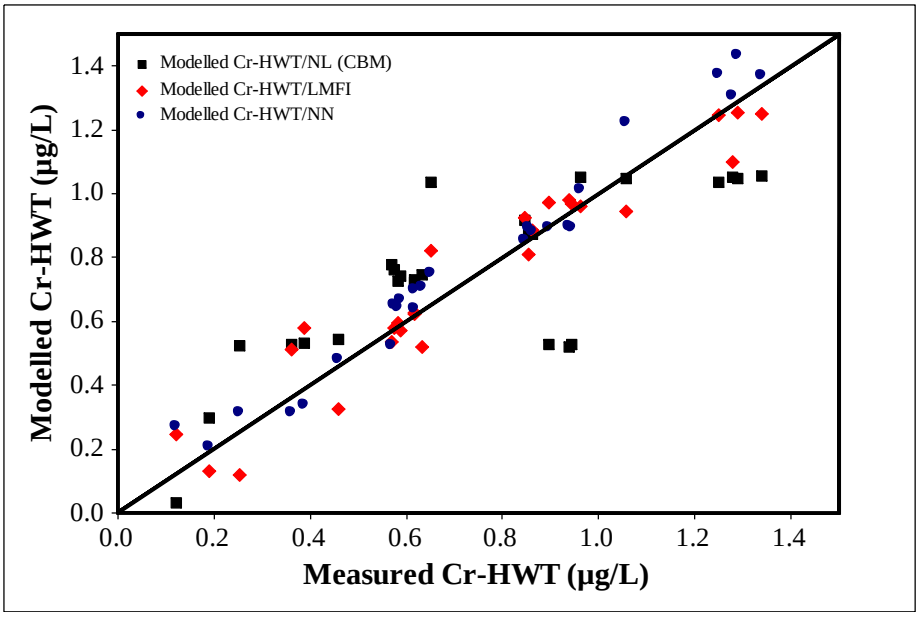


Figure 5.19: Measured and modeled concentration of Cr in HWT

(CBM: Cubic model; LMFI: Main factors, interaction and higher order terms; NN: Neural network model)

Table 5.11: Comparison of different models for Cr in HWT

| Output | Model Type | Parameters | $R^2$ | RMSE |
|---|---|---|---|---|
| Cr-HWT | LMFI | Fe-HWT, Mn-HWT, Pb-WDS, Sr-HWT | 0.92 | 0.107 |
| | NL (CBM) | Sr-HWT | 0.59 | 0.22 |
| | NN | Fe-HWT, Mn-HWT, Pb-WDS, Cr-WDS | 0.98 | 0.05 |

### 5.3.2.2 Model Validation for Cr in HWT

The predictive models for Cr in HWT were validated using an additional set of data, which were not used in model development. The average concentrations of Cr-HWT from the LMFI, NL (CBM) and NN models were 0.78, 0.80 and 0.86 µg/L respectively, and the ranges were 0.11-1.24, 0.30-1.05 and 0.20-1.53 µg/L respectively. The average of the measured concentration of Cr-HWT was 0.79 µg/L with the range of 0.19-1.34 µg/L. From the plot of predicted vs. measured data, the values of correlation coefficients (*r*) were determined and shown in Table 5.12. The values of *r* for LMFI, NL (CBM) and NN models were 0.98, 0.77 and 0.99 respectively. The comparison of different models for validation study are shown in Figure 5.20. The LMFI and NN models were much closer to LOEC and showed better fit with measured data than NL (CBM) model.

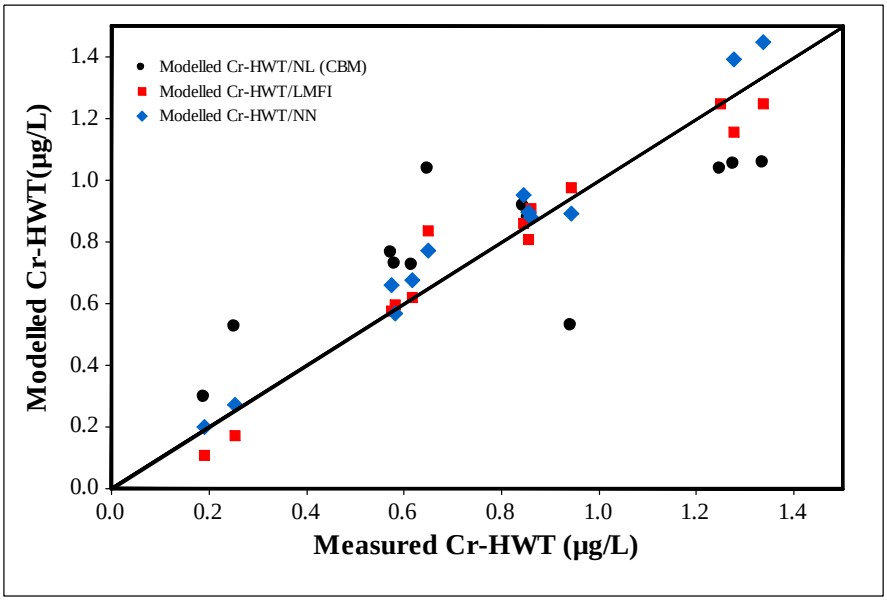


Figure 5.20: Measured and modelled concentration of Cr-HWT in validation

Table 5.12: Correlation coefficients for model validation of Cr in HWT

| Output | Model Type | r (Corr. Coef.) |
|---|---|---|
| Cr-HWT | LMFI | 0.98 |
| | CBM | 0.77 |
| | NN | 0.99 |

For the Cr-PP and Cr-HWT models, the NN models were the best while the NL models showed poor performance. The nonlinear models were developed using the most important single factors, which might be the main reason of the poor performance. Although the single factor models were easy to use, the relative poor performances were likely to inhibit their applications. Most of the models for Cr in PP and HWT showed moderate to excellent predictive capacities. The iron pipe corrosion by-products contained high level of V along with Cr, Fe and Mn, which could have increase Cr in PP. In addition, the physical and chemical disturbances of pipe inner surface might have released Cr into PP. Cr could have also been originated from leaching of WDS materials and reactions in plumbing premise [116]. The stagnation period had significant effects on Cr release from pipe network. The corrosion of nichrome coil (alloys of nickel, chromium, and iron) and stainless steel could have served as the potential sources of Cr in HWT [102]. The dissolution of hard scale deposits on the heater wall along with other corroded metals (i.e., Cr, Sr) might have caused the release of Cr in HWT along with Sr. Cr in HWT was also affected by Cr in WDS.

## 5.4 Models for Predicting Copper (Cu)

### 5.4.1 Modeling Cu in PP

**Linear Model:**

Figure 5.21 summarizes the procedure of selecting parameters and adequacy check for modeling copper (Cu) concentrations in the PP samples. Among the different linear models, the LMFI model was found to be the best and was selected (Equation 5.25). The model had the $R^2$ value of 0.89. The experimental data and predicted values were found to be consistent (Fig. 5.21d). The plot of residuals versus predicted values (Fig. 5.21b) showed the data randomness. The plot of residuals versus row number (Fig. 5.21c) confirmed that the residuals were uncorrelated. No evidence of lack of fit (P >= 0.1) was also observed. The screening effects of the main factors and main factors with interactions (Table 5.13), and the half-normal plot (Fig. 5.21a) showed that V-WDS, temperature and total residual chlorine in PP, interactions of V-WDS with T-PP and TCl-PP positively influenced the concentrations of Cu in PP.

Table 5.13: Screening effects of the factors for modeling Cu-PP

| Term | Estimate | Std Error | t Ratio | Prob>\|t\| |
|---|---|---|---|---|
| Intercept | -6.215899 | 0.902447 | -6.89 | <.0001 |
| V-WDS | 0.6225374 | 0.097251 | 6.40 | <.0001 |
| T-PP | 0.0649511 | 0.014351 | 4.53 | 0.0003 |
| (V-WDS-4.17)*(T-PP-26.8) | 0.0136735 | 0.002298 | 5.95 | <.0001 |
| (V-WDS-4.17)*(TCl-PP-0.041) | 27.124743 | 4.507237 | 6.02 | <.0001 |
| TCl-PP | 110.91148 | 18.57693 | 5.97 | <.0001 |

$$Cu-PP=\beta_0+\beta_1 V-WDS+\beta_2 T-PP+\beta_3(V-WDS-4.17)(T-PP-26.8)+\beta_4(V-WDS-4.17)(TCl-PP-0.04)+\beta_5 TCl-PP \quad (5.25)$$

Where: $\beta_0=-6.22;\ \beta_1=0.62;\ \beta_2=0.065;\ \beta_3=0.014;\ \beta_4=27.12;\ \beta_5=110.91$

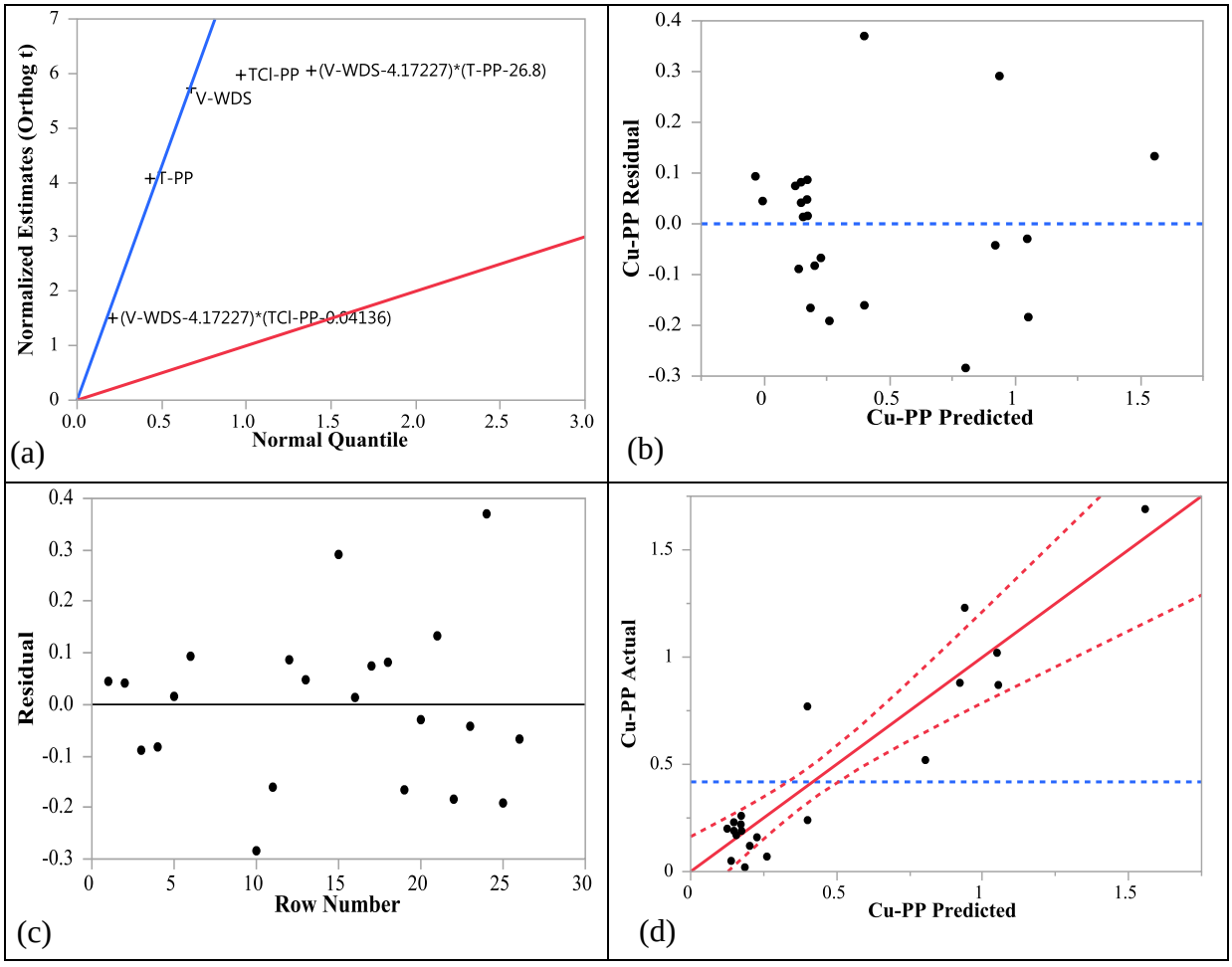


Figure 5.21: For Cu-PP model (a) half normal plot (b) residual vs predicted (c) residual vs row number and (d) actual vs predicted data

**Neural Network Model:**

The NN model for predicting Cu-PP is shown in Equation 5.26. The model had the $R^2$ and RMSE values of 0.84 and 0.20 respectively. The experimental data and predicted values were found to be consistent (Fig. 5.22). The Equation of hidden nodes (Equation 5.27-5.29) showed that Cu-WDS, Fe-WDS and Zn-PP had influence on the occurrence of Cu in PP.

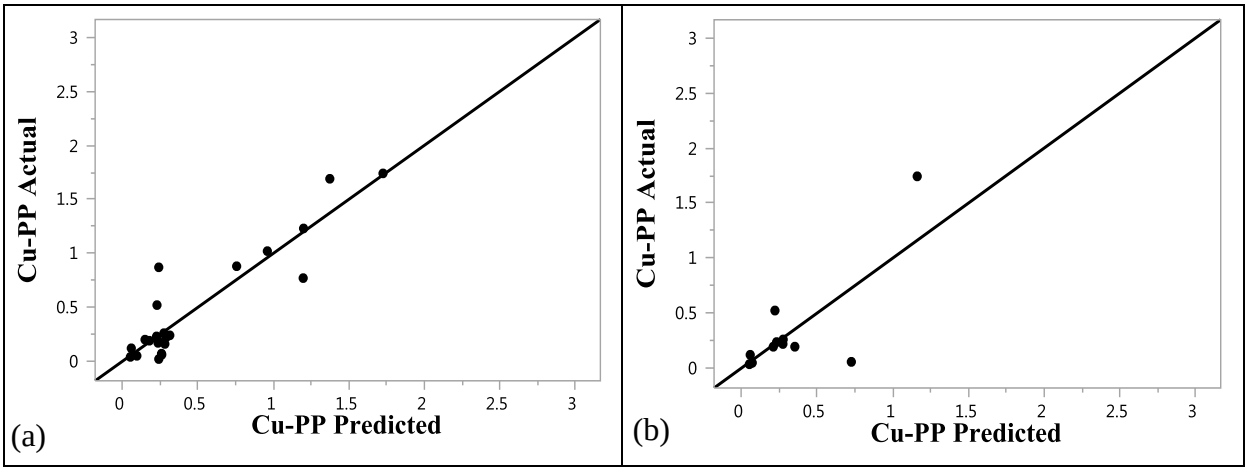


Figure 5.22: Actual vs predicted plot of Cu-PP for (a) data training (b) validation of NN model

$$Cu-PP = 2.34 + (3.58 \times \mathrm{H1}) + (\text{-}2.71 \times \mathrm{H2}) + (-3.92 \times \mathrm{H3}) \quad (5.26)$$

$$\mathrm{H1} = \tanh[0.5 \times \{2.27 + (\text{-}0.04\,\mathrm{Zn}\text{-}\mathrm{PP}) + (\text{-}0.066\,Fe-WDS + (1.35\,Cu-WDS)\}] \quad (5.27)$$

$$\mathrm{H2} = \tanh[0.5 \times \{3.44 + (0.079\,\mathrm{Zn}\text{-}\mathrm{PP}) + (\text{-}0.075\,Fe-WDS + (0.174\,Cu-WDS)\}] \quad (5.28)$$

$$\mathrm{H3} = \tanh[0.5 \times \{0.18 + (\text{-}0.07\,\mathrm{Zn}\text{-}\mathrm{PP}) + (0.0047\,Fe-WDS + (0.84\,Cu-WDS)\}] \quad (5.29)$$

### 5.4.1.1 Model Comparison for Cu in PP

The comparison of the models for predicting Cu in PP are shown in Figure 5.23. The LMFI model had $R^2$ value of 0.89, while the NN model had $R^2$ of 0.84 (Table 5.14). The lower RMSE value of LMFI (RMSE=0.177) compared to NN model (RMSE=0.20) also indicates that LMFI model is statistically better than NN model. The LMFI model used interaction of parameters, which might have improved the model efficiency (Table 5.14). None of the NL model fit with any parameters. The selected models had better fits with measured data for lower concentrations of Cu (<1.5 µg/L), where the LMFI model is much closer to the LOEC. As such, the LMFI model is the model of choice for predicting Cu in PP.

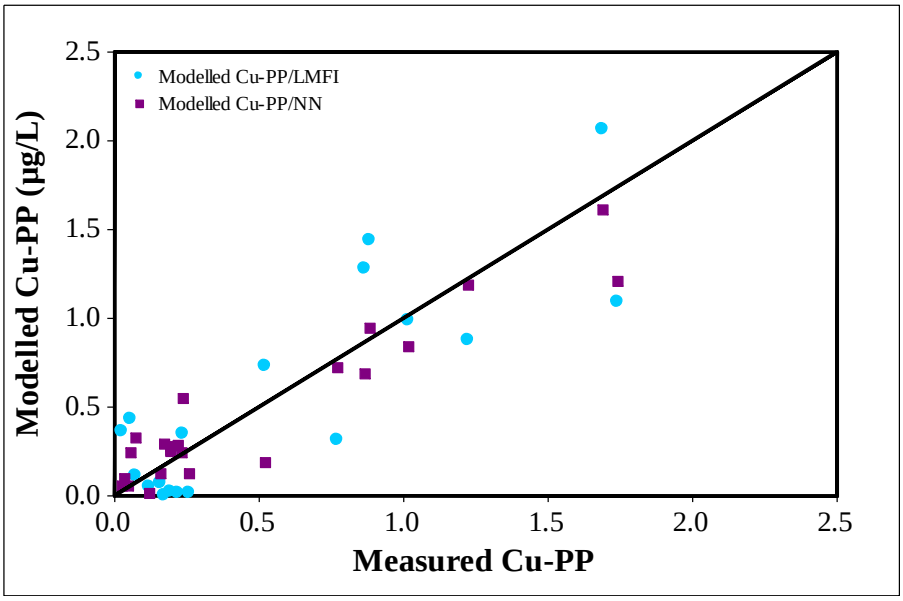


Figure 5.23: Measured and modeled concentration of Cu in PP

(LMFI: Main factors, interaction and higher order terms model; NN: Neural network model)

Table 5.14: Comparison of different models for Cu in PP

| Output | Model Type | Parameters | $R^2$ | RMSE |
|---|---|---|---|---|
| Cu-PP | LMFI | V-WDS, T-PP, TCl-PP | 0.89 | 0.177 |
| | NN | Fe-WDS, Cu-WDS, Zn-PP | 0.84 | 0.20 |

### 5.4.1.2 Model Validation for Cu in PP

The predictive models for Cu in PP were validated using an additional set of data, which were not used in model development. The average concentrations of Cu-PP from the LMFI and NN models were 3.12 and 0.18 µg/L respectively, and the ranges were 0.01-36.49 and 0.01-0.68 µg/L respectively. The average of measured concentrations of Cu-PP was 4.30 µg/L with the range of 0.035-38.28 µg/L. From the plot of predicted vs. measured data, the values of correlation coefficients (*r*) were determined and shown in Table 5.15. The values of *r* for LMFI and NN models were 0.48 and 0.45 respectively. The comparison of different models for validation study are shown in Figure 5.24. Both of the LMFI and NN models were much scattered from LOEC and did not show good predictive capacity.

Table 5.15: Correlation coefficients for model validation of Cu in PP

| Output | Model Type | *r* (Corr. Coef.) |
|---|---|---|
| Cu-PP | LMFI | 0.48 |
| | NN | 0.45 |

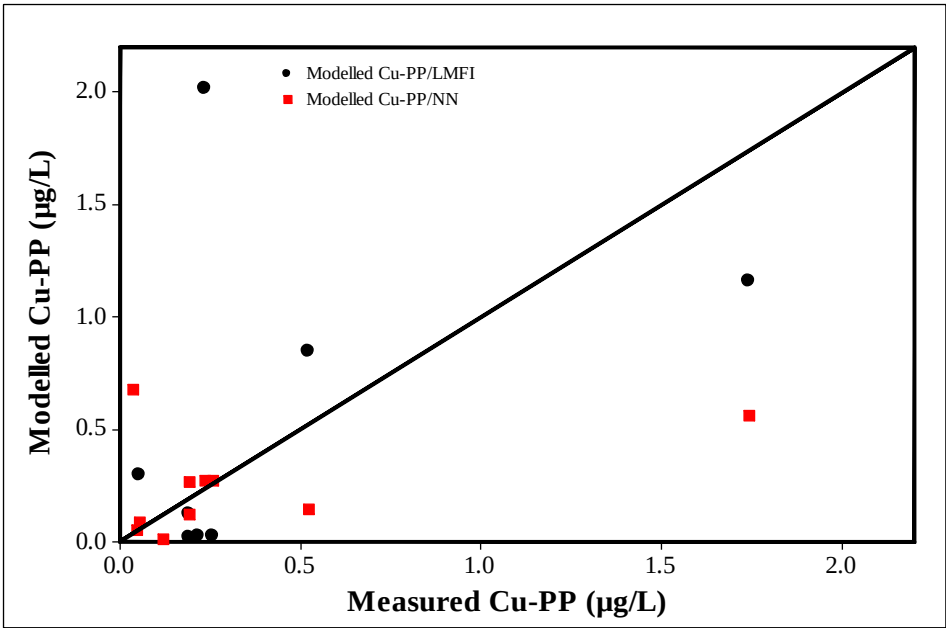


Figure 5.24: Measured and modelled concentration of Cu-PP in validation

## 5.4.2 Modeling Cu in HWT

**Linear Model:**

The procedure of selecting parameters and adequacy check for the predictive model of Cu in HWT samples is illustrated in Fig. 5.25. Table 5.16 summarizes the ANOVA with significant factors (p value < 0.01). Among the different linear models, the LMF model was found to be the best and was selected (Equation 5.30). The model had the $R^2$ value of 0.93. The experimental data and predicted values were found to be consistent (Fig. 5.25d). The plot of residuals versus predicted (Fig. 5.25b) showed data randomness. The plot of residuals versus row number (Fig. 5.25c) confirmed that the residuals were uncorrelated. No evidence of lack of fit (P >= 0.1) was also observed.

Table 5.16: Screening effects of the factors for modeling Cu-HWT

| Term | Estimate | Std Error | t Ratio | Prob>\|t\| |
|---|---|---|---|---|
| Intercept | 0.1603255 | 0.110408 | 1.45 | 0.1620 |
| Na-HWT | $2.6868\times10^{-6}$ | $2.713\times10^{-7}$ | 9.90 | <.0001 |
| DOC-HWT | -0.271858 | 0.075785 | -3.59 | 0.0018 |
| UV-HWT | 104.75572 | 25.33363 | 4.14 | 0.0005 |
| Mn-HWT | 0.1725228 | 0.071482 | 2.41 | 0.0255 |

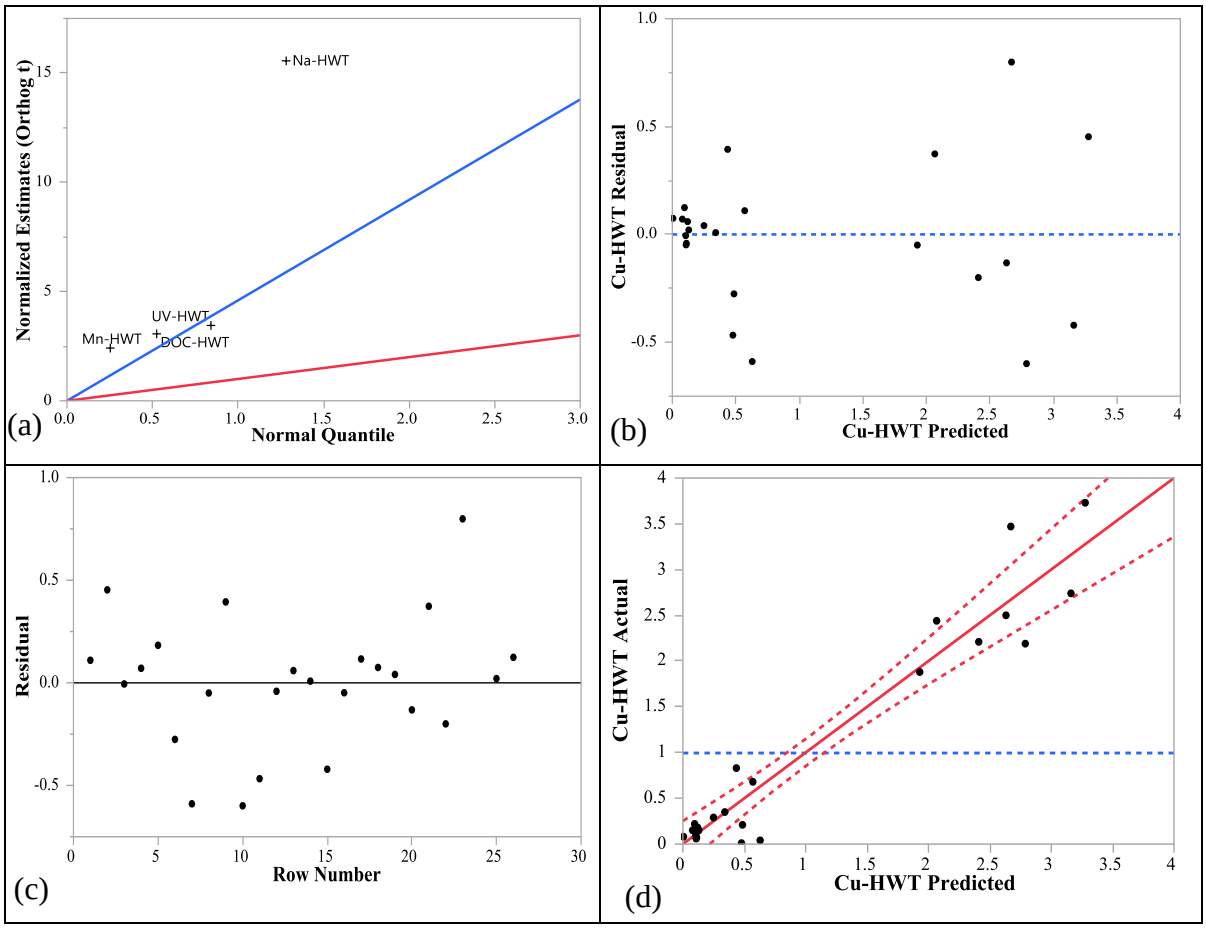


Figure 5.25: For Cu-HWT model (a) half normal plot (b) residual vs predicted (c) residual vs row number and (d) actual vs predicted data

$$Cu-HWT = \beta_0 + \beta_1 Na-HWT + \beta_2 DOC-HWT + \beta_3 UV-HWT + \beta_4 Mn-HWT \qquad (5.30)$$

Where: $\beta_0 = 0.16; \beta_1 = 2.69 \times 10^{-6}; \beta_2 = -0.27; \beta_3 = 104.76; \beta_4 = 0.173$

The screening effects of the main factors (Table 5.16) and half-normal plot (Fig. 5.25a) shows that Na-HWT, UV-HWT and Mn-HWT positively influenced the occurrence of Cu in HWT samples while DOC-HWT had negative influence.

**Neural Network Model:**

The NN model for predicting Cu-HWT is shown in Equation 5.31. The model had the $R^2$ value of 0.93 and RMSE of 0.31. The experimental data and predicted values were found to be consistent (Fig. 5.26). The Equations 5.32-5.34 showed that DOC-HWT, UV-HWT and Mn-HWT had influence on the occurrence of Cu in HWT.

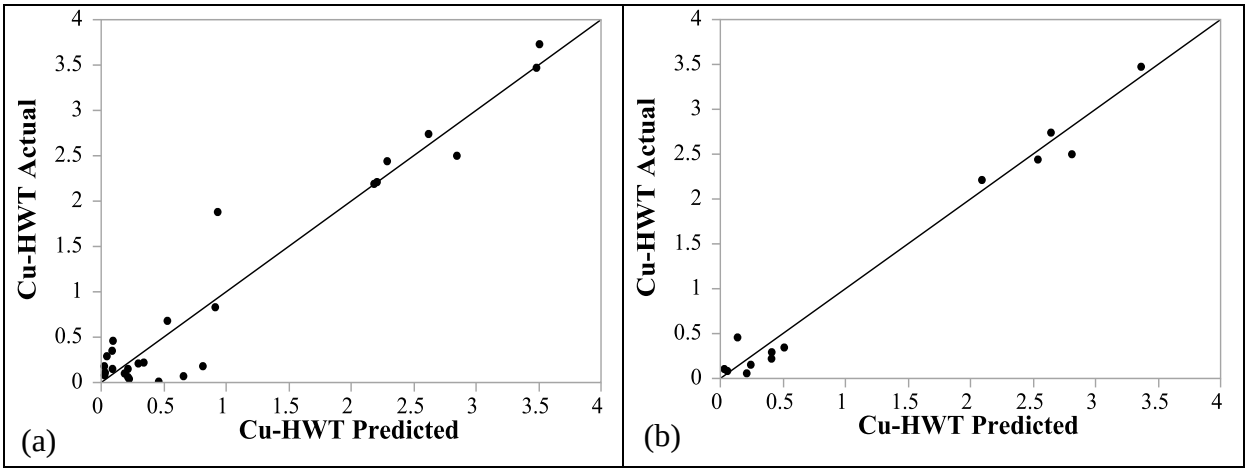


Figure 5.26: Actual vs predicted plot of Cu-HWT for (a) data training (b) validation of NN model

$$Cu - HWT = 1.86 + (-1.71 \times \mathrm{H1}) + (1.85 \times \mathrm{H2}) + (1.71 \times \mathrm{H3}) \quad (5.31)$$

$$\mathrm{H1} = \tanh[0.5 \times \{-9.58 + (4.06\,\mathrm{DOC\text{-}HWT}) + (-34.08\,\mathrm{UV\text{-}HWT}) + (7.30\,\mathrm{Mn\text{-}HWT})\}] \quad (5.32)$$

$$\mathrm{H2} = \tanh[0.5 \times \{-13.62 + (11.38\,\mathrm{DOC\text{-}HWT}) + (587.49\,\mathrm{UV\text{-}HWT}) + (2.83\,\mathrm{Mn\text{-}HWT})\}] \quad (5.33)$$

$$\mathrm{H3} = \mathrm{ttanh}[0.5 \times \{0.69 + (-10.40\,\mathrm{DOC\text{-}HWT}) + (88.48\,\mathrm{UV\text{-}HWT}) + (7.33\,\mathrm{Mn\text{-}HWT})\}] \quad (5.34)$$

### 5.4.2.1 Model Comparison for Cu in HWT

The comparison of the models for predicting Cu in HWT are shown in Figure 5.27. The NN model and LMF model for predicting Cu in HWT had the same $R^2$ of 0.93 (Table 5.17). The RMSE values for the NN and LMF models are also similar (RMSE = 0.31 and 0.352 respectively) showing fairly consistent predictive performance. None of the NL model fitted with any parameters. All the models had better fits for lower and mid-level concentrations of Cu. For the NN model, the measured data were much closer to the LOEC. The NN model is preferred over the other model for predicting Cu in HWT.

Table 5.17: Comparison of different models for Cu in HWT

| Output | Model Type | Parameters | $R^2$ | RMSE |
|---|---|---|---|---|
| Cu-HWT | LMF | UV-HWT, DOC-HWT, Mn-HWT, Na-HWT | 0.93 | 0.352 |
| | NN | UV-HWT, DOC-HWT, Mn-HWT | 0.93 | 0.31 |

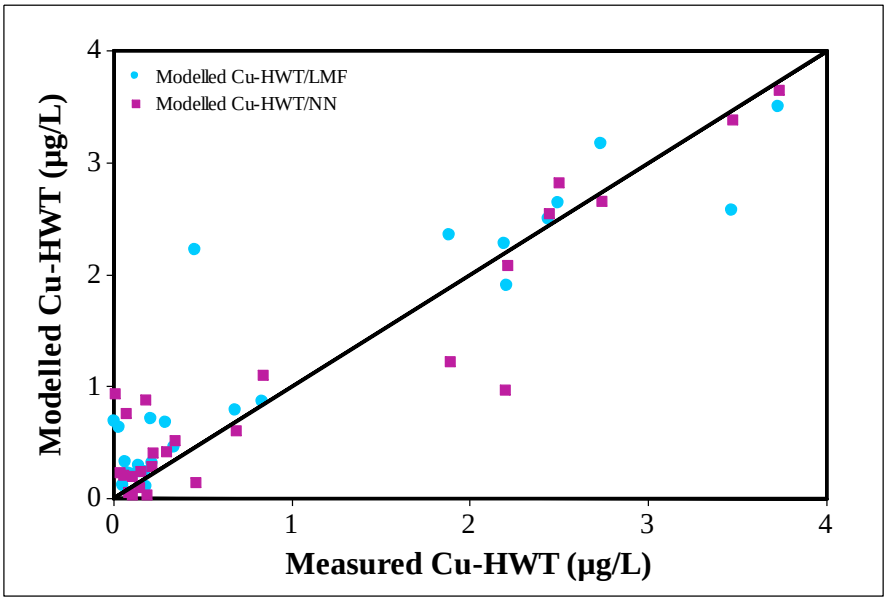


Figure 5.27: Measured and modeled concentration of Cu in HWT

(LMF: Main factors linear model; NN: Neural network model)

### 5.4.2.2 Model Validation for Cu in HWT

The predictive models for Cu in HWT were validated using an additional set of data, which were not used in model development. The average concentrations of Cu-HWT from the LMF and NN models were 1.30 and 1.19 µg/L respectively, and the ranges were 0.11-3.17 and 0.03-3.38 µg/L respectively. The average of measured concentrations of Cu-HWT was 1.16 µg/L with the range of 0.06-3.47 µg/L. From the plot of predicted vs. measured data, the values of correlation coefficients ($r$) were determined and shown in Table 5.18. The values of $r$ for LMF and NN models were 0.89 and 0.99 respectively. The comparison of different models for validation study are shown in Figure 5.28. Both of the LMF and NN models were much closer to LOEC and showed strong fits with measured data.

Table 5.18: Correlation coefficients for model validation of Cu in HWT

| Output | Model Type | r (Corr. Coef.) |
|---|---|---|
| Cu-HWT | LMF | 0.89 |
| | NN | 0.99 |

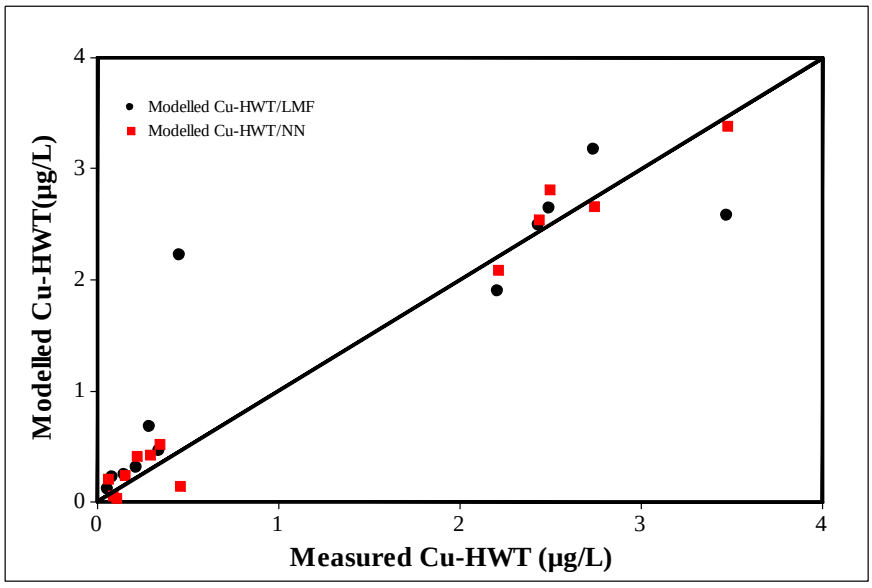


Figure 5.28: Measured and modelled concentration of Cu-HWT in validation

Most of the models for Cu in PP and HWT showed moderate to excellent predictive capacities. The iron pipe corrosion byproducts contained Cu, V, Fe and Zn. Due to the physical and chemical disturbances (i.e., changing temperature, TCl), Cu was released into PP along with other metals [115]. Cu in PP had significant effect form Cu in WDS. Cu might also have been originated from copper pipes and fixtures due to dissolution in the household plumbing system. Such dissolution was affected by the stagnation period [117]. It was indicated that Cu in HWT was not significantly

influenced by the Cu in WDS. Corrosion of brass fittings and other plumbing fixtures were some of the potential sources of Cu in HWT. Scale deposits on the heater wall along with other corroded metals (i.e., Mn, Cu and Fe) might also have served as the sources of Cu in HWT. Following the usage of hot water, the scales were sloughed off and released into hot water [103].

## 5.5 Models for Predicting Mercury (Hg)

### 5.5.1 Modeling Hg in PP

**Linear Model:**

Figure 5.29 summarizes the procedure of selecting parameters and adequacy check for developing models to predict Hg in PP. Table 5.19 summarizes the ANOVA with significant factors (p value < 0.01). Among the different linear models, the LMF model was found to be the best and was selected (Equation 5.35). The model had the $R^2$ value of 0.61. The experimental data and predicted values were found to be moderately consistent (Fig. 5.29d). The plot of residuals versus predicted values (Fig. 5.29b) showed the randomness of residuals. No evidence of lack of fit (P >= 0.1) was also observed.

The screening effects of the main factors (Table 5.19) and half-normal plot (Fig. 5.29a) showed that Hg-WDS and Sr-WDS influenced positively on the concentrations of Hg in PP while UV-PP and Fe-WDS had negative effects.

Table 5.19: Screening effects of the factors for modeling Hg-PP

| Term | Estimate | Std Error | t Ratio | Prob>\|t\| |
|---|---|---|---|---|
| Intercept | 2.5290886 | 0.731819 | 3.46 | 0.0025 |
| Fe-WDS | -0.033035 | 0.011158 | -2.96 | 0.0077 |
| Sr-WDS | 0.0011856 | 0.000539 | 2.20 | 0.0398 |
| Hg-WDS | 0.5864129 | 0.270337 | 2.17 | 0.0423 |
| UV-PP | -218.3493 | 81.10201 | -2.69 | 0.0140 |

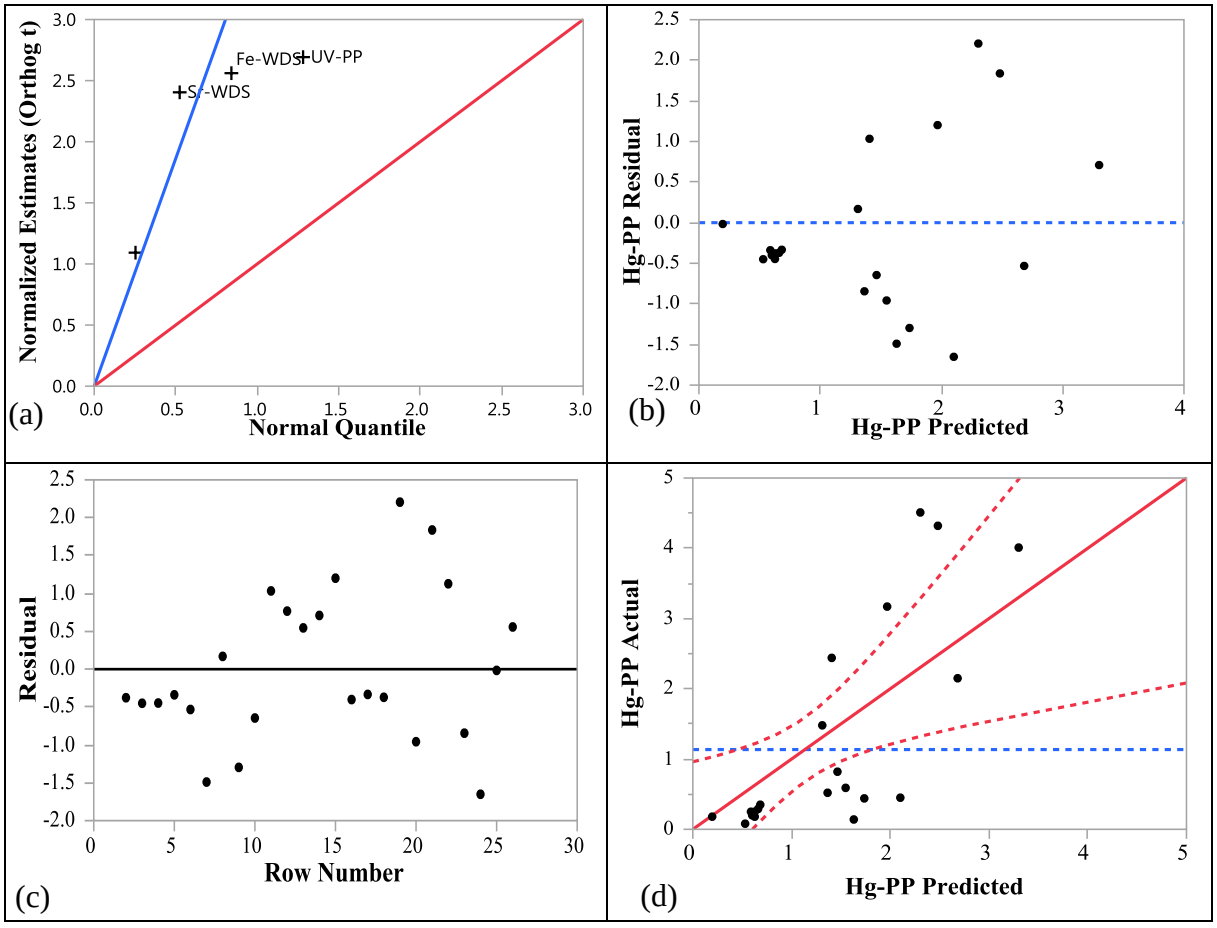


Figure 5.29: For Hg-PP model (a) half normal plot (b) residual vs predicted (c) residual vs row number and (d) actual vs predicted data

$$Hg-PP = \beta_0 + \beta_1 Hg-WDS + \beta_2 Fe-WDS + \beta_3 UV-PP + \beta_4 Sr-WDS \quad (5.35)$$

Where: $\beta_0 = 2.53$; $\beta_1 = 0.59$; $\beta_2 = -0.03$; $\beta_3 = -218.35$; $\beta_4 = 0.0012$

**Neural Network Model:**

The best NN model for predicting Hg-PP is shown in Equation 5.36. The model had the $R^2$ value of 0.93 and RMSE of 0.37. The experimental data and predicted values were found to be consistent (Fig. 5.30). The Equation of hidden nodes (Equation 5.37-5.39) showed that Hg-WDS, Fe-WDS and Sr-WDS had influence on the concentrations of Hg in PP.

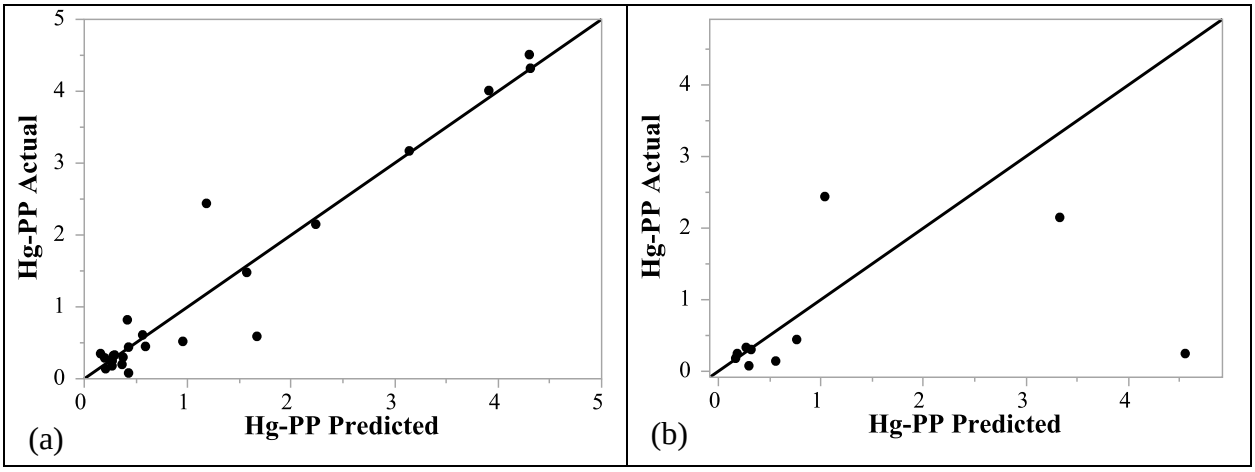


Figure 5.30: Actual vs predicted plot of Hg-PP for (a) data training (b) validation of NN model

$$Hg-PP = 6.326 + (16..285 \times \mathrm{H1}) + (10.652 \times \mathrm{H2}) + (-13.528 \times \mathrm{H3}) \quad (5.36)$$

$$\mathrm{H1} = \tanh[0.5 \times \{-3.15 + (0.481\,\mathrm{Hg\text{-}WDS}) + (0.055\,Fe-WDS + (-0.003\,Sr-WDS)\}] \quad (5.37)$$

$$H2 = \tanh[0.5 \times \{2.907 + (-1.33\,\mathrm{Hg}\text{-}\mathrm{WDS}) + (-0.049\,Fe - WDS + (0.003\,Sr - WDS)\}] \quad (5.38)$$

$$H3 = \tanh[0.5 \times \{-0.887 + (-0.403\,\mathrm{Hg}\text{-}\mathrm{WDS}) + (0.033\,Fe - WDS + (-0.0012\,Sr - WDS)\}] \quad (5.39)$$

#### 5.5.1.1 Model Comparison for Hg in PP

The comparison of the models for predicting Hg in PP are shown in Figure 5.31. The NN model showed better performance ($R^2$ = 0.93; RMSE = 0.37) than the LMF model ($R^2$ = 0.61; RMSE = 1.06). The LMF model used one additional factor (i.e., UV-PP) than the NN model (Table 5.20). None of the NL models fit with any parameters. All models showed better fits with measured data for lower concentrations of Hg (<1.0 µg/L), while for NN model, the measured data were much closer to the LOEC. The NN model is the model of choice for predicting Hg in PP.

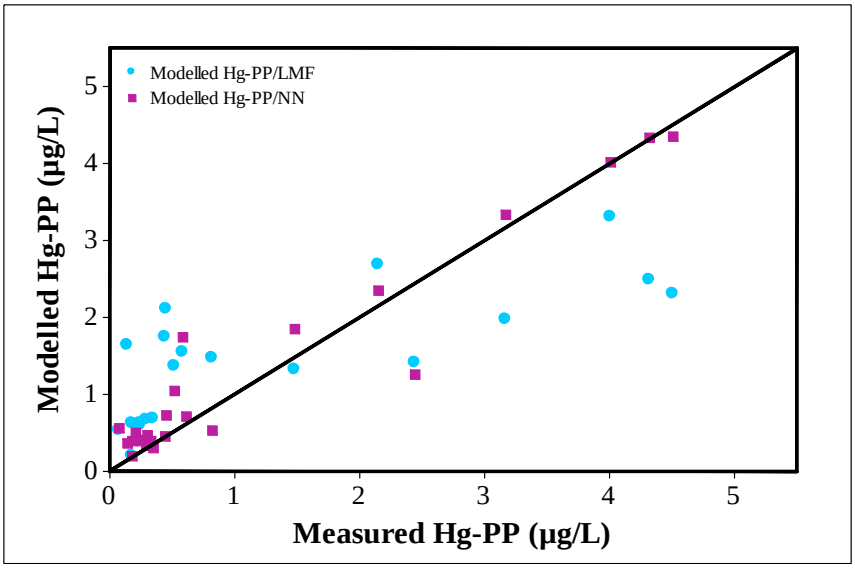


Figure 5.31: Measured and modeled concentration of Hg in PP

(LMF: Main factors linear model; NN: Neural Network)

Table 5.20: Comparison of different models for Hg in PP

| Output | Model Type | Parameters | $R^2$ | RMSE |
|---|---|---|---|---|
| Hg-PP | LMF | Hg-WDS, Fe-WDS, Sr-WDS, UV-PP | 0.61 | 1.059 |
| | NN | Hg-WDS, Fe-WDS, Sr-WDS | 0.93 | 0.37 |

### 5.5.1.2 Model Validation for Hg in PP

The predictive models for Hg in PP were validated using an additional set of data, which were not used in model development. The average concentrations of Hg-PP from the LMF and NN models were 0.79 and 4.33 µg/L respectively and the ranges were 0.02-3.90 and 0.31-19.77 µg/L respectively. The average of measured concentration of Hg-PP was 2.64 µg/L with the range of 0.08-25.40 µg/L. This maximum concentration of Hg in PP (25.40 µg/L) was considered as outlier in boxplot (Fig. 4.2). From the plot of predicted vs. measured data, the values of correlation coefficients (*r*) were determined and shown in Table 5.21. The values of *r* for LMF and NN models were 0.50 and 0.71 respectively. The comparison of different models for validation study are shown in Figure 5.32. The NN model output were much closer to LOEC and showed better fit with measured data than LMF model.

Table 5.21: Correlation coefficients for model validation of Hg in PP

| Output | Model Type | *r* (Corr. Coef.) |
|---|---|---|
| Hg-PP | LMF | 0.50 |
| | NN | 0.71 |

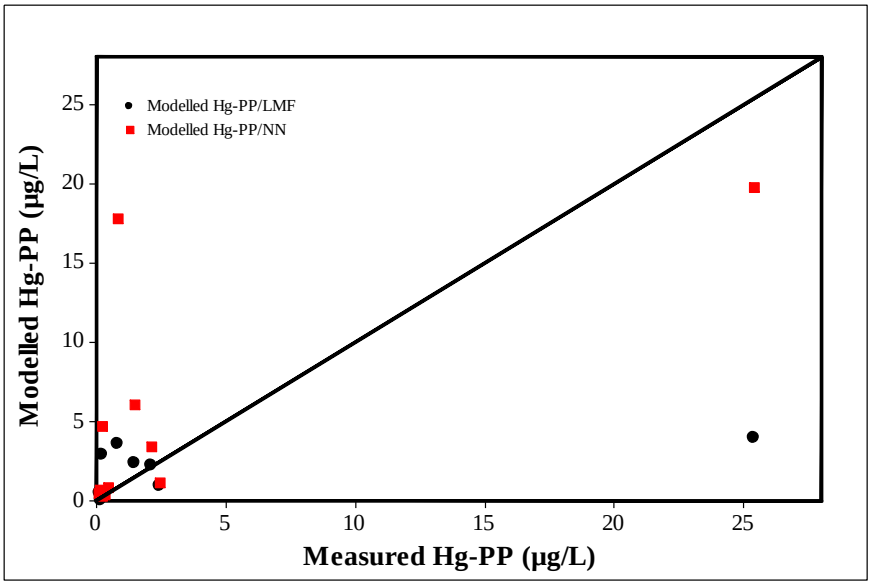


Figure 5.32: Measured and modelled concentration of Hg-PP in validation

### 5.5.2 Modeling Hg in HWT

**Nonlinear Model:**

The NL model selection for Hg in HWT samples are explained in Fig. 5.33 and Fig. 5.34. Among the different factors, Zn in WDS showed best performance with the four-parameter Weibull model (Fig. 5.33a). The model for predicting Hg-HWT with NL (WM-4P) is shown in Equation 5.40 and the model had the RMSE of 1.43. The experimental data and predicted values ($R^2$ = 0.71) were found to be fairly consistent (Fig. 5.33b).

$$Hg-HWT=\theta_1-\theta_2 Exp(-Exp[\theta_3+\theta_4 Ln\{Zn-WDS\}]) \quad (5.40)$$

Where: $\theta_1=57.07;\ \theta_2=56;\ \theta_3=-7.88;\ \theta_4=1.49$

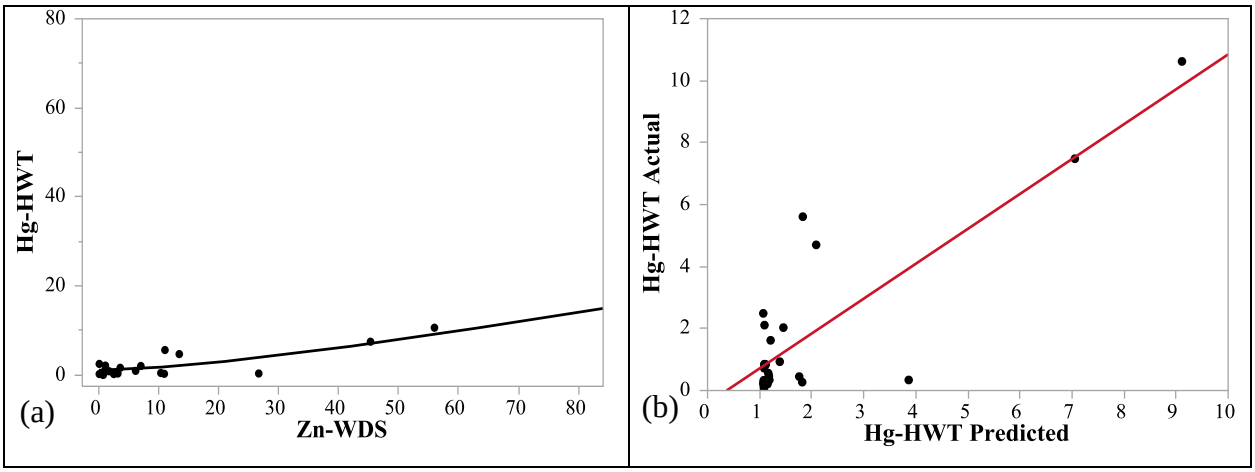


Figure 5.33: For four-parameter Weibull model of Hg-HWT (a) model fitting (b) actual vs predicted plot

In another nonlinear model, Cr-HWT showed similar performance with the four-parameter Biexponential model (Fig. 5.34a). The model for predicting Hg-HWT with NL (BEM-4P) was developed and presented in Equation 5.41, and the model had the RMSE of 1.63. The experimental data and predicted values ($R^2 = 0.62$) were found to be fairly consistent (Fig. 5.34b).

$$Hg-HWT = \theta_1 Exp(-\theta_2 Cr-HWT) + \theta_3 Exp(-\theta_4 Cr-HWT) \quad (5.41)$$

Where: $\theta_1 = 0.028; \theta_2 = -3.63; \theta_3 = 21.29; \theta_4 = 7.09$

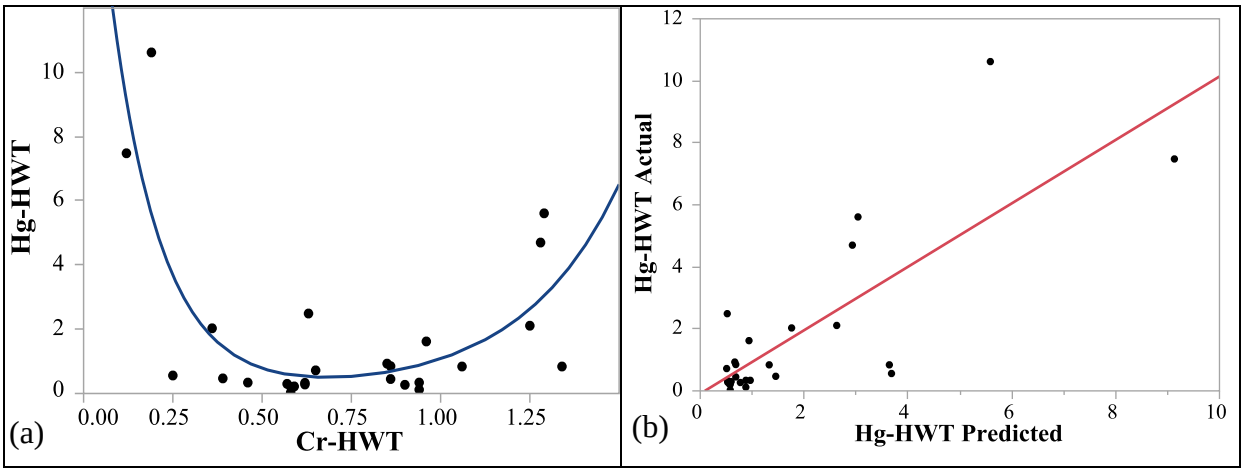


Figure 5.34: For four-parameter Biexponential model of Hg-HWT (a) model fitting (b) actual vs predicted plot

### 5.5.2.1 Model Comparison for Hg in HWT

The comparison of the models for predicting Hg in HWT are shown in Figure 5.35. None of the linear and NN models fit with any parameters. Among the two NL models, the WM-4P showed better performance ($R^2$ = 0.71; RMSE = 1.43) than the BEM-4P ($R^2$=0.62; RMSE=1.62) (Table 5.22). Both of the models showed better fits with measured data for lower concentrations of Hg (<3.0 µg/L), while for NL (WM-4P) model, the measured data were much closer to the LOEC. The NL (WM-4P) is the model of choice for predicting Hg in HWT.

Table 5.22: Comparison of different models for Hg in HWT

| Output | Model Type | Parameters | $R^2$ | RMSE |
|---|---|---|---|---|
| Hg-HWT | NL (WM-4P) | Zn-WDS | 0.71 | 1.43 |
| | NL (BEM-4P) | Cr-HWT | 0.62 | 1.63 |

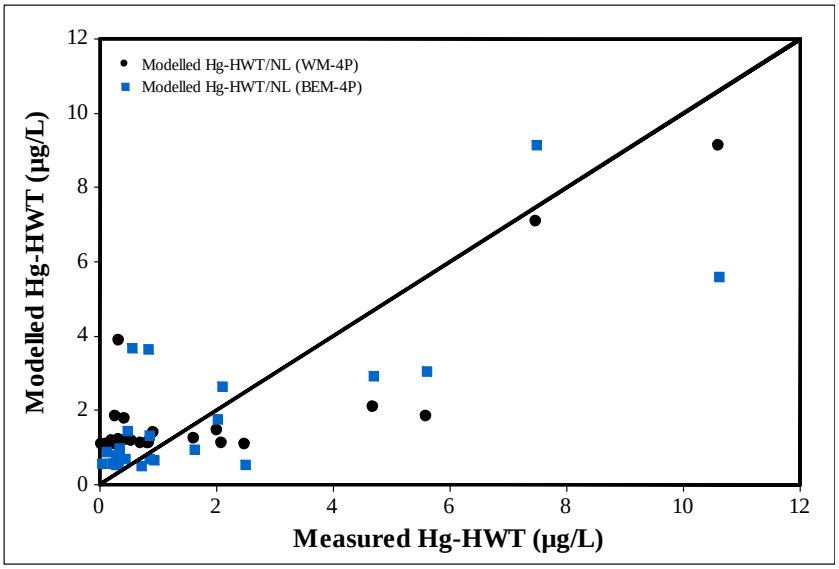


Figure 5.35: Measured and modeled concentration of Hg in HWT

(WM-4P: four-parameter Weibull model; BEM-4P: four-parameter Biexponential model)

### 5.5.2.2 Model Validation for Hg in HWT

The predictive models for Hg in HWT were validated using an additional set of data, which were not used in model development. The average concentrations of Hg-HWT from the NL (WM-4P) and NL (BEM-4P) models were 1.72 and 1.65 µg/L respectively and the ranges were 1.07-5.44 and 0.51-5.59 µg/L respectively. The average of measured concentrations of Hg-HWT was 1.84 µg/L with the range of 0.03-10.62 µg/L. From the plot of predicted vs. measured data, the values of correlation coefficients (*r*) were determined and shown in Table 5.23. The values of *r* for NL (WM-4P) and NL (BEP-4P) models were 0.92 and 0.86 respectively. The comparison of different models for validation study are shown in Figure 5.36. The NL (WM-4P) model was much closer to LOEC and showed better predictability for lower concentration of Hg-HWT (<2.0 µg/L).

Table 5.23: Correlation coefficients for model validation of Hg in HWT

| Output | Model Type | *r* (Corr. Coef.) |
|---|---|---|
| Hg-HWT | NL (WM-4P) | 0.92 |
| | NL (BEM-4P) | 0.86 |

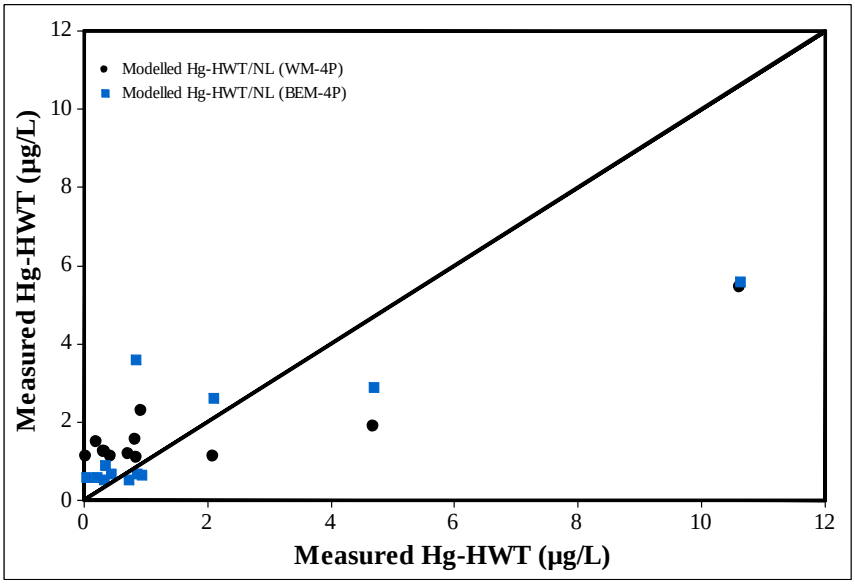


Figure 5.36: Measured and modelled concentration of Hg-HWT in validation

None of the tested NL models was found to fit with any parameter for Hg in PP while none of the linear and NN models showed acceptable fit with any parameter for Hg in HWT. The NL models for predicting Hg-HWT showed poor performance. The NL models were developed using the single factors, which could have affected their performance. Hg in consumer tap had significant effect form Hg in WDS. The oxidized form of Mercuric chloride ($HgCl_2$) might have come from the source water and remained soluble till reach the consumer's tap [118]. The corrosion by-products of iron pipe contained Hg, Sr and Fe. The physical and chemical disturbances of pipe inner surface

might have caused Hg to release into PP. The prolonged stagnation period might have also affected the release of Hg. From the models, it could be hypothesized that Hg in HWT had negligible influence from Hg in WDS. The scale deposits on the heater wall along with other corroded metals might have caused the release of Hg in HWT. Dissolution of scale due to sudden excessive usage, physical disturbance or abrupt chemical changes of water property might also have caused the release of Hg in HWT.

## 5.6 Models for Predicting Iron (Fe)

### 5.6.1 Modeling Fe in PP

**Linear Model:**

Among the different linear models, the LMF and LMFI models were found to be best for predicting Fe in PP. Figure 5.37 summarizes the procedure of selecting parameters and adequacy check for developing the LMF model to predict Fe in PP samples. Table 5.24 summarizes the ANOVA with significant factors (p value < 0.01). The model for predicting Fe-PP was developed (Equation 5.42) using the main factors. The model had the $R^2$ value of 0.95. The experimental data and predicted values were found to be consistent (Fig. 5.37d). The plot of residuals versus predicted (Fig. 5.37b) showed the randomness of residuals. The plot of residuals versus row number (Fig. 5.37c) confirmed that the residuals were uncorrelated. No evidence of lack of fit (P >= 0.1) was also observed. The screening effects of the main factors (Table 5.24) and half-normal plot (Fig. 5.37a) showed that occurrence of Fe-PP was positively influenced by the Cr in PP while V-WDS and Hg-WDS had negative impact.

Table 5.24: Screening effects of the factors for modeling Fe-PP

| Term | Estimate | Std Error | t Ratio | Prob>\|t\| |
|---|---|---|---|---|
| Intercept | 15.9835 | 4.175165 | 3.83 | 0.0009 |
| Cr-PP | 80.145531 | 5.97751 | 13.41 | <.0001 |
| V-WDS | -1.088482 | 0.174823 | -6.23 | <.0001 |
| Hg-WDS | -2.342713 | 0.455957 | -5.14 | <.0001 |

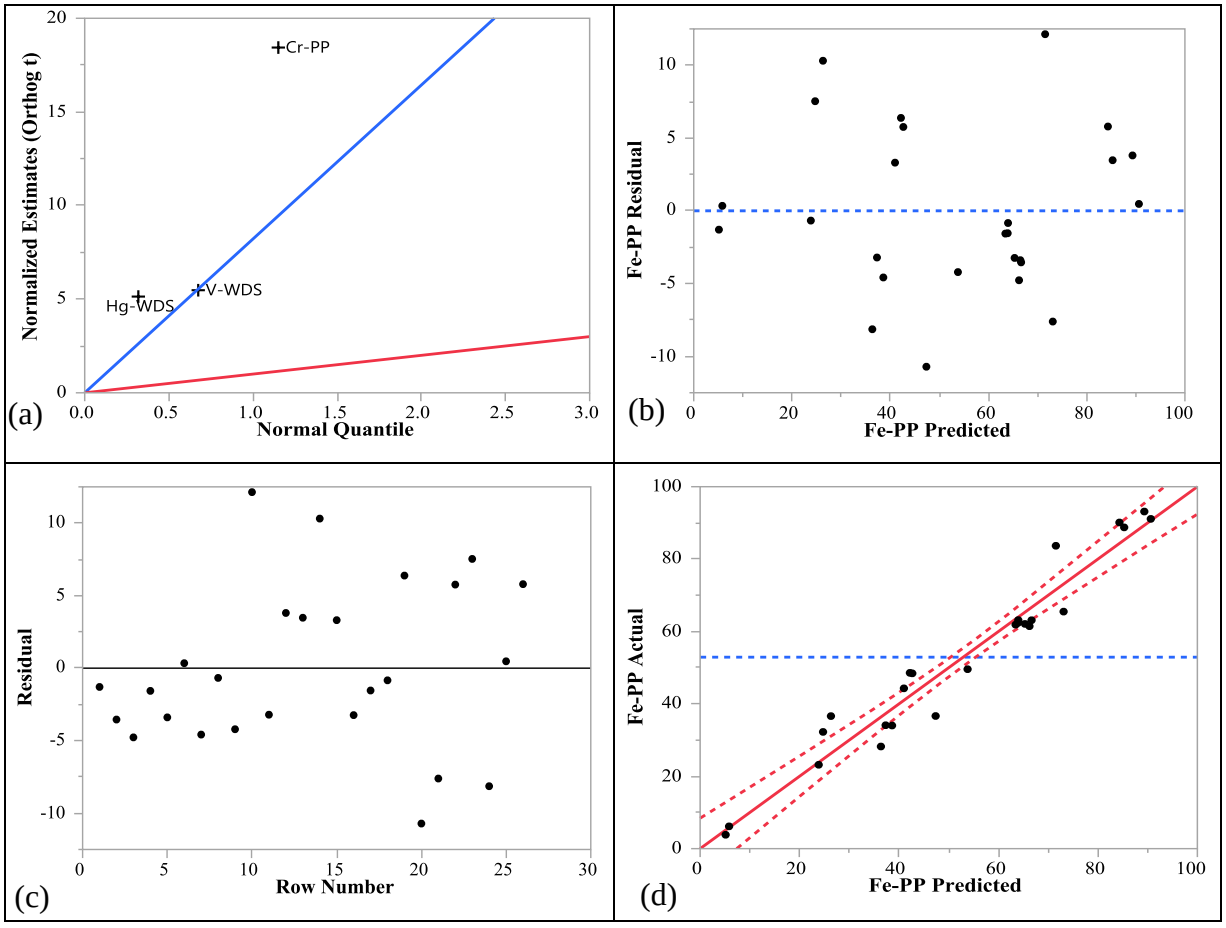


Figure 5.37: For Fe-PP model (a) half normal plot (b) residual vs predicted (c) residual vs row number and (d) actual vs predicted data

$$Fe-PP=\beta_0+\beta_1 Cr-PP+\beta_2 V-WDS+\beta_3 Hg-WDS \quad (5.42)$$

Where: $\beta_0=15.98;\ \beta_1=80.15;\ \beta_2=-1.09;\ \beta_3=-2.34$

Another linear model for predicting Fe-PP was developed (Equation 5.43) using the main factors and interaction (LMFI). The model had the $R^2$ value of 0.97. The experimental data and predicted values were fairly consistent (Fig. 5.38d). The plot of residuals versus predicted (Fig. 5.38b) showed a scattered pattern. The plot of residuals versus row number (Fig. 5.38c) confirmed that the residuals were uncorrelated. No evidence of lack of fit (P >= 0.1) was observed. The screening effects of the main factors (Table 5.25) and half-normal plot (Fig. 5.38a) showed that Zn-WDS and Cr-PP had positive effects on the concentrations of Fe in PP, while V-WDS, Hg-WDS and interaction of Cr-PP with V-WDS had negative effects.

Table 5.25: Screening effects of the factors for modeling Fe-PP

| Term | Estimate | Std Error | t Ratio | Prob>\|t\| |
|---|---|---|---|---|
| Intercept | 11.049986 | 3.532415 | 3.13 | 0.0053 |
| Cr-PP | 84.483116 | 4.88444 | 17.30 | <.0001 |
| V-WDS | -0.986293 | 0.140006 | -7.04 | <.0001 |
| Hg-WDS | -2.899459 | 0.43436 | -6.68 | <.0001 |
| Zn-WDS | 0.2944139 | 0.087259 | 3.37 | 0.0030 |
| (Cr-PP-0.57)*(V-WDS-4.89) | -1.248632 | 0.541118 | -2.31 | 0.0318 |

$$Fe-PP=\beta_0+\beta_1 Cr-PP+\beta_2 V-WDS+\beta_3 Hg-WDS+\beta_4 Zn-WDS+\beta_5(Cr-PP-0.57)(V-WDS-4.49) \quad (5.43)$$

Where: $\beta_0=11.05;\ \beta_1=84.48;\ \beta_2=-0.99;\ \beta_3=-2.9;\ \beta_4=0.29;\ \beta_5=-1.25$

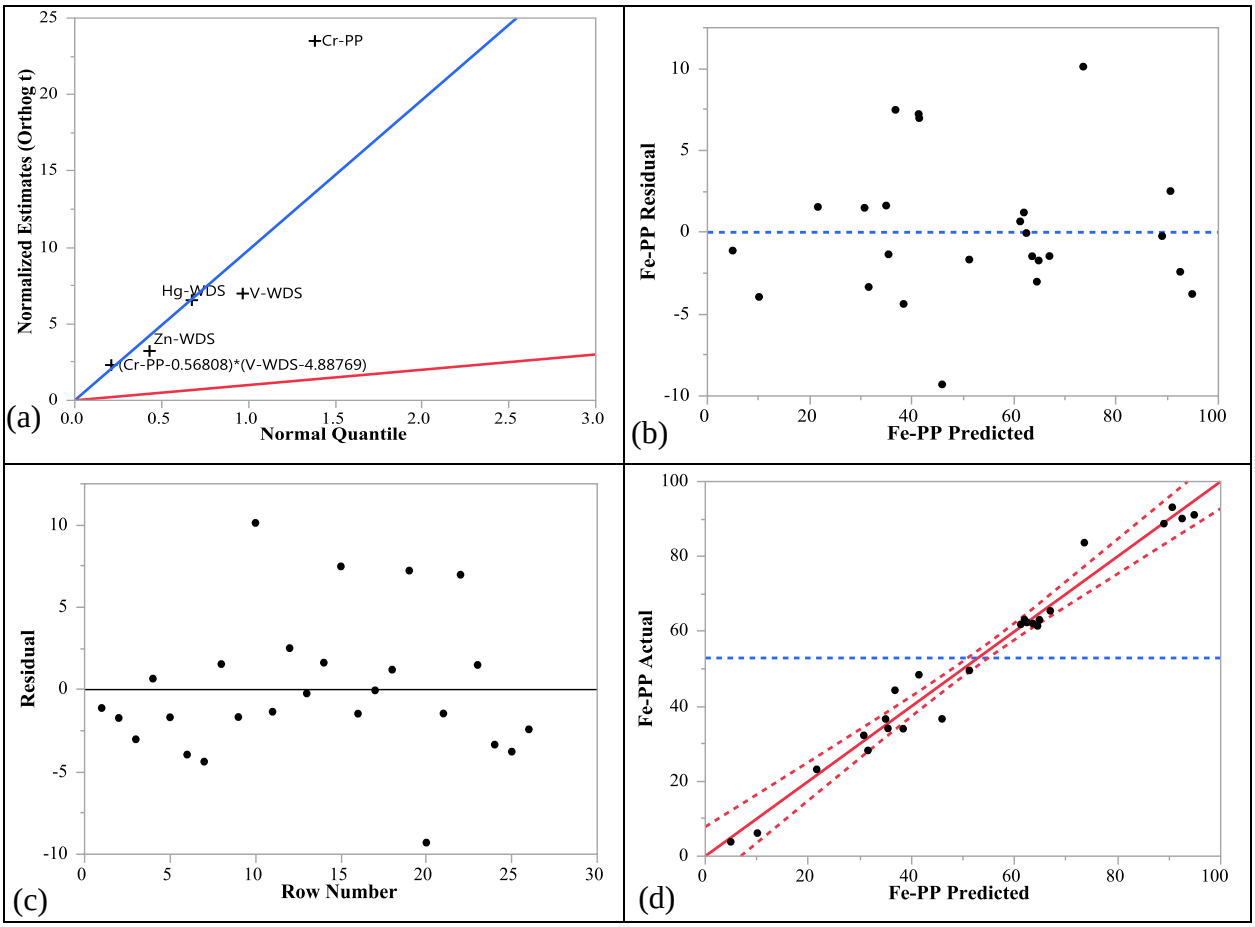


Figure 5.38: For Fe-PP model (a) half normal plot (b) residual vs predicted (c) residual vs row number and (d) actual vs predicted data

**Nonlinear Model:**

Figure 5.39 explains the nonlinear model selection process for Fe in PP samples (Fe-PP). Among the different factors, Cr in PP showed best performance with the three parameter Logistic model (Fig. 5.39a) for predicting Fe-PP concentration. The model for predicting Fe-PP was developed (Equation 5.44) and the model had the RMSE of 10.20. The experimental data and predicted values ($R^2$=0.84) were consistent (Fig. 5.39b).

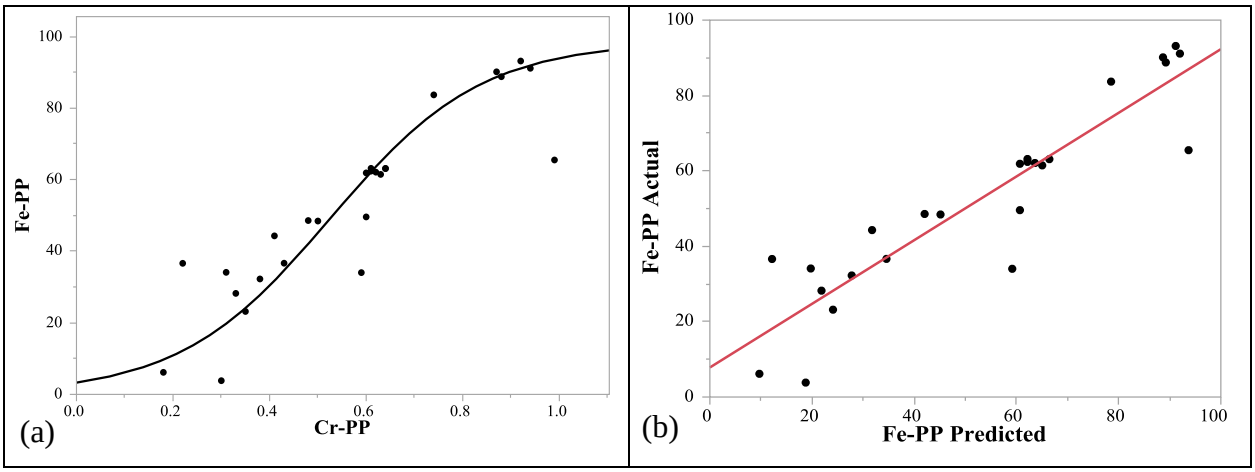


Figure 5.39: For Logistic model (3 parameters) of Fe-PP (a) model fitting (b) actual vs predicted plot

$$Fe-PP = \frac{\theta_1}{(1+\theta_2 Exp(\theta_3 Cr-PP))} \tag{5.44}$$

Where: $\theta_1 = 98.5; \theta_2 = 29; \theta_3 = -6.4$

**Neural Network Model:**

The NN model for predicting Fe-PP is shown in Equation 5.45. The model had the $R^2$ value of 0.97 and RMSE of 4.2. The experimental data and predicted values were found to be consistent (Fig. 5.40). The Equation of hidden nodes (Equation 5.46-5.48) showed that Fe-WDS, Hg-WDS, Cr-PP and V-WDS had influence on the occurrence of Fe in PP.

$$Fe-PP = 54.33 + (65.17 \times H1) + (-17.01 \times H2) + (-21.04 \times H3) \tag{5.45}$$

$$H1 = \tanh[0.5 \times \{-1.1 + (-0.021\,\text{Hg - WDS}) + (0.0025\,Fe - WDS + (-0.065\,V - WDS) + (1.819\,\text{Cr - PP})\}] \quad (5.46)$$

$$H2 = \tanh[0.5 \times \{-4.77 + (0.261\,\text{Hg - WDS}) + (0.042\,Fe - WDS + (0.09\,V - WDS) + (0.86\,\text{Cr - PP})\}] \quad (5.47)$$

$$H3 = \tanh[0.5 \times \{5.56 + (-0.059\,\text{Hg - WDS}) + (-0.015\ Fe - WDS + (-0.24\,V - WDS) + (-6.22\,\text{Cr - PP})\}] \quad (5.48)$$

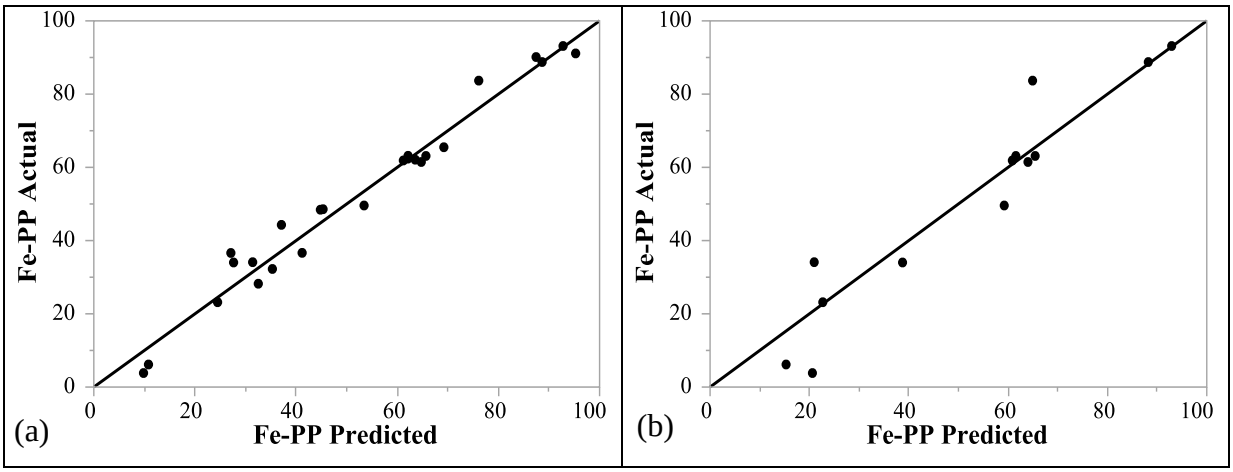


Figure 5.40: Actual vs predicted plot of Fe-PP for (a) data training (b) validation of NN model

### 5.6.1.1 Model Comparison for Fe in PP

The comparison of the models for predicting Fe in PP are shown in Figure 5.41. The NN model and LMFI model had the same $R^2$ value (0.97), while the LMF model had $R^2$ value of 0.95 (Table 5.26). The lower RMSE value of NN model (RMSE=4.20) compared to the LMFI model (RMSE=4.76) and LMF model (RMSE=6.06) also showed its better performances. The LMFI model used one additional factor (i.e., Zn-WDS) than LMF model. The use of interactive terms in LMFI model increased its efficiency over LMF model (Table 5.26). The NL model (LM-3P) showed relative weak performance than the NN, LMF and LMFI models, due to the single input factor (e.g., Cr-PP) while Fe in PP could be affected by several factors. All the models had better

fits with measured data for the whole range of concentrations of Fe while for NN model, the measured data were much closer to the LOEC. The NN model is the model of choice for predicting Fe in PP.

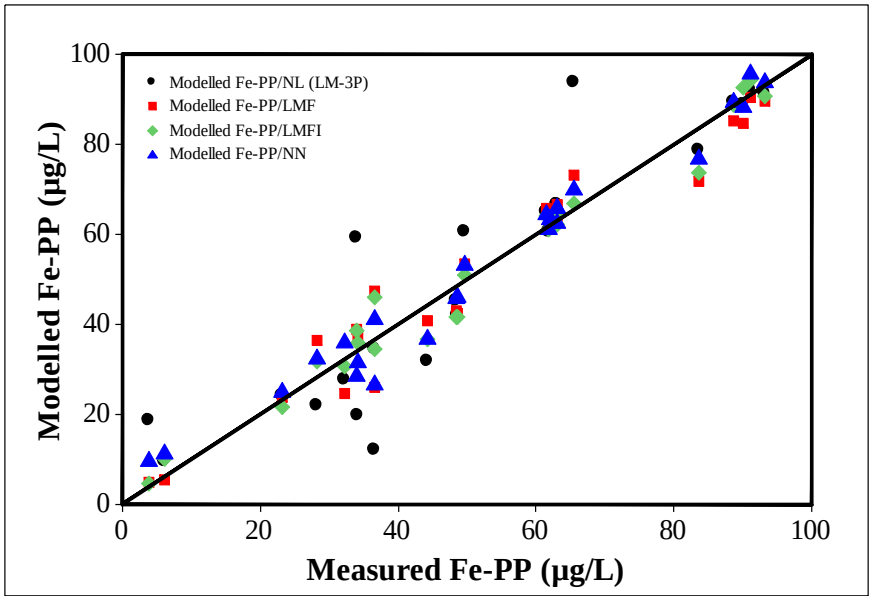


Figure 5.41: Measured and modeled concentration of Fe in PP

(LM-3P: 3 parameters Logistic model; LMF: Main factors linear model; LMFI: Main factors, interaction and higher order terms model; NN: Neural network model)

Table 5.26: Comparison of different models for Fe in PP

| Output | Model Type | Parameters | $R^2$ | RMSE |
|---|---|---|---|---|
| Fe-PP | LMF | Hg-WDS, V-WDS, Cr-PP | 0.95 | 6.06 |
| | LMFI | Hg-WDS, Zn-WDS, V-WDS, Cr-PP | 0.97 | 4.76 |
| | NL (LM-3P) | Cr-PP | 0.84 | 10.20 |
| | NN | Hg-WDS, Fe-WDS, V-WDS, Cr-PP | 0.97 | 4.20 |

### 5.6.1.2 Model Validation for Fe in PP

The predictive models for Fe in PP were validated using an additional set of data, which were not used in model development. The average concentrations of Fe-PP from the LMF, LMFI, NL (LM-3P) and NN models were 51.13, 82.35, 54.55 and 52.28 µg/L respectively and the ranges were 13.15-89.21, 19.75-417.18, 9.49-91.34 and 15.28-93.51 µg/L respectively. The average of measured concentrations of Fe-PP was 51.23 µg/L with the range of 3.83-93.14 µg/L. From the plot of predicted vs. measured data, the values of correlation coefficients (*r*) were determined and shown in Table 5.27. The values of *r* for LMF, LMFI, NL (LM-3P) and NN models were 0.91, 0.90, 0.93 and 0.94 respectively. The comparison of different models for validation study are shown in Figure 5.42. All the models were closer to LOEC and showed excellent predictability for the whole range of concentrations.

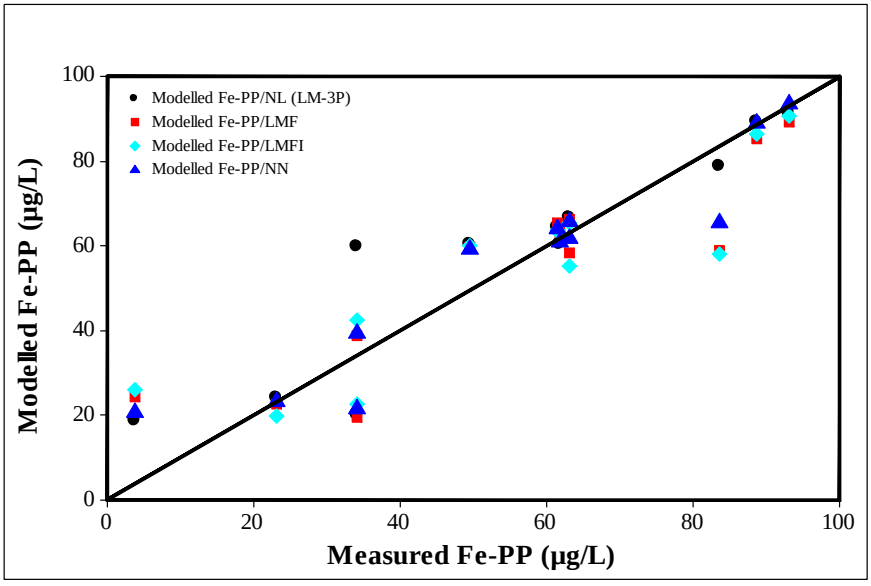


Figure 5.42: Measured and modelled concentration of Fe-PP in validation

Table 5.27: Correlation coefficients for model validation of Fe in PP

| Output | Model Type | *r* (Corr. Coef.) |
|---|---|---|
| Fe-PP | LMF | 0.91 |
| | LMFI | 0.90 |
| | NL (LM-3P) | 0.93 |
| | NN | 0.94 |

### 5.6.2 Modeling Fe in HWT

**Linear Model:**

Figure 5.43 summarizes the procedure of selecting parameters and adequacy check for modeling of Fe concentration in HWT. Table 5.28 summarizes the ANOVA with significant factors (p value < 0.01). Among the different linear models, the LMF model was found to be the best and was selected (Equation 5.49). The model had the $R^2$ value of 0.85. The experimental data and predicted values were found to be consistent (Fig. 5.43d). The plot of residuals versus predicted values (Fig. 5.43b) showed data randomness. No evidence of lack of fit (P >= 0.1) was also observed. The screening effects of the main factors (Table 5.28) and half-normal plot (Fig. 5.43a) showed that Cu-HWT, Pb-HWT and V-HWT had positive influence on the concentrations of Fe in HWT.

Table 5.28: Screening effects of the factors for modeling Fe-HWT

| Term | Estimate | Std Error | t Ratio | Prob>\|t\| |
|---|---|---|---|---|
| Intercept | 26.029997 | 5.408615 | 4.81 | 0.0001 |
| Cu-HWT | 8.5102554 | 3.140261 | 2.71 | 0.0135 |
| Pb-HWT | 5.8927495 | 0.773836 | 7.61 | <.0001 |
| V-HWT | 2.2159506 | 0.479486 | 4.62 | 0.0002 |

$$Fe-HWT = \beta_0 + \beta_1 Cu-HWT + \beta_2 Pb-HWT + \beta_3 V-HWT \quad (5.49)$$

Where: $\beta_0 = 26.03; \beta_1 = 8.51; \beta_2 = 5.89; \beta_3 = 2.21$

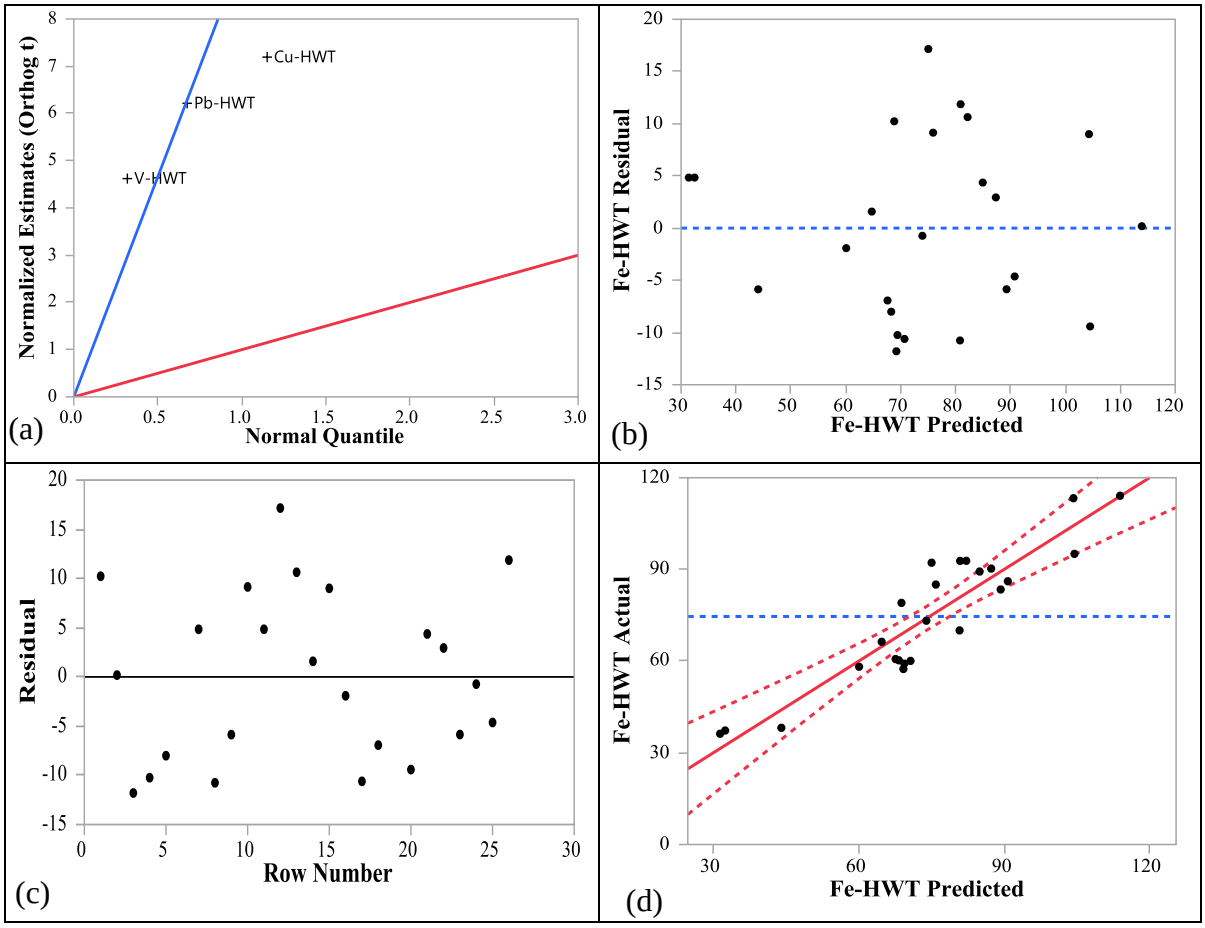


Figure 5.43: For Fe-HWT model (a) half normal plot (b) residual vs predicted (c) residual vs row number and (d) actual vs predicted data

**Nonlinear Model:**

The process of nonlinear model selection for predicting Fe concentrations in HWT samples is explained in Figure 5.44. Among the different factors, Cu in HWT showed best performance with

the Quintic model (Fig. 5.44a). The model is shown in Equation 5.50 and the model had the RMSE of 18.04. The experimental data and predicted values ($R^2$=0.47) were found to be moderately consistent (Fig. 5.44b).

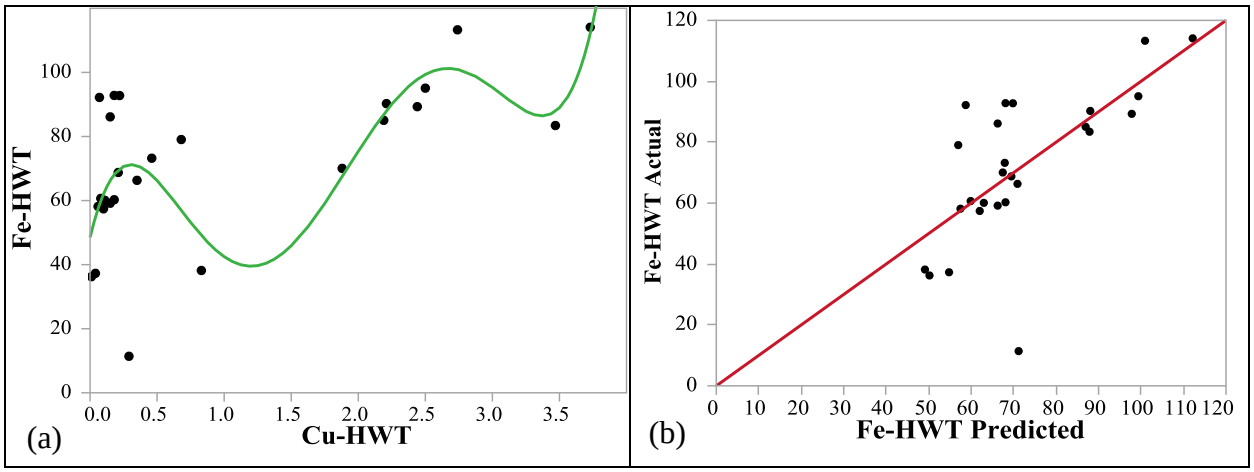


Figure 5.44: For Quintic model of Fe-HWT (a) model fitting (b) actual vs predicted plot

$$Fe-HWT=\theta_1+\theta_2 Cu-HWT+\theta_3(Cu-HWT)^2+\theta_4(Cu-HWT)^3+\theta_5(Cu-HWT)^4+\theta_6(Cu-HWT)^5 \quad (5.50)$$

Where: $\theta_1=48.5;\ \theta_2=173.4;\ \theta_3=-413.83;\ \theta_4=322.9;\ \theta_5=-98.97;\ \theta_6=10.49$

**Neural Network Model:**

The NN model for predicting Fe-HWT is shown in Equation 5.51. The model had the $R^2$ value of 0.95 and RMSE of 5.56. The experimental data and predicted values were found to be consistent (Fig. 5.45). The Equations 5.52-5.54 showed that Cu-HWT, Pb-HWT and V-HWT had influence on the occurrence of Fe in HWT.

$$Fe-HWT = -248.1 + (-217.5 \times H1) + (240.28 \times H2) + (-334.18 \times H3) \quad (5.51)$$

$$H1 = \tanh[0.5 \times \{-11.61 + (0.93\,Cu - HWT) + (0.97\,Pb - HWT) + (0.83\,V - HWT)\}] \quad (5.52)$$

$$H2 = \tanh[0.5 \times \{-7.15 + (1.04\,Cu - HWT) + (0.59\,Pb - HWT) + (0.47\,V - HWT)\}] \quad (5.53)$$

$$H3 = \tanh[0.5 \times \{-2.76 + (0.67\,Cu - HWT) + (-0.09\,Pb - HWT) + (-0.23\,V - HWT)\}] \quad (5.54)$$

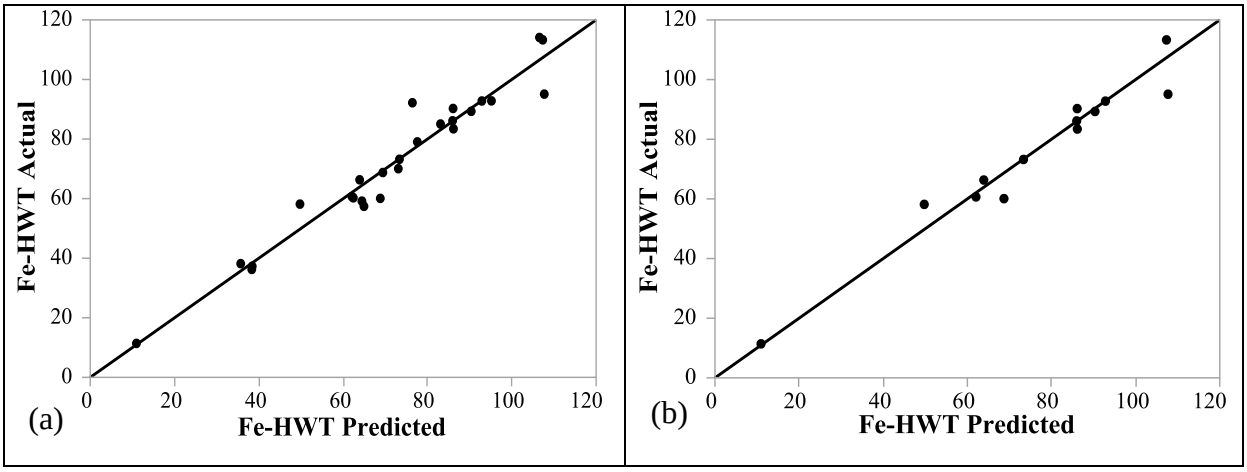


Figure 5.45: Actual vs predicted plot of Fe-HWT for (a) data training (b) validation of NN model

### 5.6.2.1 Model Comparison for Fe in HWT

The comparison of the models for predicting Fe in HWT are shown in Figure 5.46. The NN, LMF and NL (QUM) model had $R^2$ values of 0.95, 0.85 and 0.47 respectively (Table 5.29). The lower RMSE value of NN model (RMSE=5.56) than LMF and NL model indicated the better performance of NN model. However, the NN and LMF models had the same input factors (Table 5.29). The NL (QUM) showed poor performance than the NN and LMF models, due to the single input factor (e.g., Cu-HWT) while Fe in HWT could be affected by several factors. All the models

had better fits with measured data for mid-level concentrations of Fe (60-100 µg/L), while for NN model, the measured data were much closer to the LOEC. The NN model is the model of choice for predicting Fe in HWT.

Table 5.29: Comparison of different models for Fe in HWT

| Output | Model Type | Parameters | $R^2$ | RMSE |
|---|---|---|---|---|
| Fe-HWT | LMF | Cu-HWT, Pb-HWT, V-HWT | 0.85 | 9.11 |
| | NL (QUM) | Cu-HWT | 0.47 | 18.04 |
| | NN | Cu-HWT, Pb-HWT, V-HWT | 0.95 | 5.56 |

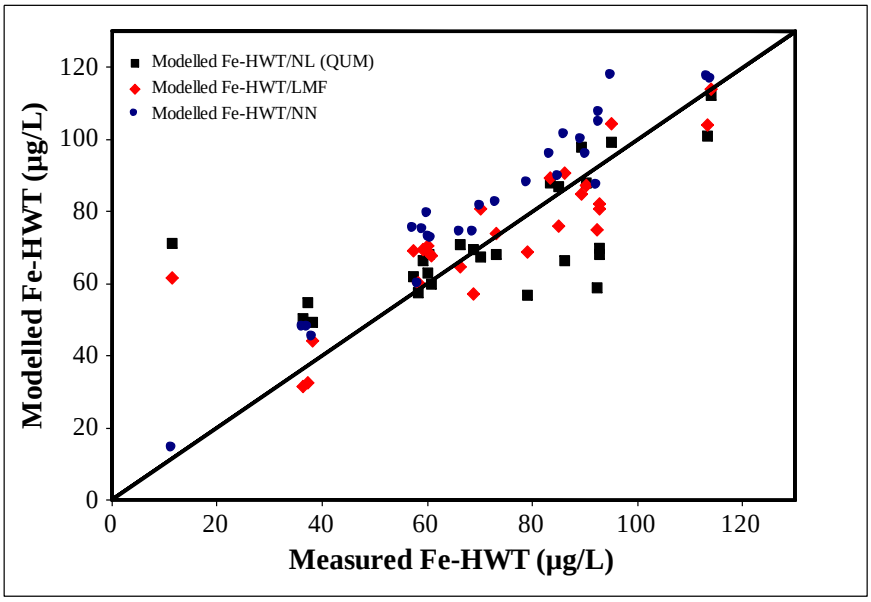


Figure 5.46: Measured and modeled concentration of Fe in HWT

(QUM: Quintic model; LMF: Main factors linear model; NN: Neural network model)

### 5.6.2.2 Model Validation for Fe in HWT

The predictive models for Fe in HWT were validated using an additional set of data, which were not used in model development. The average concentrations of Fe-HWT from the LMF, NL (QUM) and NN models were 79.97, 76.88 and 85.78 µg/L respectively, and the ranges were 60.05-104.33, 57.10-100.76 and 14.48-117.75 µg/L respectively. The average of measured concentrations of Fe-HWT was 75.40 µg/L with the range of 11.40-113.3 µg/L. From the plot of predicted vs. measured data, the values of correlation coefficients (*r*) were determined and shown in Table 5.30. The values of *r* for LMF, NL (QUM) and NN models were 0.83, 0.61 and 0.98 respectively. The comparison of different models for validation study are shown in Figure 5.47. All the models were fairly good while for NN model, the measured data were much closer to the LOEC.

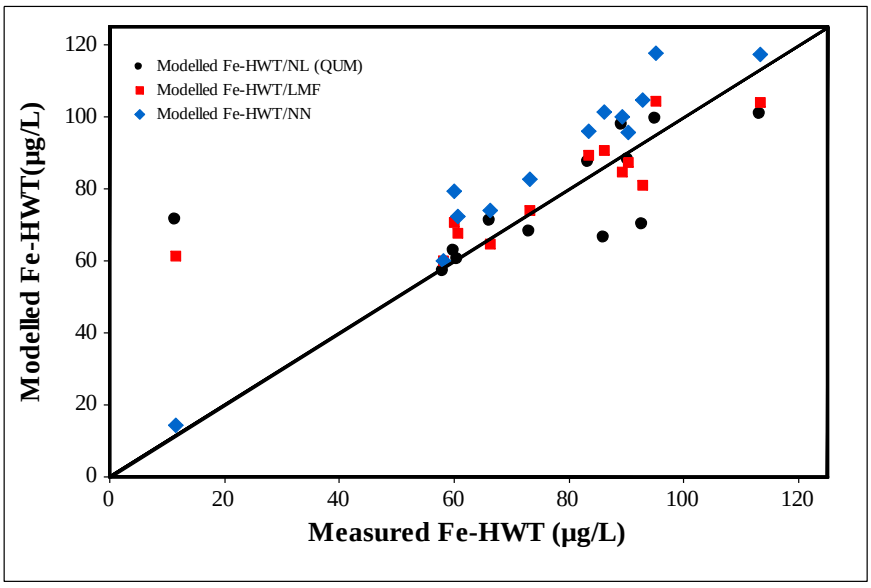


Figure 5.47: Measured and modelled concentration of Fe-HWT in validation

Table 5.30: Correlation coefficients for model validation of Fe in HWT

| Output | Model Type | *r* (Corr. Coef.) |
|---|---|---|
| Fe-HWT | LMF | 0.83 |
| | NL (QUM) | 0.61 |
| | NN | 0.98 |

For the Fe-PP and Fe-HWT models, NN models were the best while the NL models showed poor performance, due possibly to the same reasons as discussed in the earlier models. The inclusion of interaction effects in the LMFI model showed better performance than the LMF model. Most of the models for Fe in PP and HWT showed moderate to excellent predictive capacities. Fe in consumer tap (PP) had significant effect form Fe in WDS. The relatively acidic water was likely to increase the release of Fe through corrosive action, increased reaction with the pipe coatings and plumbing materials. In addition, mechanical disturbances (e.g., repeated activation of the faucet, water hammer) could have also released Fe in PP [72]. Flushing of consumer tap after long stagnation might have caused the release of Fe along with other metals. Fe in HWT was not strongly correlated to Fe in WDS. The scale deposits (Ca and Mg ions) on the heater wall along with other corroded metals (i.e., Fe, Cu, Pb, V) might have served as the potential sources of Fe in HWT. Following the usage of hot water, the scales were sloughed off and released into hot water [103].

## 5.7 Models for Predicting Arsenic (As)

### 5.7.1 Modeling As in PP

**Linear Model:**

Among the different linear models, the LMF model was found to be the best and was selected for predicting As-PP (Equation 5.55). The model had the $R^2$ value of 0.97. The experimental data and predicted values were found to be consistent (Fig. 5.48d). The plot of residuals versus predicted (Fig. 5.48b) showed that the residuals were scattered. The plot of residuals versus row number (Fig. 5.48c) confirmed that the residuals were uncorrelated. No evidence of lack of fit (P >= 0.1) was also observed.

Table 5.31: Screening effects of the factors for modeling As-PP

| Term | Estimate | Std Error | t Ratio | Prob>\|t\| |
|---|---|---|---|---|
| Intercept | 0.08845 | 0.044566 | 1.98 | 0.0636 |
| Na-PP | $5.71 \times 10^{-6}$ | $5.296 \times 10^{-6}$ | 10.78 | <.0001* |
| Zn-WDS | 0.02227 | 0.004633 | 4.81 | 0.0002* |
| Mn-WDS | -0.1225 | 0.029882 | -4.10 | 0.0007* |

$$As - PP = \beta_0 + \beta_1 Na - PP + \beta_2 Zn - WDS + \beta_3 Mn - WDS \qquad (5.55)$$

Where: $\beta_0 = 0.088; \beta_1 = 5.71 \times 10^{-6}; \beta_2 = 0.022; \beta_3 = -0.122$

The screening effects of the main factors (Table 5.31) and half-normal plot (Fig. 5.48a) showed that the Zn-WDS and Na-PP had positive influence on the concentrations of As in PP while Mn-WDS had negative effects.

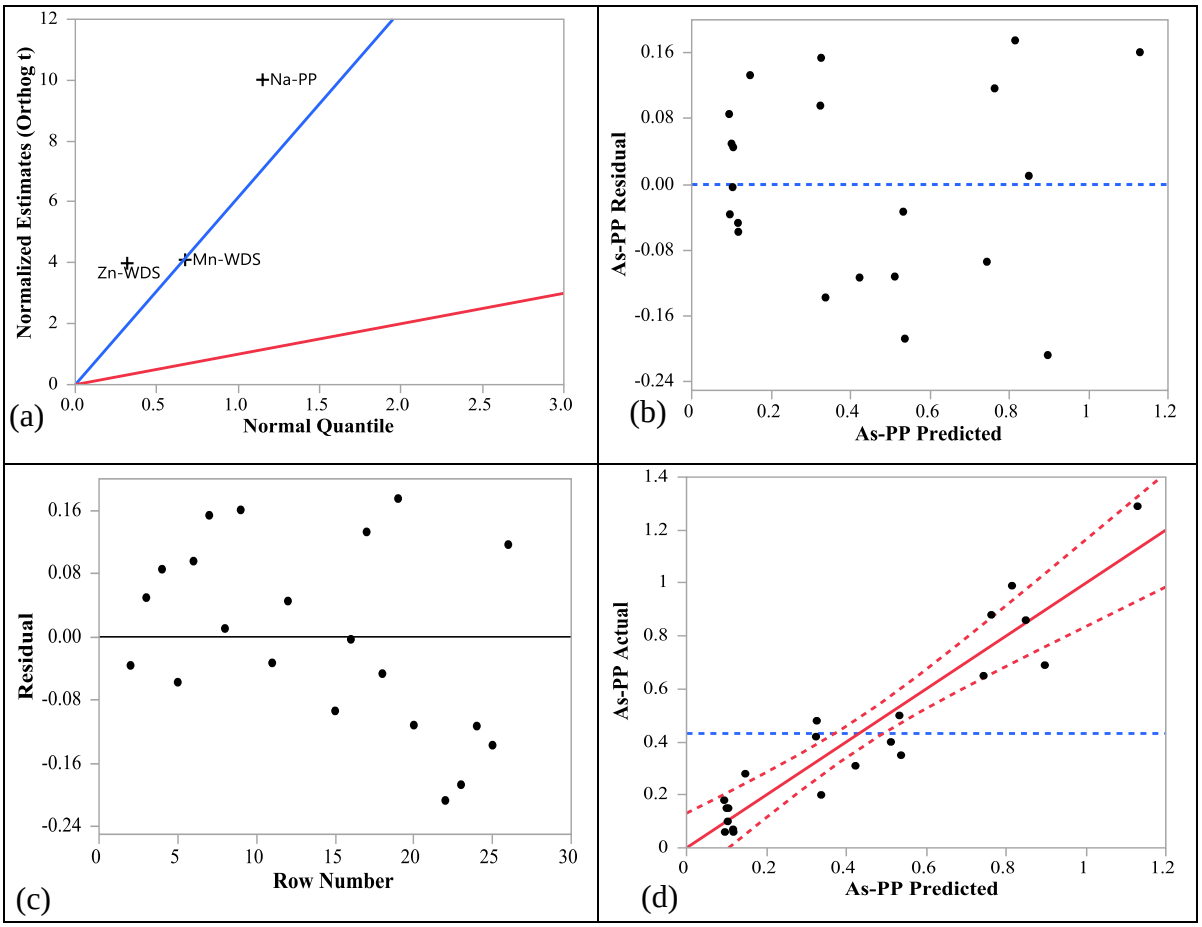


Figure 5.48: For As-PP model (a) half normal plot (b) residual vs predicted (c) residual vs row number and (d) actual vs predicted data

**Nonlinear Model:**

Figure 5.49 explains the nonlinear model selection process for As in PP samples (As-PP). Among the different factors, Zn in WDS showed the best performance with the four parameter Logistic model for predicting As-PP (Fig. 5.49a). The model was developed (Equation 5.56) and the model had the RMSE value of 0.93. The experimental data and predicted values ($R^2$=0.56) were moderately consistent (Fig. 5.49b).

$$As - PP = \theta_1 + \frac{(\theta_2 - \theta_1)}{(1 + Exp\{\theta_3[Zn - WDS - \theta_4]\})} \quad (5.56)$$

Where: $\theta_1 = 7.22; \theta_2 = 0.16; \theta_3 = 0.066; \theta_4 = 47.5$

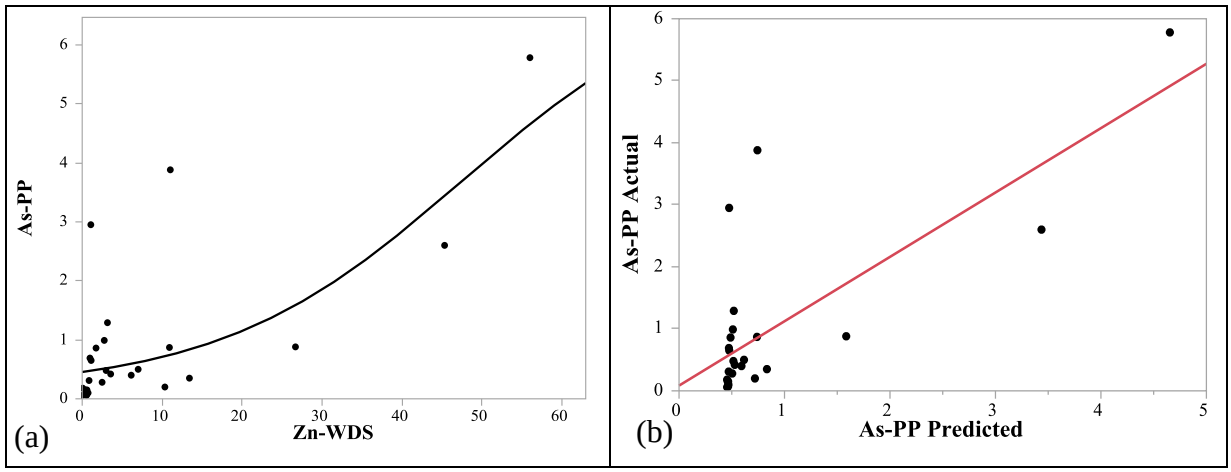


Figure 5.49: For Logistic model (4 parameters) of As-PP (a) model fitting (b) actual vs predicted plot

**Neural Network Model:**

The neural network model for predicting As concentrations in PP (As-PP) is shown in Equation 5.57. The model had the $R^2$ value of 0.97 and RMSE of 0.12. The experimental data and predicted values for training and validation dataset were consistent (Fig. 5.50). The Equation of hidden nodes (Equation 5.58-5.60) showed that Zn-WDS, Mn-WDS and Na-PP had influence on the concentrations of As in PP.

$$As - PP = 1.99 + (3.56 \times H1) + (1.24 \times H2) + (5.42 \times H3) \quad (5.57)$$

$$H1 = \tanh[0.5\times\{-9.67 + (0.0000029\,\text{Na-PP}) + (0.188\,\text{Zn-WDS}) + (0.602\,\text{Mn-WDS})\}] \quad (5.58)$$

$$H2 = \tanh[0.5\times\{-1.12 + (0.000006\,\text{Na-PP}) + (0.1005\,\text{Zn-WDS}) + (-0.655\,\text{Mn-WDS})\}] \quad (5.59)$$

$$H3 = \tanh[0.5\times\{0.899 + (0.000002\,\text{Na-PP}) + (-0.012\,\text{Zn-WDS}) + (0.071\,\text{Mn-WDS})\}] \quad (5.60)$$

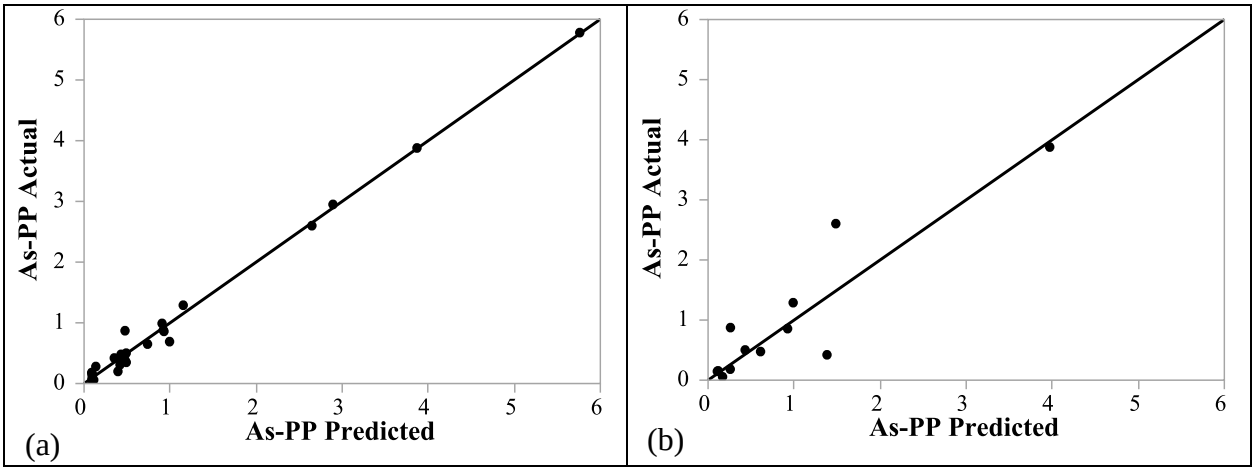


Figure 5.50: Actual vs predicted plot of As-PP for (a) data training (b) validation of NN model

### 5.7.1.1 Model Comparison for As in PP

The comparison of the models for predicting As in PP are shown in Figure 5.51. The NN model showed better performance ($R^2$ = 0.99; RMSE = 0.12) than the LMF model ($R^2$ = 0.89; RMSE = 0.13). However, these two models had the same input factors (Table 5.32). The NL model (LM-4P) showed poor performance than the NN and LMF models, due to the single input factor (e.g., Zn-WDS) while As in PP could be affected by several factors. All models showed better fit at lower concentrations (< 2.0 µg/L) (Figure 5.51), while for NN model, the measured data were much closer to the LOEC. The NN model is the model of choice for predicting As in PP.

Table 5.32: Comparison of different models for As in PP

| Output | Model Type | Parameters | $R^2$ | RMSE |
|---|---|---|---|---|
| As-PP | LMF | Na-PP, Zn-WDS, Mn-WDS | 0.89 | 0.13 |
| | NL (LM-4P) | Zn-WDS | 0.56 | 0.93 |
| | NN | Na-PP, Zn-WDS, Mn-WDS | 0.99 | 0.12 |

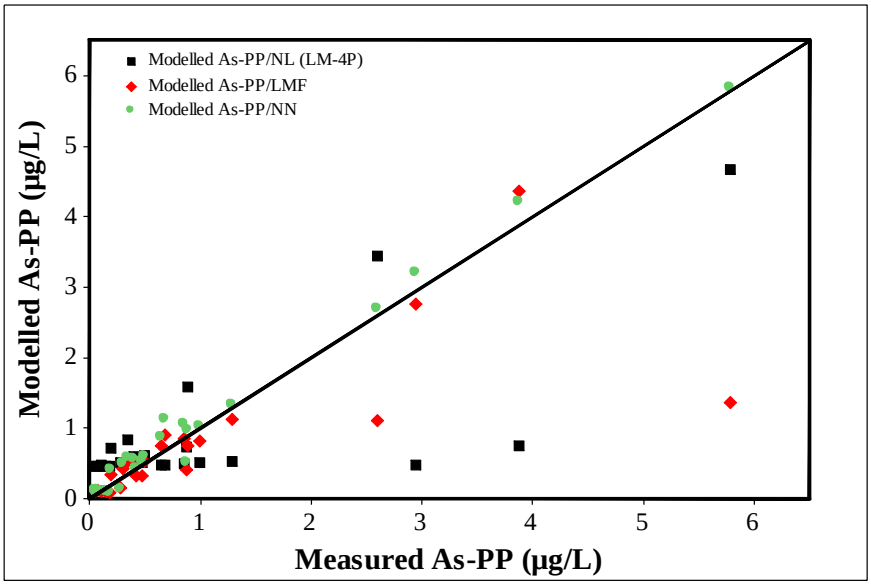


Figure 5.51: Measured and modeled concentration of As in PP

(LM-4P: 4 parameters Logistic model; LMF: Main factors linear model; NN: Neural network model)

### 5.7.1.2 Model Validation for As in PP

The predictive models for As in PP were validated using an additional set of data, which were not used in model development. The average concentrations of As-PP from the LMF, NL (LM-4P) and NN models were 0.74, 0.74 and 0.85 µg/L respectively, and the ranges were 0.12-4.22, 0.46-2.49 and 0.11-4.28 µg/L respectively. The average of measured concentrations of As-PP was 0.92

µg/L with the range of 0.06-3.88 µg/L. From the plot of predicted vs. measured data, the values of correlation coefficients (*r*) were determined and shown in Table 5.33. The values of *r* for LMF, NL (LM-4P) and NN models were 0.89, 0.53 and 0.94 respectively. The comparison of different models for validation study are shown in Figure 5.52. All the models were closer to LOEC for lower concentration of As-PP (<1.5 µg/L) while for NN model, the measured data were much closer to the LOEC.

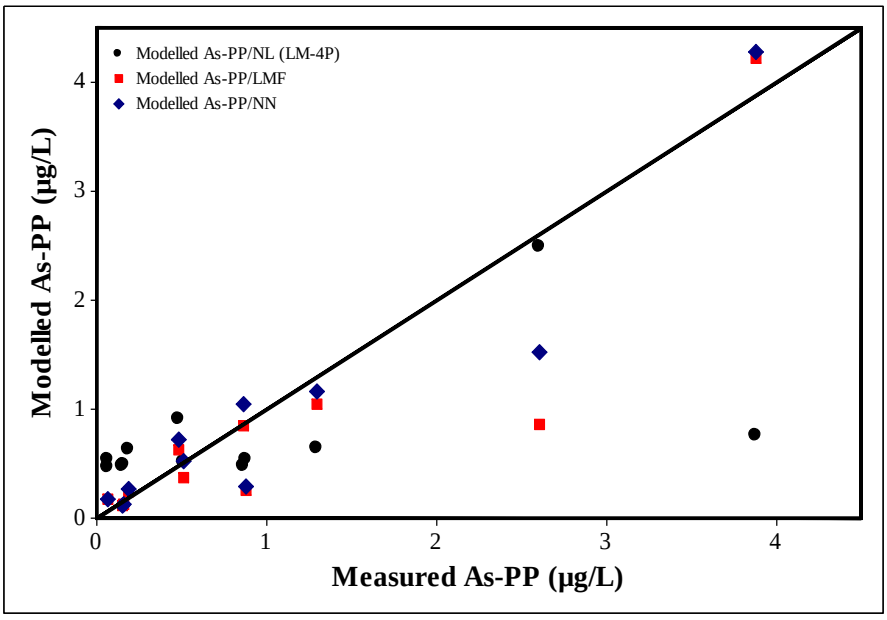


Figure 5.52: Measured and modelled concentration of As-PP in validation

Table 5.33: Correlation coefficients for model validation of As in PP

| Output | Model Type | *r* (Corr. Coef.) |
|---|---|---|
| As-PP | LMF | 0.89 |
| | NL (LM-4P) | 0.53 |
| | NN | 0.94 |

### 5.7.2 Modeling As in HWT

**Linear Model:**

The procedure of selecting parameters and adequacy check for modeling of As in HWT is illustrated in Fig. 5.53. Table 5.34 summarizes the ANOVA with significant factors (p value < 0.01). Among the different linear models, the LMF model was found to be the best and was selected (Equation 5.61). The model had the $R^2$ value of 0.98. The experimental data and predicted values were consistent (Fig. 5.53d). The plot of residuals versus predicted (Fig. 5.53b) showed data randomness. The plot of residuals versus row number (Fig. 5.53c) confirmed that the residuals were uncorrelated. No evidence of lack of fit (P >= 0.1) was also observed. The screening effects of the main factors (Table 5.34) and half-normal plot (Fig. 5.53a) showed that Na-HWT, Ba-HWT and Cr-HWT positively influenced the concentrations of As in HWT samples.

Table 5.34: Screening effects of the factors for modeling As-HWT

| Term | Estimate | Std Error | t Ratio | Prob>\|t\| |
|---|---|---|---|---|
| Intercept | -0.304585 | 0.156303 | -1.95 | 0.0642 |
| Na-HWT | $5.3426\times10^{-6}$ | $1.786\times10^{-7}$ | 29.92 | <.0001 |
| Ba-HWT | 0.0001139 | $1.074\times10^{-5}$ | 10.61 | <.0001 |
| Cr-HWT | 0.4420359 | 0.18535 | 2.38 | 0.0261 |

$$As - HWT = \beta_0 + \beta_1 Na - HWT + \beta_2 Ba - HWT + \beta_3 Cr - HWT \quad (5.61)$$

Where: $\beta_0 = -0.30; \beta_1 = 5.34\times10^{-6}; \beta_2 = 0.00011; \beta_3 = 0.44$

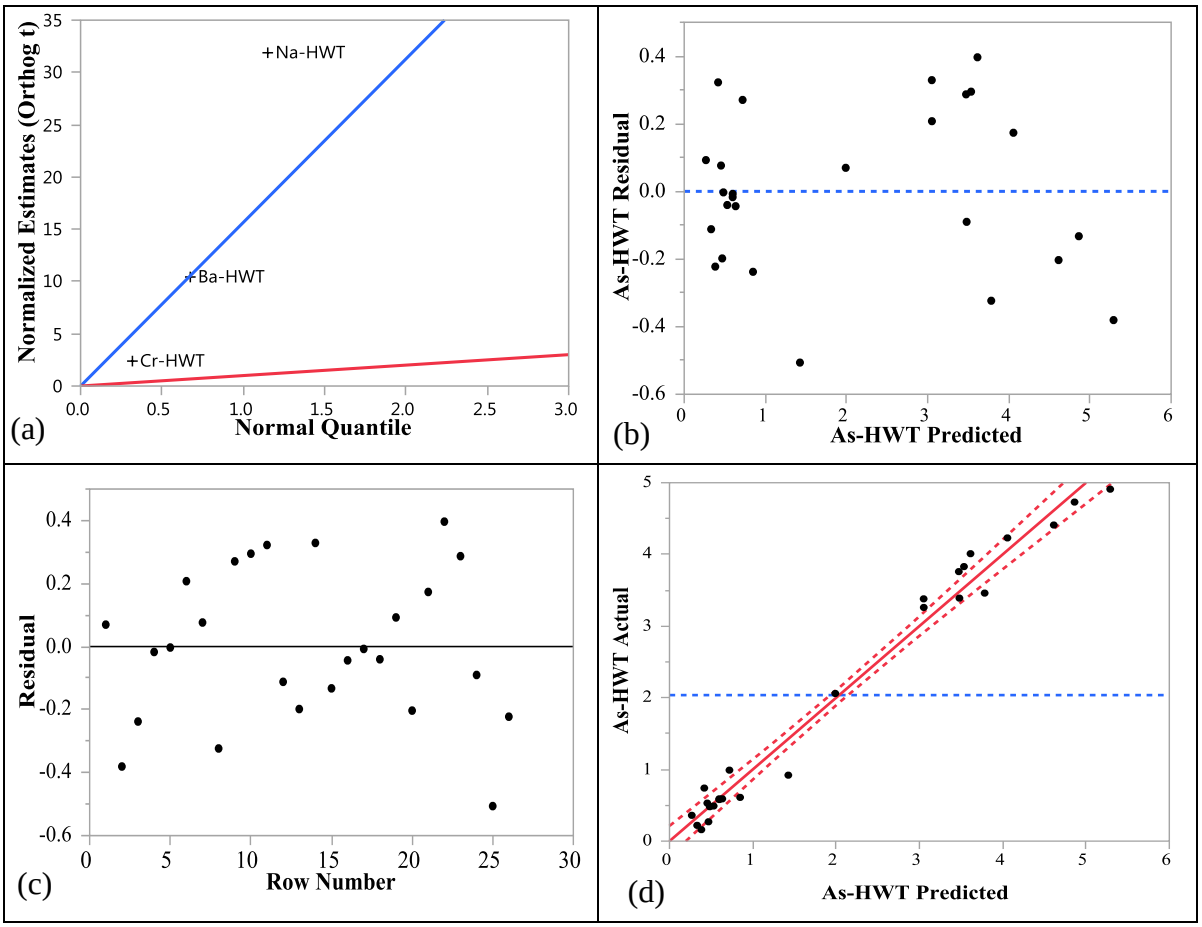


Figure 5.53: For As-HWT model (a) half normal plot (b) residual vs predicted (c) residual vs row number and (d) actual vs predicted data

**Nonlinear Model:**

Among the different nonlinear models, the LM-3P and QRM were found to be best for predicting As in HWT. The NL model (LM-3P) selection for As in HWT is explained in Fig. 5.54. Among the different factors, Na in HWT showed best performance with the LM-3P (Fig. 5.54a). The model for predicting As-HWT is presented in Equation 5.62. The model had the RMSE of 0.63. The experimental data and predicted values ($R^2$=0.87) were found to be consistent (Fig. 5.54b).

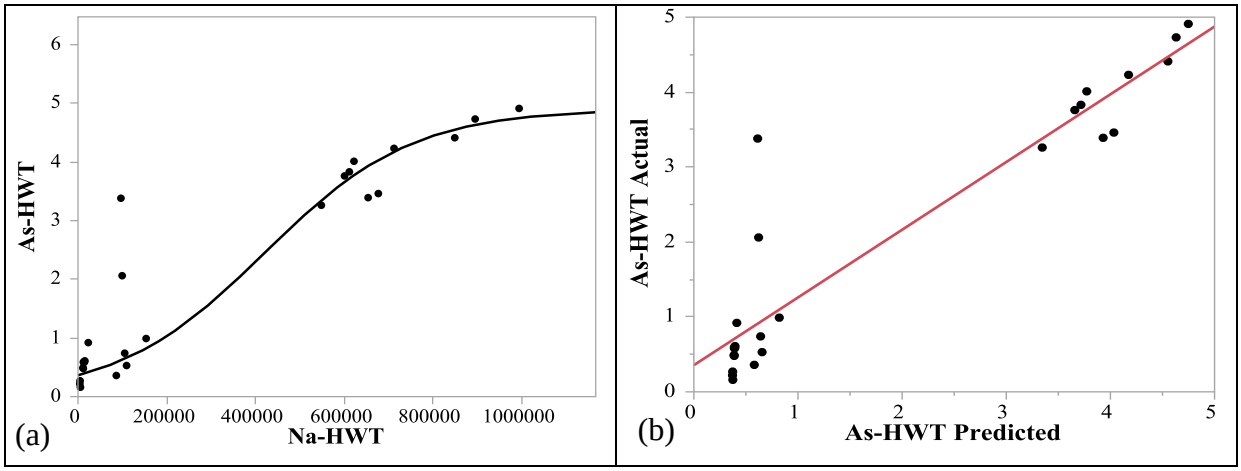


Figure 5.54: For three parameter Logistic model of As-HWT (a) model fitting (b) actual vs predicted plot

$$As-HWT=\frac{\theta_1}{(1+\theta_2 Exp(\theta_3 Na-HWT))} \tag{5.62}$$

Where: $\theta_1=4.9;\ \theta_2=12.5;\ \theta_3=-0.000006$

For As in HWT, another nonlinear model was trained and selected (Fig. 5.55). Lead (Pb) in HWT showed best performance with the Quartic model (Fig. 5.55a). The model for predicting As-HWT is shown in Equation 5.63 and the model had the RMSE value of 1.21. The experimental data and predicted values ($R^2$=0.53) were found to be weakly correlated (Fig. 5.55b).

$$As-HWT=\theta_1+\theta_2 Pb-HWT+\theta_3(Pb-HWT)^2+\theta_4(Pb-HWT)^3+\theta_5(Pb-HWT)^4 \tag{5.63}$$

Where: $\theta_1=2.12;\ \theta_2=2.36;\ \theta_3=-0.79;\ \theta_4=0.076;\ \theta_5=-0.0022$

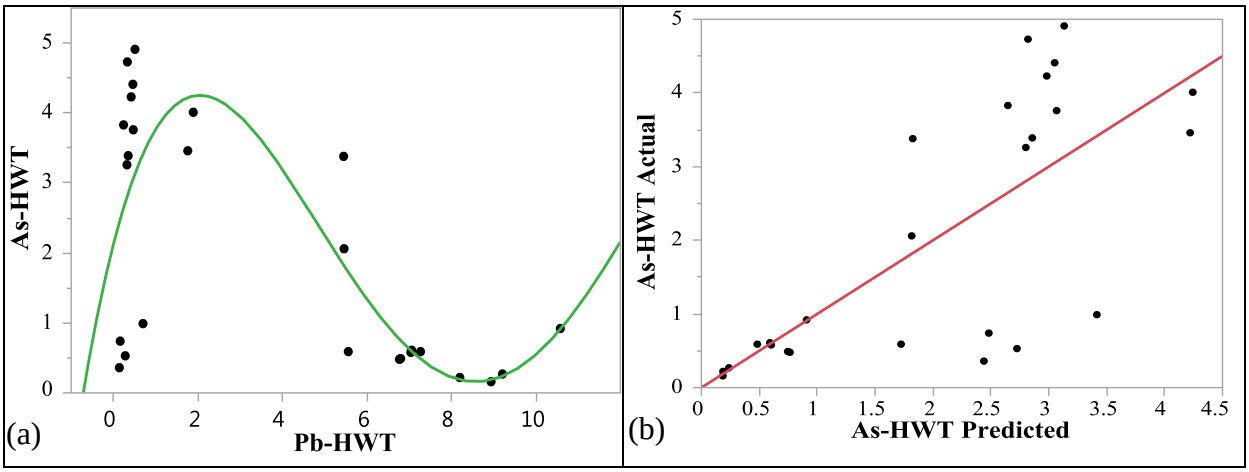


Figure 5.55: For Quartic model of As-HWT (a) model fitting (b) actual vs predicted plot

**Neural Network Model:**

The NN model for predicting As-HWT is shown in Equation 5.64. The model had the $R^2$ value of 0.99 and RMSE of 0.05. The experimental data and predicted values were found to be consistent (Fig. 5.56). The Equations 5.65-5.67 showed that Na-HWT, Ba-HWT and Cr-HWT had influence on the occurrence of As in HWT.

$$As - HWT = 2.25 + (-2.783 \times H1) + (-0.685 \times H2) + (-0.747 \times H3) \quad (5.64)$$

$$H1 = \tanh[0.5 \times \{1.6 + (-0.000008 Na - HWT) + (-0.00008 Ba - HWT) + (0.62 Cr - HWT)\}] \quad (5.65)$$

$$H2 = \tanh[0.5 \times \{33.8 + (-0.00003 Na - HWT) + (-0.001 Ba - HWT) + (-9.39 Cr - HWT)\}] \quad (5.66)$$

$$H3 = \tanh[0.5 \times \{-0.08 + (0.00002 Na - HWT) + (-0.00005 Ba - HWT) + (-6.71 Cr - HWT)\}] \quad (5.67)$$

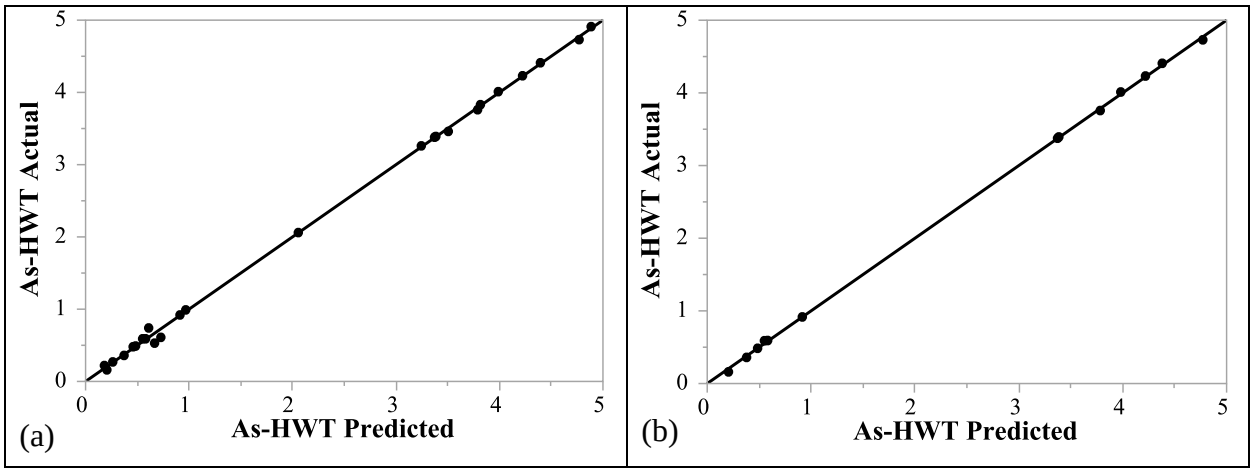


Figure 5.56: Actual vs predicted plot of As-HWT for (a) data training (b) validation of NN model

### 5.7.2.1 Model Comparison for As in HWT

The comparison of the models for predicting As in HWT are shown in Figure 5.57. The NN model had the maximum $R^2$ value of 0.99, while the LMF model had $R^2$ value of 0.98 (Table 5.35). However, the NN and LMF models had the same input factors (Table 5.35). The NL model showed poor performance than the NN and LMF models, due to the single input factor (e.g., Pb-HWT and Na-HWT separately) while As in HWT could be affected by several factors. Between the two NL models, better statistical performance was obtained for LM-3P ($R^2$=0.87) than Quartic model ($R^2$=0.53). The lowest RMSE value of NN model (RMSE=0.05) than the other models also showed better performance of NN model (Table 5.35). Most of the models had better fits for lower and mid-level concentrations of As (<5.0 µg/L), while for NN model, the measured data were much closer to the LOEC. The NN model is the model of choice for predicting As in HWT.

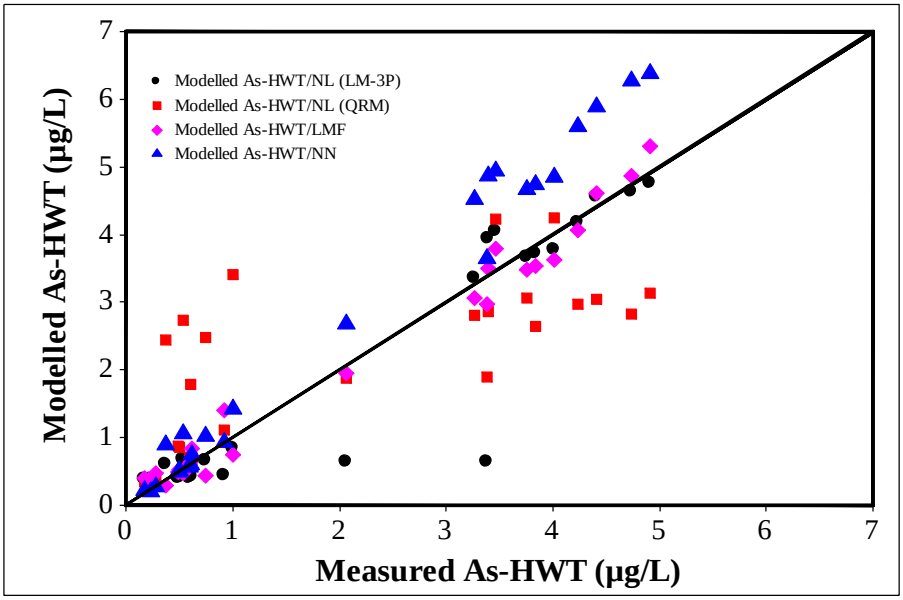


Figure 5.57: Measured and modeled concentration of As in HWT

(LM-3P: 3 parameters Logistic model; QRM: Quartic model; LMF: Main factors linear model; NN: Neural network model)

Table 5.35: Comparison of different models for As in HWT

| Output | Model Type | Parameters | $R^2$ | RMSE |
|---|---|---|---|---|
| As-HWT | LMF | Na-HWT, Ba-HWT, Cr-HWT | 0.98 | 0.256 |
| | NL (LM-3P) | Na-HWT | 0.87 | 0.63 |
| | NL (QRM) | Pb-HWT | 0.53 | 1.21 |
| | NN | Na-HWT, Ba-HWT, Cr-HWT | 0.99 | 0.05 |

### 5.7.2.2 Model Validation for As in HWT

The predictive models for As in HWT were validated using an additional set of data, which were not used in model development. The average concentrations of As-HWT from the LMF, NL (LM-3P), NL (QRM) and NN models were 2.37, 2.14, 2.15 and 3.03 µg/L respectively, and the ranges

were 0.27-4.86, 0.37-4.63, 0.33-4.24 and 0.20-6.27 µg/L respectively. The average of measured concentrations of As-HWT was 2.39 µg/L with the range of 0.16-4.73 µg/L.

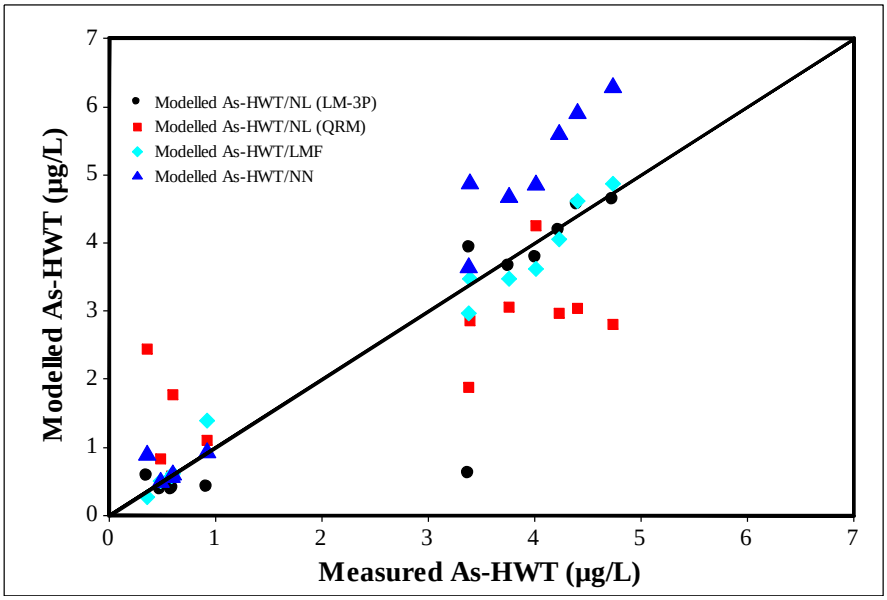


Figure 5.58: Measured and modelled concentration of As-HWT in validation

Table 5.36: Correlation coefficients for model validation of As in HWT

| Output | Model Type | *r* (Corr. Coef.) |
|---|---|---|
| As-HWT | LMF | 0.99 |
| | NL (LM-3P) | 0.91 |
| | NL (QRM) | 0.81 |
| | NN | 0.99 |

From the plot of predicted vs. measured data, the values of correlation coefficients (*r*) were determined and shown in Table 5.36. The values of *r* for LMF, NL (LM-3P), NL (QRM) and NN models were 0.99, 0.91, 0.81 and 0.99 respectively. The comparison of different models for

validation study are shown in Figure 5.58. All the models were closer to LOEC for the whole range of concentrations of As-HWT while for NN and LMF models, the measured data were much closer to the LOEC.

For As-PP and As-HWT models, the NN models were the best while the NL models showed poor performance. Most of the models for As in PP and HWT showed moderate to excellent predictive capacities. As in PP had negligible contribution form As in WDS. Arsenic in plumbing system was accumulated along with the calcite in the iron pipe and released into consumer tap [119]. The relatively acidic water was likely to increase the release of As through corrosive action, enhanced reaction with pipe coatings and plumbing materials. The stagnation period might have significant effects on As release from pipe network. The hard scale deposits (Ca and Mg ions) on the heater wall and the other corroded metals (i.e., Mn, Cu, Fe, As, Pb, Sr, Hg) might have served as the potential sources of As in HWT. Following the usage of hot water, the scales were sloughed off and released into hot water [103]. As in HWT had negligible contribution form As in WDS.

## 5.8 Models for Predicting Manganese (Mn)

### 5.8.1 Modeling Mn in HWT

**Linear Model:**

Figure 5.59 summarizes the procedure of selecting parameters and adequacy check for developing the model for predicting Mn concentrations in HWT. Table 5.37 summarizes the ANOVA with significant factors (p value < 0.01). Among the different linear models, the LMF model was found to be the best and was selected (Equation 5.68). The model had the $R^2$ value of 0.83. The experimental data and predicted values were found to be consistent (Fig. 5.59d). The plot of

residuals versus predicted (Fig. 5.59b) showed data randomness. The plot of residuals versus row number (Fig. 5.59c) confirmed that the residuals were uncorrelated. No evidence of lack of fit (P >= 0.1) was also observed. The screening effects of the main factors (Table 5.37) and half-normal plot (Fig. 5.59a) showed that Fe-HWT and V-HWT positively influenced the concentrations of Mn in HWT samples while Cr-HWT had negative influence.

Table 5.37: Screening effects of the factors for modeling Mn-HWT

| Term | Estimate | Std Error | t Ratio | Prob>\|t\| |
|---|---|---|---|---|
| Intercept | 0.9386493 | 0.345835 | 2.71 | 0.0134 |
| V-HWT | 0.1333557 | 0.014088 | 9.47 | <.0001 |
| Cr-HWT | -2.34296 | 0.352337 | -6.65 | <.0001 |
| Fe-WDS | 0.0113169 | 0.00471 | 2.40 | 0.0261 |

$$Mn - HWT = \beta_0 + \beta_1 V - HWT + \beta_2 Cr - HWT + \beta_3 Fe - HWT \quad (5.68)$$

Where: $\beta_0 = 0.94; \beta_1 = 0.133; \beta_2 = -2.34; \beta_3 = 0.011$

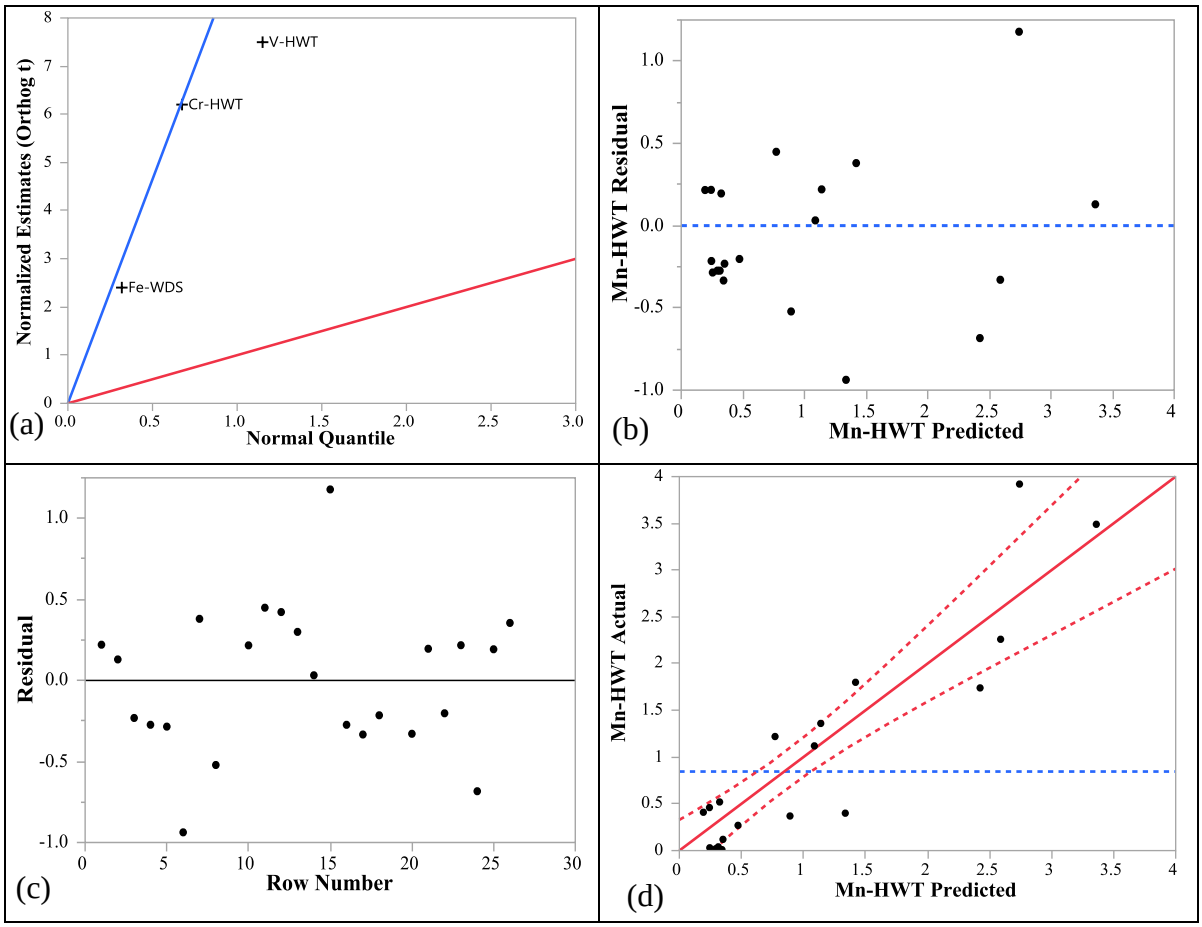


Figure 5.59: For Mn-HWT model (a) half normal plot (b) residual vs predicted (c) residual vs row number and (d) actual vs predicted data

**Neural Network Model:**

The NN model for predicting Mn-HWT is shown in Equation 5.69. The model had the $R^2$ value of 0.99 and RMSE of 0.14. The experimental data and predicted values were found to be consistent (Fig. 5.60). The Equations 5.70-5.72 showed that Fe-HWT, V-HWT, Cr-HWT and Mn-WDS had influence on the occurrence of Mn in HWT.

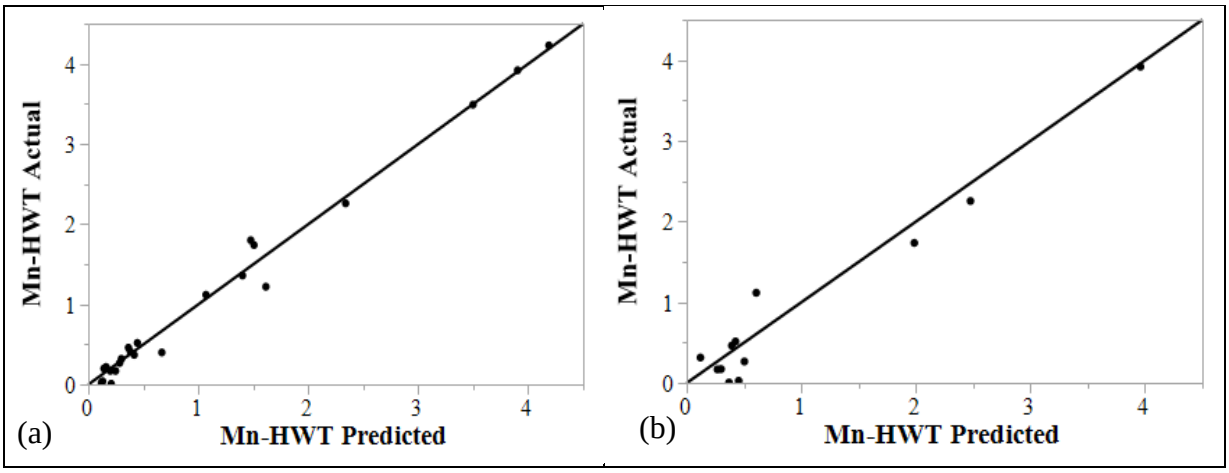


Figure 5.60: Actual vs predicted plot of Mn-HWT for (a) data training (b) validation of NN model

$$Mn-HWT = 1.76 + (-4.38 \times H1) + (-7.27 \times H2) + (9.18 \times H3) \quad (5.69)$$

$$H1 = \tanh[0.5 \times \{1.8 + (2.8\,Cr\text{-}HWT) + (0.03\,V\text{-}HWT) + (-0.04\,Fe\text{-}HWT) + (-0.06\,Mn\text{-}WDS)\}] \quad (5.70)$$

$$H2 = \tanh[0.5 \times \{-9.18 + (3.62\,Cr\text{-}HWT) + (0.19\,V\text{-}HWT) + (0.07\,Fe\text{-}HWT) + (3.45\,Mn\text{-}WDS)\}] \quad (5.71)$$

$$H3 = \tanh[0.5 \times \{-5.47 + (5.32\,Cr\text{-}HWT) + (0.15\,V\text{-}HWT) + (0.004\,Fe\text{-}HWT) + (2.98\,Mn\text{-}WDS)\}] \quad (5.72)$$

### 5.8.1.1 Model Comparison for Mn in HWT

The comparison of the models for predicting Mn in HWT are shown in Figure 5.61. The NN model had the maximum $R^2$ value of 0.99 while the LMF model had $R^2$ value of 0.83 (Table 5.38). The NN model used one additional factor (i.e., Mn-WDS) than LMF model (Table 5.38). None of the NL models fit with any parameters. All models showed better fit with measured data for the whole range of concentrations of Mn while for NN model, the measured data were much closer to the LOEC (Fig. 5.61).

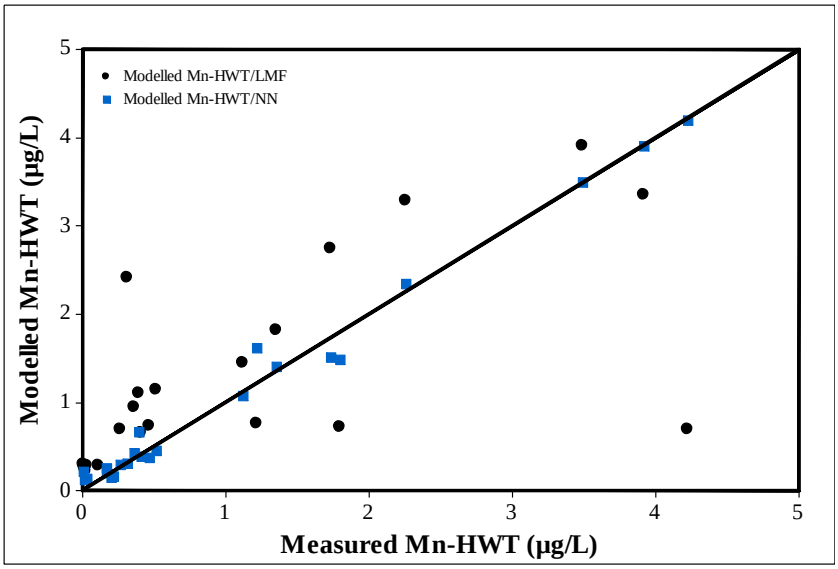


Figure 5.61: Measured and modeled concentration of Mn in HWT

(LMF: Main factors linear model; NN: Neural network model)

Table 5.38: Comparison of different models for Mn in HWT

| Output | Model Type | Parameters | $R^2$ | RMSE |
|---|---|---|---|---|
| Mn-HWT | LMF | V-HWT, Cr-HWT, Fe-HWT | 0.83 | 0.48 |
| | NN | V-HWT, Cr-HWT, Fe-HWT, Mn-WDS | 0.99 | 0.14 |

### 5.8.1.2 Model Validation for Mn in HWT

The predictive models for Mn in HWT were validated using an additional set of data, which were not used in model development. The average concentrations of Mn-HWT from the LMF and NN models were 1.25 and 0.88 µg/L respectively, and the ranges were 0.21-3.35 and 0.10-3.93 µg/L respectively. The average of measured concentrations of Mn-HWT was 0.85 µg/L with the range of 0.006-3.92 µg/L. From the plot of predicted vs. measured data, the values of correlation

coefficients (*r*) were determined and shown in Table 5.39. The values of *r* for LMF and NN models were 0.84 and 0.98 respectively. The comparison of different models for validation study are shown in Figure 5.62. Both the models were closer to LOEC for lower concentration of Mn-HWT (<3 µg/L), while for NN model, the measured data were much closer to the LOEC.

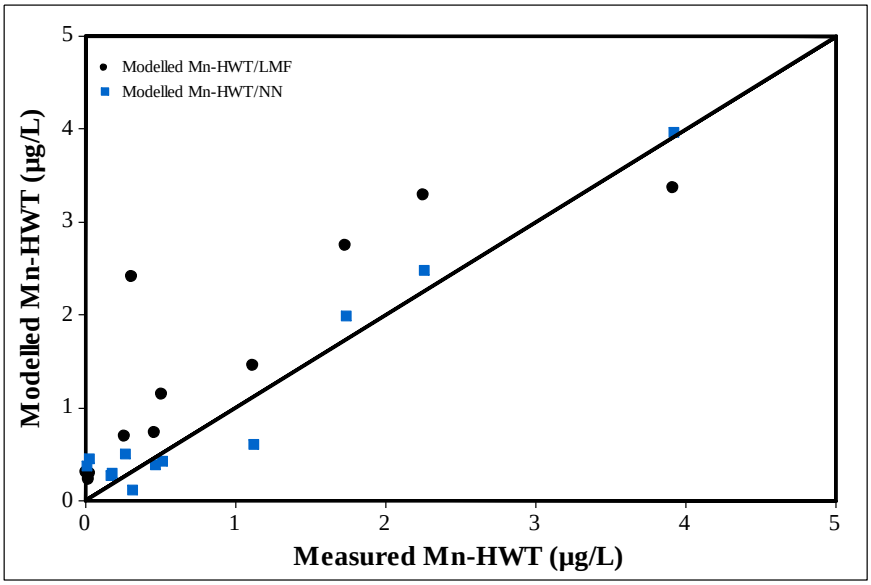


Figure 5.62: Measured and modelled concentration of Mn-HWT in validation

Table 5.39: Correlation coefficients for model validation of Mn in HWT

| Output | Model Type | *r* (Corr. Coef.) |
|---|---|---|
| Mn-HWT | LMF | 0.84 |
| | NN | 0.98 |

For Mn in HWT, the NN models showed the best performance, while none of the NL models showed good fit with any parameters. The models for Mn in HWT showed moderate to excellent predictive capacities. Mn in HWT was affected by its concentration in WDS. The hard scale of the heater wall were deposited along with other corroded metals (i.e., Fe, V, Mn), which might have served as the potential sources of Mn in HWT. Following the usage of hot water, the scales were sloughed off and released into hot water [103]. It is likely that Mn co-existed with Fe and rarely found alone in a water source [120].

## 5.9 Models for Predicting Zinc (Zn)

### 5.9.1 Modeling Zn in PP

**Neural Network Model:**

The NN model for predicting Zn-PP is shown in Equation 5.73. The model had the $R^2$ value of 0.92 and RMSE of 5.24. The experimental data and predicted values were found to be consistent (Fig. 5.63). The Equation of hidden nodes (Equation 5.74-5.76) showed that total chlorine in WDS, temperature in PP and Cu-PP had influence on the concentrations of Zn in PP.

$$Zn-PP = 136.67 + (439.20 \times \mathrm{H1}) + (-759.64 \times \mathrm{H2}) + (-453.27 \times \mathrm{H3}) \quad (5.73)$$

$$\mathrm{H1} = \tanh[0.5 \times \{-6.29 + (55.94\,\mathrm{TCl\text{-}WDS}) + (0.04\,T-PP + (-0.99\,C\mathrm{u}-PP)\}] \quad (5.74)$$

$$\mathrm{H2} = \tanh[0.5 \times \{11.26 + (14.47\,\mathrm{TCl\text{-}WDS}) + (-0.49\,T-PP + (-5.82\,C\mathrm{u}-PP))\}] \quad (5.75)$$

$$\mathrm{H3} = \tanh[0.5 \times \{-19.20 + (-5.78\,\mathrm{TCl\text{-}WDS}) + (0.76\,T-PP + (7.33\,C\mathrm{u}-PP)\}] \quad (5.76)$$

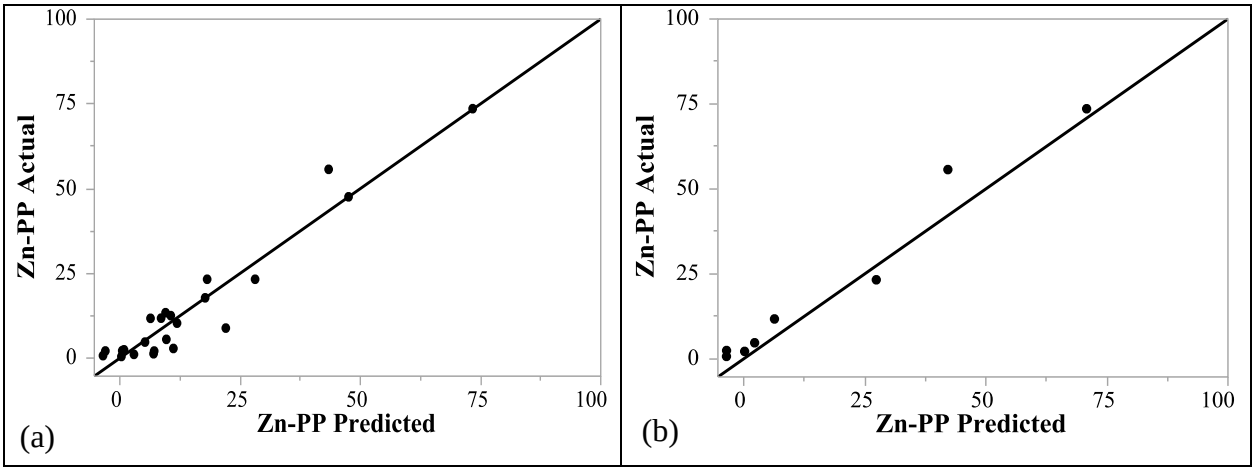


Figure 5.63: Actual vs predicted plot of Zn-PP for (a) data training (b) validation of NN model

### 5.9.1.1 Model Validation for Zn in PP

The predictive model for Zn in PP was validated using an additional set of data, which were not used in model development. The average concentrations of Zn-PP from the NN model was 16.27 µg/L and the range was 0.19-70.82 µg/L. The average measured concentration of Zn-PP was 19.97 µg/L with the range of 0.72-73.59 µg/L. From the plot of predicted vs. measured data, the value of correlation coefficient ($r$=0.96) was determined (Fig. 5.64). The measured data were much closer to the LOEC.

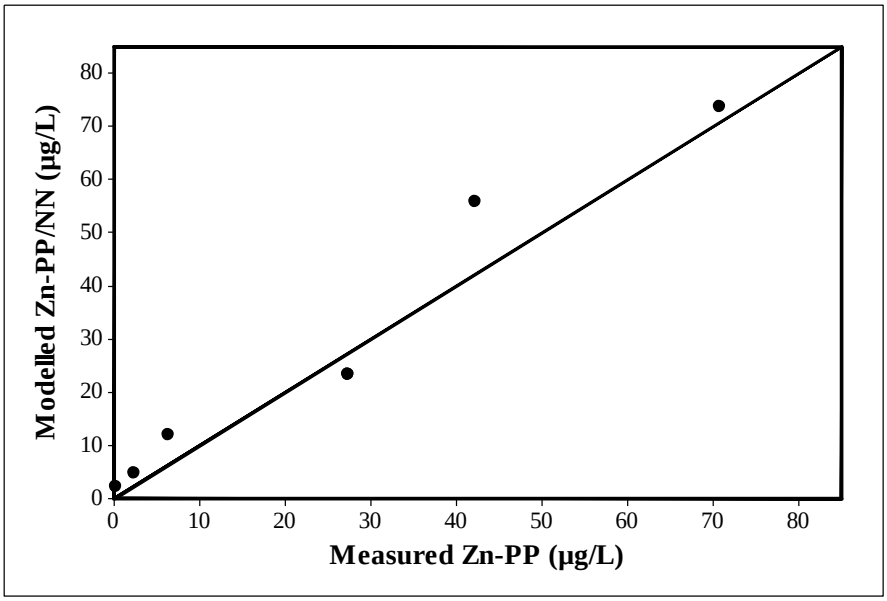


Figure 5.64: Measured and modelled concentration of Zn-PP in validation

For Zn in PP, the NN model showed excellent predictive capacities, while none of the liner or NL models showed good fits. Zn in PP had negligible effect form Zn in WDS. The relatively acidic water was likely to increase the release of Zn through corrosive action, increased reaction with pipe coatings and plumbing materials. The stagnation period might have affected the release of Zn from pipe network. Changes of the concentrations of disinfectant or water temperature could cause the release of Zn from corrosion scale deposits. Application of zinc orthophosphate inhibitor for corrosion control might have also served as a potential source of Zn in consumer tap [121].

## 5.10 Models for Predicting Magnesium (Mg)

### 5.10.1 Modeling Mg in HWT

**Linear Model:**

Figure 5.65 summarizes the procedure of selecting parameters and adequacy check to develop models for Mg concentrations in HWT samples. Table 5.40 summarizes the ANOVA with significant factors (p value < 0.01). Among the different linear models, the LMF model was found to be the best and was selected (Equation 5.77). The model had the $R^2$ value of 0.99. The experimental data and predicted values were found to be consistent (Fig. 5.65d). The plot of residuals versus predicted (Fig. 5.65b) showed the randomness of residuals. The plot of residuals versus row number (Fig. 5.65c) indicated that the residuals were uncorrelated. No evidence of lack of fit (P > = 0.1) was observed. The screening effects of the main factors (Table 5.40) and half-normal plot (Fig. 5.65a) showed that Sr-HWT, Ca-HWT, Hg-HWT and Ba-HWT positively influenced the occurrence of Mg in HWT samples.

Table 5.40: Screening effects of the factors for modeling Mg-HWT

| Term | Estimate | Std Error | t Ratio | Prob>\|t\| |
|---|---|---|---|---|
| Intercept | -578.8981 | 170.8677 | -3.39 | 0.0031 |
| Sr-HWT | 11.914251 | 1.000989 | 11.90 | <.0001 |
| Ca-HWT | 0.1625284 | 0.036439 | 4.46 | 0.0003 |
| Hg-HWT | 496.12657 | 88.56081 | 5.60 | <.0001 |
| Ba-HWT | 0.1394185 | 0.050987 | 2.73 | 0.0132 |

$$Mg - HWT = \beta_0 + \beta_1 Sr - HWT + \beta_2 Ca - HWT + \beta_3 Hg - HWT + \beta_4 Ba - HWT \qquad (5.77)$$

Where: $\beta_0 = -578.9;\ \beta_1 = 11.91;\ \beta_2 = 0.163;\ \beta_3 = 496.13;\ \beta_4 = 0.139$

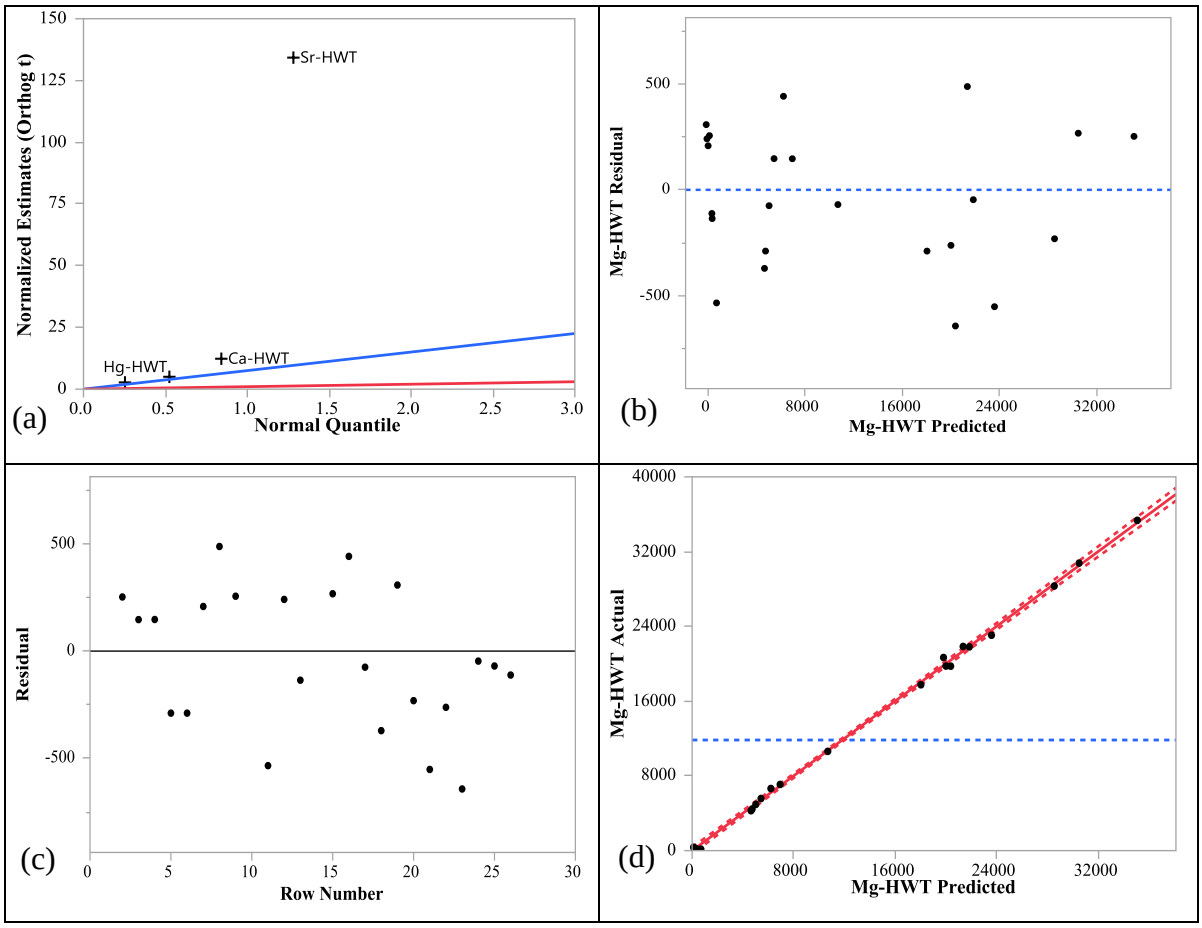


Figure 5.65: For Mg-HWT model (a) half normal plot (b) residual vs predicted (c) residual vs row number and (d) actual vs predicted data

**Nonlinear Model:**

Among the different NL models, the LM-4P and QRM were found to be best for predicting Mg in HWT. The NL (QRM) selection for Mg in HWT samples is explained in Fig. 5.66. Among the

different factors, Sr in HWT showed the best performance with the Quartic model (Fig. 5.66a) for predicting Mg in HWT. The model for predicting Mg-HWT is shown in Equation 5.78 and the model had the RMSE value of 1778.4. The experimental data and predicted values ($R^2$=0.99) were consistent (Fig. 5.66b).

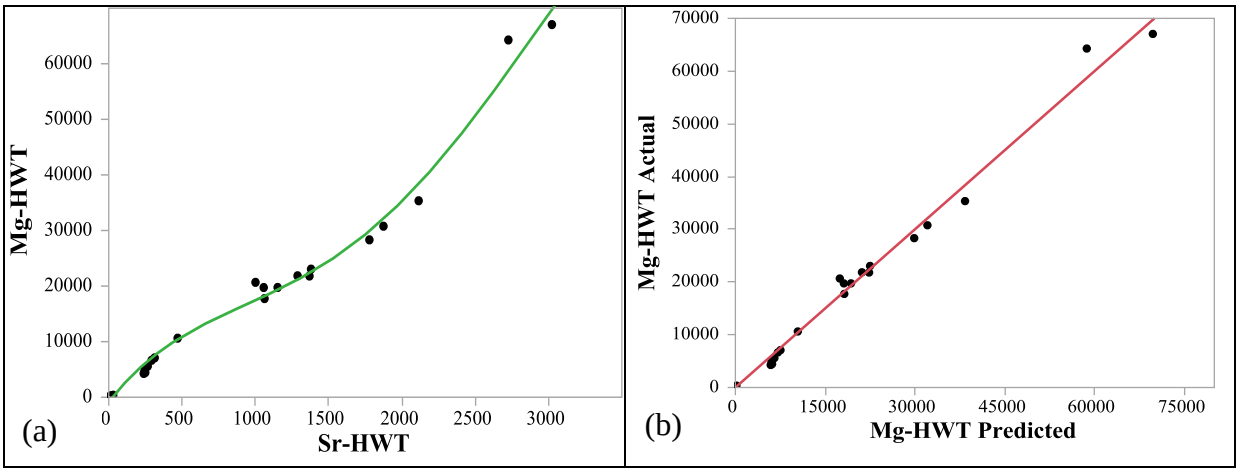


Figure 5.66: For Quartic model of Mg-HWT (a) model fitting (b) actual vs predicted plot

$$Mg-HWT = \theta_1 + \theta_2 Sr-HWT + \theta_3 (Sr-HWT)^2 + \theta_4 (Sr-HWT)^3 + \theta_5 (Sr-HWT)^4 \quad (5.78)$$

Where: $\theta_1 = -822.36; \theta_2 = 33.78; \theta_3 = -0.026; \theta_4 = 0.000013; \theta_5 = -1.65 \times 10^{-9}$

Another nonlinear model for Mg-HWT showed similar performance where Ca-HWT was used in the four parameter Logistic model (Fig. 5.67a). This model is shown in Equation 5.79 and the model had the RMSE value of 1964.77. The experimental data and predicted values were found to be consistent (Fig. 5.67b) with the $R^2$ of 0.99.

$$Mg-HWT = \theta_1 + \frac{(\theta_2 - \theta_1)}{(1 + Exp\{\theta_3[Ca-HWT-\theta_4]\})} \quad (5.79)$$

Where: $\theta_1 = 65590; \theta_2 = -185.76; \theta_3 = 0.000053; \theta_4 = 53500$

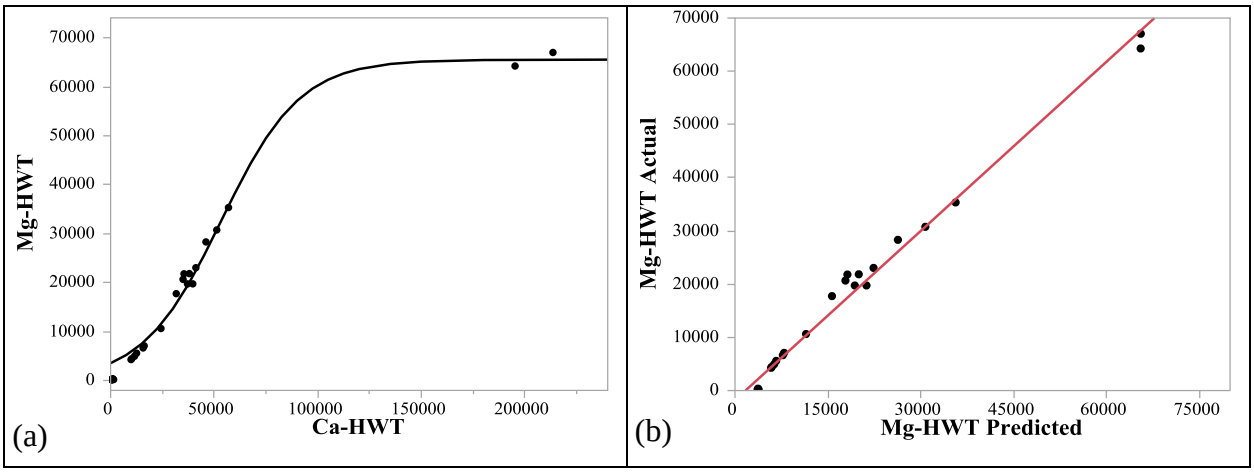


Figure 5.67: For four parameter Logistic model of Mg-HWT (a) model fitting (b) actual vs predicted plot

**Neural network Model:**

The NN model for predicting Mg-HWT is shown in Equation 5.80. The model had the $R^2$ value of 0.99 and RMSE of 191.9. The experimental data and predicted values were found to be consistent (Fig. 5.68). The Equations 5.81-5.83 showed that Sr-HWT, Ca-HWT, Hg-WDS and Ba-HWT had influence on the occurrence of Hg in HWT.

$$Mg - HWT = 51040.8 + (56808 \times \mathrm{H1}) + (\text{-}12680 \times \mathrm{H2}) + (49234 \times \mathrm{H3}) \quad (5.80)$$

$$\mathrm{H1} = \tanh[0.5 \times \{-0.38 + (0.00001\,\mathrm{Ca}\text{ - HWT}) + (0.0002\,\mathrm{Sr}\text{ - HWT}) + (0.000006\,\mathrm{Ba}\text{ - HWT}) + (\text{-}0.15\,\mathrm{Hg}\text{ - HWT})\}] \quad (5.81)$$

$$\mathrm{H2} = \tanh[0.5 \times \{1.91 + (\text{-}0.00002\,\mathrm{Ca}\text{ - HWT}) + (0.0005\,\mathrm{Sr}\text{ - HWT}) + (\text{-}0.00006\,\mathrm{Ba}\text{ - HWT}) + (0.07\,\mathrm{Hg}\text{ - HWT})\}] \quad (5.82)$$

$$\mathrm{H3} = \tanh[0.5 \times \{-1.47 + (\text{-}0.00001\,\mathrm{Ca}\text{ - HWT}) + (0.0005\,\mathrm{Sr}\text{ - HWT}) + (\text{-}0.00003\,\mathrm{Ba}\text{ - HWT}) + (0.23\,\mathrm{Hg}\text{ - HWT})\}] \quad (5.83)$$

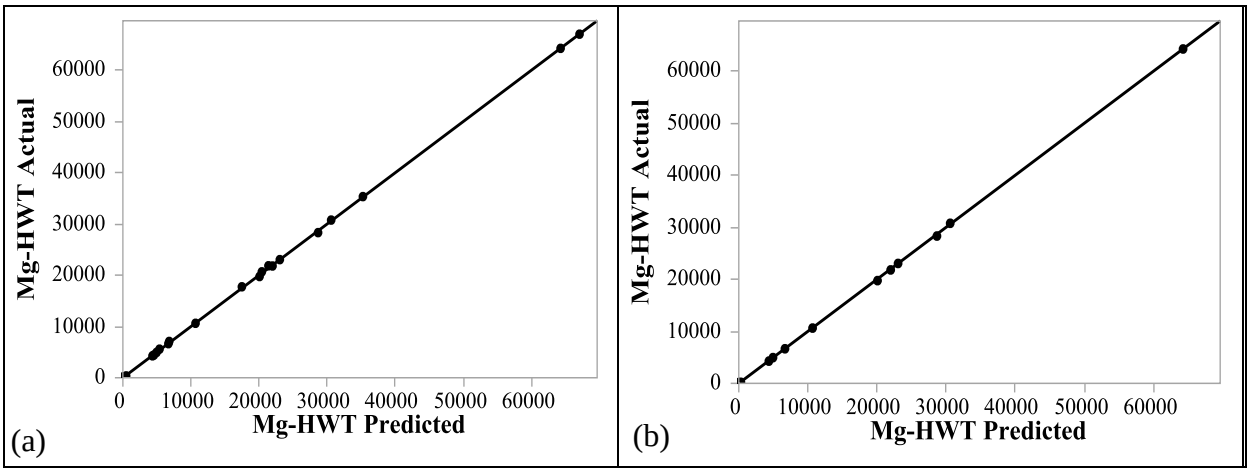


Figure 5.68: Actual vs predicted plot of Mg-HWT for (a) data training (b) validation of NN model

## 5.10.2 Model Comparison for Mg in HWT

The comparison of the models for predicting Mg in HWT are shown in Figure 5.69. All the four models had the similar $R^2$ value of 0.99. Between the two NL models, QRM (RMSE=1778.4) showed better performance than LM-4P (RMSE=1964.7). The lowest RMSE value of NN model (RMSE=191.92) than others indicate that the NN model is statistically better than other models

(Table 5.41). The nonlinear models were developed using single factor, while the formation of Mg in HWT can be affected by several parameters. Most of the models had better fit for lower half part of the dataset (<45000 µg/L) while for NN model, the measured data were much closer to the LOEC. The NN model is the model of choice for predicting Mg in HWT.

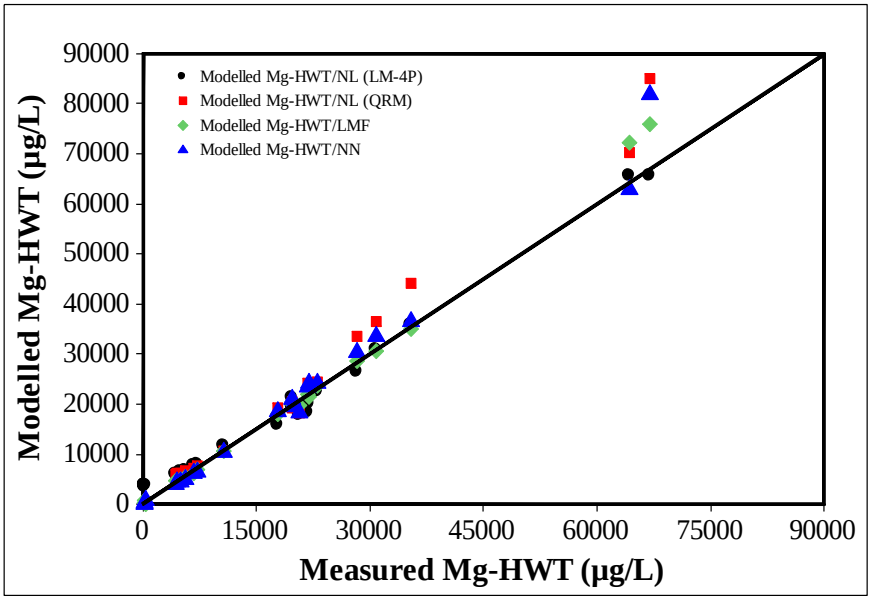


Figure 5.69: Measured and modeled concentration of Mg in the hot water tank samples (NLM-4P: 4 parameters Logistic model; QRM: Quartic model; LMF: Main factors linear model; NN: Neural network model)

Table 5.41: Comparison of different models for Mg in HWT

| Output | Model Type | Parameters | $R^2$ | RMSE |
|---|---|---|---|---|
| Mg-HWT | LMF | Ca-HWT, Sr-HWT, Ba-HWT, Hg-HWT | 0.99 | 401.89 |
| | NL (LM-4P) | Ca-HWT | 0.99 | 1964.7 |
| | NL (QRM) | Sr-HWT | 0.99 | 1778.4 |
| | NN | Ca-HWT, Sr-HWT, Ba-HWT, Hg-HWT | 0.99 | 191.92 |

### 5.10.3 Model Validation for Mg in HWT

The predictive models for Mg in HWT were validated using an additional set of data, which were not used in model development. The average concentrations of Mg-HWT from the LMF, NL (LM-4P), NL (QRM) and NN models were 18773, 18581, 19814 and 18993 µg/L respectively, and the ranges were 304-72351, 3497-65554, 5928-70281 and 4008-63953 µg/L respectively. The average of measured concentrations of Mg-HWT was 18042 µg/L with the range of 148-64280 µg/L. From the plot of predicted vs. measured data, the values of correlation coefficients (*r*) were determined and shown in Table 5.42. All the four models had the same *r* (0.99). The comparison of different models for validation study are shown in Figure 5.70. All the models were closer to LOEC for lower concentration of Mg-HWT (<40000 µg/L), while for NN model, the measured data were much closer to the LOEC.

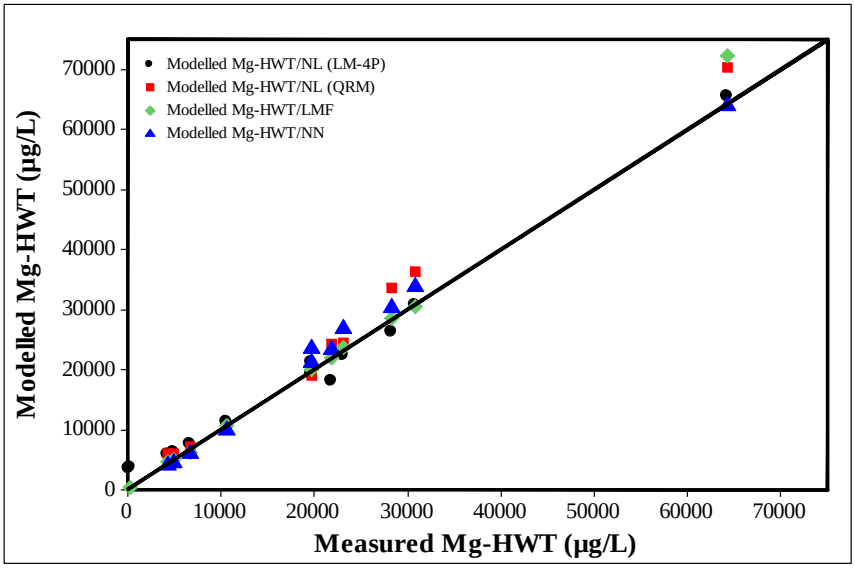


Figure 5.70: Measured and modelled concentration of Mg-HWT in validation

Table 5.42: Correlation coefficients for model validation of Mg in HWT

| Output | Model Type | *r* (Corr. Coef.) |
|---|---|---|
| Mg-HWT | NL (LM-4P) | 0.99 |
| | NL (QRM) | 0.99 |
| | LMF | 0.99 |
| | NN | 0.99 |

All the models for Mg in HWT showed excellent predictive capacities. The hard scale deposits (Ca and Mg ions) on the heater wall along with other corroded metals (i.e., Sr, Hg) might have caused the release of Mg in HWT. The sacrificial anodes (A rod screwed into the top of HWT and made of Mg or Al that is formed around a steel core wire) used for rust protection of HWT could also be a potential source of Mg [122].

# CHAPTER 6

# CONCLUSIONS

In this study, occurrences and variability of different heavy metals in WDS, PP and HWT samples were investigated for a period of 7 month (Nov 2015 – May 2016). The samples were collected and analyzed following the standard procedures. Concentrations of metals were variable, and several metals showed wide ranges of coefficient of variation. Concentrations of most of the metals were found to be higher in HWT than those in the WDS and PP. The blended water (mixture of desalinated and treated groundwater) is supplied through the WDS in Saudi Arabia. This water is relatively corrosive, which can react with the pipe materials and pipe coatings during transport through the WDS, resulting in the release of heavy metals into drinking water. The diurnal and seasonal variability of temperature also affected the reactivity of desalinated/blended water with the pipe materials and inner coatings. Between WDS and tap in the house, water spends a significant amount of time in the PP and HWT depending on the size of the plumbing premise. This allows an additional reaction time and the water quality is often degrades between the WDS and the tap. During the off-peak hours (e.g., midnight to early morning), stagnation period of water in the PP and HWT can be much higher, which can increase the concentrations of several heavy metals in water.

This study developed three major types of models for predicting the changes of heavy metal concentrations from the WDS to the PP and HWT. The linear and neural network models were found to be very good to excellent while the nonlinear models showed relatively weak

performance. In model validation study with additional set of data, all these models showed moderate to excellent predictability.

The predictive models for Pb, Fe, Cu and Hg in PP were found to be partially affected by their concentrations in WDS. In case of HWT models, formation of Pb and Cr were partially due to the concentrations in the WDS samples. Among the WQP, temperature, TCl and $UV_{254}$ were the important parameters in model formation. In addition, co-occurrence with other metals were a significant criterion for few models. Incorporation of interaction effects of several factors has improved the efficiency of few models. Better understanding of interaction effects of the factors is essential for developing the best models. The models may provide the baseline information to identify the policies for improving the quality of drinking water in consumer's tap and establishing regulatory guidelines for heavy metals.

The findings of this study will provide supportive information in taking necessary steps for controlling metal release and to protect human health. However, this study has few limitations in context of study period and sample analysis. The availability of standard chemicals, maintenance of equipment's due to sudden failure and lack of the expert technical staffs had some implications on the analytical schedule. Furthermore, the study period was limited to 7 months. Extension of the sampling process over additional period may enhance the understanding of the occurrences and variability of metals in WDS, PP and HWT.

# CHAPTER 7

# RECOMMENDATIONS

The study recommends the following research to better understand the occurrences and variability of heavy metals in tap water, and to develop models for predicting heavy metals in plumbing pipe and hot water tanks.

The sampling program of this study was limited to a single source. The sampling program in multiple sources of different locations may provide better insights on the occurrences and variability of metals in WDS, PP and HWT. In addition, the span of this study was also limited. Extension of the sampling process over additional period may enhance reliability of the findings. The validation study for the models was accomplished by the dataset of similar source, which were excluded during the model formation process. Model validation by additional set of data from separate sampling location may provide better explanation regarding the model acceptability.

The indoor handling of tap water (e.g., storing in the refrigerator, household filtration, heating) may also serve as a potential source of metal exposure. The effects of such factors might be investigated in future.

Despite few limitations, this study provides the basic understanding regarding the changes and variability of metal concentrations in PP and HWT. Consumption of metal contaminated drinking water over prolonged period may affect the humans. There is a need to perform human exposure and risk analysis from heavy metals in tap water in future.

# References


[1] L. Jarup, Hazards of heavy metal contamination, *Br. Med. Bull.* 68 (2003) 167–182.

[2] W.D. Glanze, K. Anderson, L.E. Anderson, *The Signet Mosby medical encyclopedia, Signet*, 1996.

[3] S. Chowdhury, M.A.J. Mazumder, O. Al-Attas, T. Husain, Heavy metals in drinking water: Occurrences, implications, and future needs in developing countries, *Sci. Total Environ.* 569–570 (2016) 476–488.

[4] M.A. Islam, M.R. Karim, T. Higuchi, H. Sakakibara, M. Sekine, Comparison of the trace metal concentration of drinking water supply options in southwest coastal areas of Bangladesh, *Appl. Water Sci.* 4 (2014) 183–191.

[5] T. He, X. Feng, Y. Guo, G. Qiu, Z. Li, L. Liang, J. Lu, The impact of eutrophication on the biogeochemical cycling of mercury species in a reservoir: A case study from Hongfeng Reservoir, Guizhou, China, *Environ. Pollut.* 154 (2008) 56–67.

[6] F. Yoshida, A. Hata, H. Tonegawa, Itai-Itai disease and the countermeasures against cadmium pollution by the Kamioka mine, Environ. *Econ. Policy Stud.* 2 (1999) 215–229.

[7] C. Jane Wyatt, C. Fimbres, L. Romo, R.O. Méndez, M. Grijalva, Incidence of Heavy Metal Contamination in Water Supplies in Northern Mexico, *Environ. Res.* 76 (1998) 114–119.

[8] UESPA (U.S. Environmental Protection Agency), National Primary Drinking Water Regulations, (2017). https://www.epa.gov/ground-water-and-drinking-water/national-primary-drinking-water-regulations#Inorganic (accessed October 29, 2017).

[9] WHO (World Health Organization), Guidelines for Drinking-water Quality FOURTH EDITION WHO Library Cataloguing-in-Publication Data, World Heal. Organ. (2011). http://www.who.int (accessed October 29, 2017).

[10] J.P. Bourdineaud, Heavy metals toxicity at very low, yet environmentally relevant doses: The cases of human mercurial contaminations through fish consumption, uranium in drinking water, and gold nanoparticles in aquatic systems, Comp. Biochem. Physiol. Part A Mol. Integr. Physiol. 157 (2010) S35.

[11] E.J. Kim, J.E. Herrera, D. Huggins, J. Braam, S. Koshowski, Effect of pH on the concentrations of lead and trace contaminants in drinking water: A combined batch, pipe loop and sentinel home study, *Water Res.* 45 (2011) 2763–2774.

[12] G. Tamasi, R. Cini, Heavy metals in drinking waters from Mount Amiata (Tuscany, Italy). Possible risks from arsenic for public health in the Province of Siena, *Sci. Total Environ*. 327 (2004) 41–51.

[13] I.A. Alam, M. Sadiq, Metal contamination of drinking water from corrosion of distribution pipes, *Environ. Pollut*. 57 (1989) 167–178.

[14] M.A. El-Harouny, S.A. El-Dakroory, S.M. Attalla, N.A. Hasan, R. Hegazy, The Internet journal of nutrition and wellness., *Internet Scientific Publications*, 2005. https://www.cabdirect.org/cabdirect/abstract/20103382092 (accessed October 29, 2017).

[15] AI Alabdulaaly, Trace metals in Riyadh public waters supplies, *Arab. J. Sci. Eng*. 22 (1997) 165–174

[16] A. Rakić, J. Perić, L. Foglar, Influence of temperature, chlorine residual and heavy metals on the presence of Legionella pneumophila in hot water distribution systems, *Ann. Agric. Environ. Med*. 19 (2012) 431-436

[17] R.P. Maas, S.C. Patch, A.M. Gagnon, The Dynamics of Lead in Drinking Water in U.S. Workplaces and Schools, *Am. Ind. Hyg. Assoc. J.* 55 (1994) 829–832.

[18] I.A. Al-Saleh, Trace elements in drinking water coolers collected from primary schools, Riyadh, Saudi Arabia, *Sci. Total Environ.* 181 (1996) 215–221.

[19] W.F. Davis, A Case Study of Lead in Drinking Water: Protocol, Methods, and Investigative Techniques, Am. *Ind. Hyg. Assoc. J.* 51 (1990) 620–624.

[20] A.I. Alabdula'aly, M.A. Khan, Heavy metals in cooler waters in Riyadh, Saudi Arabia, *Environ. Monit. Assess.* 157 (2009) 23–28.

[21] P.C.M. Kutty, A. a Nomani, S. Al-sulami, A. Al-rabeh, Monitoring of trace metals in desalinated drinking water and their permissible levels, Pap. Present. *IDA Conf. Abu Dhabi*. (1995) 1180-1190.

[22] ATSDR (Agency for Toxic Substances and Disease Registry), Toxicologial Profiles, Toxic Substances Portal (2015). Available at: http://www.atsdr.cdc.gov/toxprofiles/index.asp (accessed October 29, 2017).

[23] A. Garza, R. Vega, E. Soto, Cellular mechanisms of lead neurotoxicity., *Med. Sci. Monit*. 12 (2006) RA57-65.

[24] M.F. Bouchard, S. Sauvé, B. Barbeau, M. Legrand, M.-È. Brodeur, T. Bouffard, E. Limoges, D.C. Bellinger, D. Mergler, Intellectual Impairment in School-Age Children Exposed to Manganese from Drinking Water, *Environ. Health Perspect*. 119 (2010) 138–143.

[25] K. Jomova, Z. Jenisova, M. Feszterova, S. Baros, J. Liska, D. Hudecova, C.J. Rhodes, M. Valko, Arsenic: toxicity, oxidative stress and human disease, *J. Appl. Toxicol*. 31 (2011)

[26] J. Burger, K.R. Campbell, S. Murray, T.S. Campbell, K.F. Gaines, C. Jeitner, T. Shukla, S. Burke, M. Gochfeld, Metal levels in blood, muscle and liver of water snakes (Nerodia spp.)

from New Jersey, Tennessee and South Carolina, *Sci. Total Environ*. 373 (2007) 556–563.

[27] N. Johri, G. Jacquillet, R. Unwin, Heavy metal poisoning: the effects of cadmium on the kidney, *BioMetals*. 23 (2010) 783–792.

[28] F. Fernández-Luqueño, F. López-Valdez, P. Gamero-Melo, S. Luna-Suárez, E. Aguilera-González, A. Martínez, M. García-Guillermo, G. Hernández-Martínez, R. Herrera-Mendoza, M. Álvarez-Garza, I. Pérez-Velázquez, Heavy metal pollution in drinking water - a global risk for human health: A review, *African J. Environ. Sci. Technol.* (2013) 567-584.

[29] R.R. Dietert, M.S. Piepenbrink, Lead and Immune Function, Crit. Rev. *Toxicol.* 36 (2006) 359–385.

[30] MOEP (Ministry of Economy and Planning), The General Population and Housing Census. General Authority for Statistics, (2010). https://www.stats.gov.sa/en/13 (accessed October 29, 2017).

[31] MWE, (2012). http://www.worldwatercouncil.org/fileadmin/wwc/Prizes/Hassan_II/Candidates_2011/16%0A.Ministry_ SA.pdf %0A..

[32] MOEP(Ministry of Economy and Planning), Kingdom of Saudi Arabia, (2010). http://climateobserver.org/wp-content/uploads/2014/09/Saudi-Arabia_Ninth Development-Plan-2010-2014.pdf (accessed October 29, 2017).

[33] S. Chowdhury, M. Al-Zahrani, Characterizing water resources and trends of sector wise water consumptions in Saudi Arabia, *J. King Saud Univ. - Eng. Sci*. 27 (2015) 68–82.

[34] SWCC (Saline Water Conversion Corporation), SWCC Annual Report (2015). http://www.swcc.gov.sa/english/MediaCenter/SWCCPublications/Publication Files/AnnualReport2015EN.pdf (accessed October 29, 2017).

[35] D. Kim, G.L. Amy, T. Karanfil, Disinfection by-product formation during seawater desalination: A review, *Water Res.* 81 (2015) 343–355.

[36] R.A. Mandour, Y.A. Azab, The prospective toxic effects of some heavy metals overload in surface drinking water of Dakahlia Governorate, Egypt, *Int. J. Occup. Environ. Med.* (2011) 245-253.

[37] M.R. Lasheen, C.M. Sharaby, N.G. El-Kholy, I.Y. Elsherif, S.T. El-Wakeel, Factors influencing lead and iron release from some Egyptian drinking water pipes, *J. Hazard. Mater.* 160 (2008) 675–680.

[38] D.A. Lytle, T.J. Sorg, C. Frietch, Accumulation of Arsenic in Drinking Water Distribution Systems, *Environ. Sci. Technol.* 38 (2004) 5365–5372.

[39] S. Kim, Pyrolysis kinetics of waste PVC pipe, *Waste Manag.* 21 (2001) 609–616.

[40] AWWA (American Water Works Association), Internal Corrosion of Water Distribution Systems, Second Edition :: 9780898677591, (1996). https://www.bookdepository.com/Internal-Corrosion-Water-Distribution-Systems-Second-Edition-AWWA-American-Water-Works-Association/9780898677591 (accessed October 29, 2017.

[41] D.A. Lytle, M.R. Schock, Impact of stagnation time on metal dissolution from plumbing materials in drinking water, *J. Water Supply Res. Technol. - Aqua*. 49 (2000).

[42] M. Al-Malack, Migration of lead from unplasticized polyvinyl chloride pipes, *J. Hazard. Mater.* 82 (2001) 263–274.

[43] Y. Xie, Y. Wang, V. Singhal, D.E. Giammar, Effects of pH and Carbonate Concentration on Dissolution Rates of the Lead Corrosion Product $PbO_2$, *Environ. Sci. Technol.* 44 (2010) 1093–1099.

[44] Boffardi BP, Minimization of lead corrosion in drinking water. Materials performance. 1990; 29(8) 45-9.

[45] P. SARIN, J.A. CLEMENT, V.L. SNOEYINK, W.M. KRIVEN, Iron Release from corroded, unlined cast-iron pipe, *J. Am. Water Works Assoc.* 95 (2003) 85–96.

[46] P. Sarin, V.L. Snoeyink, D.A. Lytle, W.M. Kriven, Iron Corrosion Scales: Model for Scale Growth, Iron Release, and Colored Water Formation, *J. Environ. Eng.* 130 (2004) 364–373.

[47] Edwards, M., Jacobs, S., & Dodrill, D. (1999). Desktop guidance for mitigating pb and cu corrosion by-products. *American Water Works Association.Journal*, 91(5), 66.

[48] H. Liu, G. V. Korshin, J.F. Ferguson, Investigation of the Kinetics and Mechanisms of the Oxidation of Cerussite and Hydrocerussite by Chlorine, *Environ. Sci. Technol*. 42 (2008) 3241–3247.

[49] M.R. Schock, R.N. Hyland, M.M. Welch, Occurrence of Contaminant Accumulation in Lead Pipe Scales from Domestic Drinking-Water Distribution Systems, *Environ. Sci. Technol.* 42 (2008) 4285–4291.

[50] D.A. LYTLE, M.R. SCHOCK, Formation of Pb(IV) oxides in chlorinated water, *J. Am. Water Works Assoc*. 97 (2005) 102–114.

[51] M. EDWARDS, A. DUDI, role of chlorine and chloramine in corrosion of lead-bearing plumbing materials, *J. Am. Water Works Assoc.* 96 (2004) 69–81.

[52] Y.-P. Lin, R.L. Valentine, Release of Pb(II) from Monochloramine-Mediated Reduction of Lead Oxide (PbO 2 ), *Environ. Sci. Technol.* 42 (2008) 9137–9143.

[53] Y. Xie, Y. Wang, D.E. Giammar, Impact of Chlorine Disinfectants on Dissolution of the

Lead Corrosion Product PbO 2, *Environ. Sci. Technol.* 44 (2010) 7082–7088.

[54] C. Volk, Practical evaluation of iron corrosion control in a drinking water distribution system, *Water Res.* 34 (2000) 1967–1974.

[55] N. Boulay, M. Edwards, Role of temperature, chlorine, and organic matter in copper corrosion by-product release in soft water, *Water Res.* 35 (2001) 683–690.

[56] B. Johnson, R. Yorton, T. Tran, J. Kim, Evaluation of corrosion control alternatives to meet the lead and copper rule for Eastern Massachusetts, *J. NEWWA*. 3 (1993) 24–45..

[57] Le Gouellec, Y. A., & Cornwell, D. (2007). Installation, condition assessment, and reliability of service lines. Water Environment Research Foundation.

[58] G.R. Boyd, S.H. Reiber, M.S. McFadden, G. V. Korshin, Effect of changing water quality on galvanic coupling, *J. Am. Water Works Assoc.* 104 (2012).

[59] S Triantafyllidou, S., & Edwards, M. Contribution of galvanic corrosion to lead in water after partial lead service line replacements. Water Res. Found. Report, (2010). (4088).

[60] H. Zidouh, Velocity Profiles and Wall Shear Stress in Turbulent Transient Pipe Flow, Int. *J. Dyn. Fluids*. 5 (2009) 61-83.

[61] C. Cartier, R.B. Arnold, S. Triantafyllidou, M. Prévost, M. Edwards, Effect of Flow Rate and Lead/Copper Pipe Sequence on Lead Release from Service Lines, *Water Res.* 46 (2012) 4142–4152.

[62] S. Triantafyllidou, M. Edwards, Critical evaluation of the NSF 61 Section 9 test water for lead, *J. Am. Water Works Assoc*. 99 (2007) 133–143.

[63] G.R. Boyd, G.L. Pierson, G.J. Kirmeyer, M.D. Britton, R.J. English, Lead release from new end-use plumbing components in Seattle Public Schools, *J. Am. Water Works Assoc.* 100 (2008) 105–114.

[64] P. Scardina, M. Edwards, Lead-Contaminated Water from Brass Plumbing Devices in New Buildings, *J. Am. Water Works Assoc.* 102 (1914) 66–76.

[65] D.E. Kimbrough, Brass Corrosion as a source of lead and copper in traditional and all-plastic distribution systems, *J. Am. Water Works Assoc.* 99 (2007) 70–76.

[66] E. Sarver, Y. Zhang, M. Edwards, Review of Brass Dezincification Corrosion in Potable Water Systems, *Corros. Rev.* 28 (2010) 155–196.

[67] Y. Zhang, M. Edwards, Zinc content in brass and its influence on lead leaching, *J. Am. Water Works Assoc*. (2011).

[68] E. Brandl, R. Malke, T. Beck, A. Wanner, T. Hack, Stress corrosion cracking and selective corrosion of copper-zinc alloys for the drinking water installation, *Mater. Corros.* 60 (2009)

251–258.

[69] C. Cartier, S. Nour, B. Richer, E. Deshommes, M. Prévost, Impact of water treatment on the contribution of faucets to dissolved and particulate lead release at the tap, *Water Res.* 46 (2012) 5205–5216.

[70] S.. O'Reilly, M.F. Hochella, Lead sorption efficiencies of natural and synthetic Mn and Fe-oxides, Geochim. *Cosmochim. Acta.* 67 (2003) 4471–4487.

[71] M. Mohapatra, K. Rout, B.K. Mohapatra, S. Anand, Sorption behavior of Pb(II) and Cd(II) on iron ore slime and characterization of metal ion loaded sorbent, *J. Hazard. Mater*. 166 (2009) 1506–1513.

[72] E. Deshommes, L. Laroche, S. Nour, C. Cartier, M. Prévost, Source and occurrence of particulate lead in tap water, *Water Res.* 44 (2010) 3734–3744.

[73] R. Goyer, M. Golub, H. Choudhury, M. Hughes, E. Kenyon, M. Stifelman, Issue Paper on The Human Health Effects of Metals, 2004. https://www.epa.gov/sites/production/files/2014-11/documents/human_health_effects.pdf (accessed October 30, 2017).

[74] M. Bauer, C. Blodau, Arsenic distribution in the dissolved, colloidal and particulate size fraction of experimental solutions rich in dissolved organic matter and ferric iron, Geochim. *Cosmochim. Acta.* 73 (2009) 529–542.

[75] Michael R Schock, D.A. Lytle, J.A. Clement, Effect of pH, DIC, orthophosphate and sulfate on drinking water cuprosolvency (PDF Download Available), 1995. https://www.researchgate.net/publication/236378088_Effect_of_pH_DIC_orthophosphate_and_sulfate_on_drinking_water_cuprosolvency (accessed October 30, 2017).

[76] US EPA (United States Environmental Protection Agency). Integrated Risk Information System (2017). https://www.epa.gov/iris (accessed October 30, 2017).

[77] ATSDR (Agency for Toxic Substances and Disease Registry), Toxicologial Profiles, Toxic Substances Portal (2015). https://www.atsdr.cdc.gov/toxprofiles/index.asp (accessed October 30, 2017).

[78] A. Garza, R. Vega, E. Soto, Cellular mechanisms of lead neurotoxicity., *Med Sci Monit*. (2006).

[79] K. Jomova, Z. Jenisova, M. Feszterova, S. Baros, J. Liska, D. Hudecova, C.J. Rhodes, M. Valko, Arsenic: toxicity, oxidative stress and human disease, *J. Appl. Toxicol.* (2011)

[80] J. Burger, K.R. Campbell, S. Murray, T.S. Campbell, K.F. Gaines, C. Jeitner, T. Shukla, S. Burke, M. Gochfeld, Metal levels in blood, muscle and liver of water snakes (Nerodia spp.) from New Jersey, Tennessee and South Carolina, *Sci. Total Environ.* 373 (2007) 556–563.

[81] N. Johri, G. Jacquillet, R. Unwin, Heavy metal poisoning: the effects of cadmium on the kidney, *BioMetals.* 23 (2010) 783–792.

[82] R.R. Dietert, M.S. Piepenbrink, Lead and Immune Function, Crit. Rev. *Toxicol.* 36 (2006) 359–385.

[83] F. Fernández-Luqueño, F. López-Valdez, P. Gamero-Melo, S. Luna-Suárez, E. Aguilera-González, A. Martínez, M. García-Guillermo, G. Hernández-Martínez, R. Herrera-Mendoza, M. Álvarez-Garza, I. Pérez-Velázquez, Heavy metal pollution in drinking water - a global risk for human health: A review, *African J. Environ. Sci. Technol.* (2013).

[84] US EPA (United States Environmental Protection Agency), National Primary Drinking Water Regulations, (2017). https://www.epa.gov/ground-water-and-drinking water/national-primary-drinking-water-regulations#Inorganic (accessed October 30, 2017).

[85] US EPA (United States Environmental Protection Agency), Drinking Water Contaminants – Standards and Regulations, 2017. https://www.epa.gov/dwstandardsregulations (accessed October 30, 2017).

[86] HC (Health Canada), Guidelines for Canadian Drinking Water Quality Summary Table, (2017). https://www.canada.ca/content/dam/hc-sc/migration/hc-sc/ewh-semt/alt_formats/pdf/pubs/water-eau/sum_guide-res_recom/sum_guide-res_recom-eng.pdf (accessed October 30, 2017).

[87] WHO, (The World Health Organization) Guidelines For Drinking-Water Quality, (2011). http://www.who.int/water_sanitation_health/publications/2011/9789241548151_ch08.pdf (accessed October 30, 2017).

[88] NZ (New Zealand), Drinking-water Standards for New Zealand 2005 (Revised 2008), 2005. http://www.health.govt.nz/publication/drinking-water-standards-new-zealand-2005-revised-2008.

[89] AUS, Australian Drinking Water Guidelines (2011) - Updated October 2017, National Health and Medical Research Council, (2011). https://www.nhmrc.gov.au/guidelines-publications/eh52 (accessed October 30, 2017).

[90] UK (United Kingdom) Drinking Water guideline, (2015). http://www.dwi.gov.uk (accessed October 30, 2017).

[91] US EPA (United States Environmental Protection Agency), Drinking Water Unit, Quick Guide To Drinking Water Sample Collection - Second Edition Updated, (2016). https://www.epa.gov/sites/production/files/2015-11/documents/drinking_water_sample_collection.pdf (accessed October 30, 2017).

[92] APHA. (American Public Health Association), Standard Methods for the Examination of Water and Wastewater Order Form, 1995. https://www.mwa.co.th/download/file_upload-/SMWW_10900end.pdf (accessed October 30, 2017).

[93] US EPA (United States Environmental Protection Agency), ICP MS, Method 200.8, Revision 5.4: Determination of Trace Elements in Waters and Wastes by Inductively Coupled Plasma – Mass Spectrometry, (1994). https://www.epa.gov/sites/production/files/2015-08/documents/method_200-8_rev_5-4_1994.pdf (accessed October 30, 2017).

[94] SAS Inc, Statistical Software, JMP Software from SAS, (2009). https://www.jmp.com/en_us/home.html (accessed October 30, 2017).

[95] Minitab Inc, (2016.). The Statistical Software Package. http://www.minitab.com/en-us/?_sm_au_=iVV63ZTW6Hq4k540 (accessed October 30, 2017).

[96] M.T. Alexander, D.C. Montgomery, G. Runger, Applied Statistics and Probability for Engineers, *Technometrics*. 37 (1995) 455.

[97] N.K. Kasabov, Foundations of neural networks, fuzzy systems, and knowledge engineering, *Comput. Math. with Appl*. 33 (1997) 136.

[98] WHO (The World Health Organization). Lead poisoning and health, WHO. (2017). http://www.who.int/mediacentre/factsheets/fs379/en/ (accessed October 30, 2017).

[99] S. Martin, W. Griswold, Human Health Effects of Heavy Metals, *Environ. Sci. Technol. Briefs Citizens.*15 (2009).

[100] M. Jaishankar, T. Tseten, N. Anbalagan, B.B. Mathew, K.N. Beeregowda, Toxicity, mechanism and health effects of some heavy metals, *Interdiscip. Toxicol*. 7 (2014).

[101] A. Wigginton, S. McSpirit, C.D. Sims, Heavy Metal Accumulation in Hot Water Tanks in a Region Experiencing Coal Waste Pollution and Comparison Between Regional Water Systems, Bull. *Environ. Contam. Toxicol.* 79 (2007) 405–409.

[102] E.A. Gulbransen, K.F. Andrew, Oxidation Studies on the Nickel-Chromium and Nickel-Chromium-Aluminum Heater Alloys, *J. Electrochem. Soc.* 106 (1959) 941.

[103] USEPA(United States Environmental Protection Agency), (2007). https://www.epa.gov/sites/production/files/201509/documents/-fs_arsenic_dist-_sys_factsheet_final.pdf (accessed October 1, 2017).

[104] K. Gerin, O.; Bleys, B.; De Cuyper, Seasonal variation of hot and cold water consumption in apartment buildings, *CIBW06 Symp*. (2014).

[105] Y. Xie, Y. Wang, V. Singhal, D.E. Giammar, Effects of pH and carbonate concentration on dissolution rates of the lead corrosion product PbO2, *Environ. Sci. Technol.* 44 (2010) 1093–1099.

[106] Y. Xie, Y. Wang, D.E. Giammar, Impact of chlorine disinfectants on dissolution of the lead corrosion product PbO2, *Environ. Sci. Technol.* 44 (2010) 7082–7088.

[107] M. Edwards, A. Dudi, role of chlorine and chloramine in corrosion of lead-bearing plumbing materials, *J. Am. Water Works Assoc.* 96 (2004) 69–81..

[108] Y.-P. Lin, R.L. Valentine, Release of Pb(II) from Monochloramine-Mediated Reduction of Lead Oxide (PbO 2 ), *Environ. Sci. Technol*. 42 (2008) 9137–9143.

[109] M. Mohapatra, K. Rout, B.K. Mohapatra, S. Anand, Sorption behavior of Pb(II) and Cd(II) on iron ore slime and characterization of metal ion loaded sorbent, *J. Hazard. Mater.* 166 (2009) 1506–1513.

[110] S.. O'Reilly, M.F. Hochella, Lead sorption efficiencies of natural and synthetic Mn and Fe-oxides, *Geochim. Cosmochim. Acta*. 67 (2003) 4471–4487.

[111] M.R. Lasheen, C.M. Sharaby, N.G. El-Kholy, I.Y. Elsherif, S.T. El-Wakeel, Factors influencing lead and iron release from some Egyptian drinking water pipes, *J. Hazard. Mater.* 160 (2008) 675–680.

[112] I.A. Alam, M. Sadiq, Metal contamination of drinking water from corrosion of distribution pipes, *Environ. Pollut.* 57 (1989) 167–178.

[113] ATSDR (Agency for Toxic Substances and Disease Registry), Toxicologial Profiles, Toxic Substances Portal (2015). Available at: http://www.atsdr.cdc.gov/toxprofiles/index.asp (accessed October 29, 2017).

[114] US EPA (United States Environmental Protection Agency), Drinking Water Contaminants – Standards and Regulations, 2017. https://www.epa.gov/dwstandardsregulations (accessed October 30, 2017)

[115] T.L. Gerke, K.G. Scheckel, J.B. Maynard, Speciation and distribution of vanadium in drinking water iron pipe corrosion by-products, *Sci. Total Environ.* 408 (2010) 5845–5853.

[116] L. Mcneill, J. Mclean, M. Edwards, J. Parks, State of the Science of Hexavalent Chromium in Drinking Water State of the Science of Hexavalent Chromium in Drinking Water 1, (2012).

[117] MDH, Copper in Drinking Water: Health Effects and How to Reduce Exposure Fact Sheet - EH: Minnesota Department of Health, 2005. http://www.health.state.mn.us/divs/eh/water/factsheet/com/copper.html?_sm_au_=iVV63ZTW6Hq4k540 (accessed October 30, 2017).

[118] U.S. EPA. Decontamination of Drinking Water Infrastructure: A Literature Review and Summary, 2014. https://cfpub.epa.gov/si/si_public_record_report.cfm?dirEntryId=274760 (accessed October 30, 2017).

[119] F. Bardelli, M. Benvenuti, P. Costagliola, F. Di Benedetto, P. Lattanzi, C. Meneghini, M. Romanelli, L. Valenzano, Arsenic uptake by natural calcite: An XAS study, *Geochim. Cosmochim. Acta*. 75 (2011) 3011–3023.

[120] The Clemson University Cooperative Extension Service, Iron and Manganese, 1990. http://lubbock.tamu.edu/files/2011/10/WQL9.pdf?_sm_au_=iVV63ZTW6Hq4k540 (accessed October 30, 2017).

[121] USEPA(United States Environmental Protection Agency), Investigation of Potential Environmental Impacts due to the use of Phosphate-based Corrosion Inhibitors in the District of Columbia, 2004. http://taskmediator.com/op/op.Download.php?documentid=2153&version=1.

[122] Hot water heater anodes and rust protection, (2017). http://www.waterheaterrescue.com/Longevity/water-heater-anodes.html (accessed October 30, 2017).

# Vitae


Name : Fayzul Kabir

Nationality : Bangladeshi

Date of Birth :8/15/1990

Email :g201509710@kfupm.edu.sa; fkabirceesust@gmail.com

Address : Village: Jangalia, Post Office: Adampur, Police Station: Kamalganj, District: Moulvibazar, Bangladesh


Academic Background :

Fayzul Kabir attended Shahjalal University of Science and Technology, Sylhet, Bangladesh from where he obtained Bachelor of Science in Civil Engineering in 2012 and he placed second position in his batch. After graduation, he joined at Civil Engineering Discipline, Leading University, Bangladesh as a faculty member in January 2013. After that, he attended King Fahd University of Petroleum and Minerals, Dhahran, Saudi Arabia and obtained Master of Science in Civil Engineering in January 2018. He has published three peer reviewed journal papers, and several of his works are currently under review process.

Research Interest :

His research interests lie primarily in the area of water quality, water treatment, contaminant transport, human exposure and risk analysis, hydrological processes, effects of climate change and mitigation strategy, climate change impacts on water resources.

Publications:

Peer Reviewed Journal Papers

1. **Kabir, F.,** and Chowdhury, S. (2017). Arsenic Removal Methods for Drinking Water in the Developing Countries: Technological Developments and Research Needs. *Environmental Science and Pollution Research*, 24, 24102–24120
2. Ahmed, A.M., **Kabir, F**., and Ali, S.M. (2013). Analysis of Different Types of Aerators for Conventional Iron Removal Plant. *Journal of Applied Technology in Environmental Sanitation*, 3(4), 159-164.
3. **Kabir, F**., Chakrabarty, S., and Ali, S.M., (2014). Use of Recycled Coarse Aggregate as an Alternative of Natural Coarse Aggregate for Structural Construction. *International Journal of Advances in Engineering Sciences*, 4 (4) 35-38

Refereed Conference Proceedings

1. Hasan, G.M.J., **Kabir, F.,** and Hossain, S.Z. (2012). Estimation of suspended sediment concentration of different water bodies using low cost portable cameras, *Proceedings of the Second International Conference on Environmental Technology and Construction Engineering for Sustainable Development (ICETCESD 2012)*, Sylhet, Bangladesh, 10-12 March, 2012.